Università degli Studi di Cagliari

DOTTORATO DI RICERCA
Ingegneria Industriale

XXVI Ciclo

Soft pneumatic devices for blood circulation improvement

Settore scientifico disciplinare di afferenza
ING-IND/13 - MECCANICA APPLICATA ALLE MACCHINE

Presentata da	Silvia Meili
Coordinatore Dottorato	prof. Roberto Baratti
Tutor	prof. Maria Teresa Pilloni
Relatore	prof. Andrea Manuello Bertetto

Esame finale anno accademico 2013 – 2014

Dottorato di Ricerca in Ingegneria Industriale

Soft pneumatic devices for blood circulation improvement

Silvia Meili

Università degli Studi di Cagliari
Dipartimento di Ingegneria Meccanica, Chimica e dei Materiali

Abstract

The research activity I am presenting in this thesis lies within the framework of a cooperation between the University of Cagliari (Applied Mechanics and Robotics lab, headed by professor Andrea Manuello Bertetto, and the research group of physicians referencing to professor Alberto Concu at the Laboratory of Sports Physiology, Department of Medical Sciences), and the Polytechnic of Turin (professor Carlo Ferraresi and his équipe at the Group of Automation and Robotics, Department of Mechanical and Aerospace Engineering)

This research was also funded by the Italian Ministry of Research (MIUR – PRIN 2009).

My activity has been mainly carried on at the Department of Mechanics, Robotics lab under the supervision of prof. Manuello; I have also spent one year at the Control Lab of the School of Electrical Engineering at Aalto University (Helsinki, Finland). The tests on the patients were taken at the Laboratory of Sports Physiology, Cagliari.

I will be describing the design, development and testing of some soft pneumatic flexible devices meant to apply an intermittent massage and to restore blood circulation in lower limbs in order to improve cardiac output and wellness in general. The choice of the actuators, as well as the pneumatic circuits and air distribution system and PLC control patterns will be outlined. The trial run of the devices have been field-tested as soon a prototype was ready, so as to tune its features step-by-step.

I am also giving a characterization of a commercial thin force sensor after briefly reviewing some other type of thin pressure transducer. It has been used to gauge the contact pressure between the actuator and the subject's skin in order to correlate the level of discomfort to the supply pressure, and to feed this value back to regulate the supply air flow.

In order for the massage to be still effective without causing pain or distress or any cutoff to the blood flow, some control objective have been set, consisting in the regulation of the contact force so that it comes to the constant set point smoothly and its value holds constant until unloading occurs.

The targets of such mechatronic devices range from paraplegic patients lacking of muscle tone because of their spinal cord damage, to élite endurance athletes needing a circulation booster when resting from practicing after serious injuries leading to bed rest.

Encouraging results have been attained for both these two categories, based on the monitored hemodynamic variables.

Contents

1 Introduction

Reduction of the hemodynamic response leading to poor oxygen delivery has been observed in paraplegic patients; hence a means to replace muscle action on deep leg blood vessels to restore venous return when tonus is lost is seriously sought after. Inflatable pneumatic devices are particularly suited for human interaction and rehabilitation purposes.

1.1 Motivation

Some lightweight, low-cost, customizable pneumatic devices for blood flow recovery have been developed and tested for their effectiveness in modifying cardiac output. They mainly consist of some pneumatic compliant actuators, of different shape size and number resulting in different actuation mechanisms, performing an intermittent massage on different leg segments at controlled law and pressure level. The actuators, which are toroidal balloons each consisting of an inflatable bladder bounded by an inextensible fabric coat acting as a constraint, were chosen for their geometrical, mechanical, pneumatic and shape properties. Actuation can be performed either by means of the only inflatable bladders or adopting a further constraining stiff shell. The pneumatic circuits supplying air to the actuators has been kept as compact as possible and designed so as not to get too high pressure drops caused by piping resistance, neither suffer the relatively large air mass responsible for high inertial (inductive) features as well as properly feeding the relatively large bladder volumes behaving as capacitors. The devices, meant for people having chronic or transient muscular inefficiencies or diseases up to paraplegia as well as for élite athletes, were first tested on a group of paraplegic patients to preliminarily assess their effectiveness in modifying some indexes of

heart efficiency (as stroke volume and ventricular pre-ejection time/ventricular ejection time), then, after some modifications, underwent several tests on healthy subjects in order to monitor either different hemodynamic parameters. The effects of applying different intermittent pressure patterns on patients legs are thus highlighted and related to impedance cardiography measures of heart efficiency parameters.

1.2 Statement of the problem

In normal subjects, the arterial blood pressure adjustment during dynamic exercise is regulated through a balance between systemic vascular resistance (SVR) and cardiac output (CO). The integrity of the central nervous system, which operates an effective integration between these components, is essential to reach a normal hemodynamic response. In spinal cord-injured (SCI) individuals, there is a partial loss of nervous control over circulation, and this reaches to the absent peripheral vasoconstriction below the level of the spinal lesion and the lower stroke volume (SV). Moreover, in paraplegic subjects, due to absence of leg muscle contraction, venous return to the heart is reduced and this may cause a diastolic deficit with a reduction of (CO) and oxygen delivery that, in turn, would reduce the aerobic capacity in these patients.

Many medical and biomechanical researchers evaluate the possibility of replacing the striate muscle pump on limb veins with the application to legs of mechanical actuators, thus restoring end diastolic filling pressure of ventricles. In this occurrence, cardiac output compensation would occur and aerobic capacity would be restored in these patients.

1.3 Outline

This section gives a summary of the thesis

Chapter 2: Background

The framework within this thesis has been developed. Generalities on flexible pneumatic actuators as well as the physiological fundamentals for the choice of using those as an aid device for restoring blood circulation are presented.

Chapter 3: Flexible pneumatic systems

A review on the wide range on such class of actuators is given. Following an overview of their functioning principles, and finally a description of the design and development of the devices set up and tested in this thesis.

Chapter 4: Preliminary experimental

Very encouraging results of the preliminary tests on paraplegic patients, showing how the patients cardiac function improves when having pressure applied on their legs under incremental effort will be given, along with the description of the circuit, the actuators, the acquisition system and the improvement of the hemodynamic parameters values showing blood circulation improvement.

Chapter 5: Contact experimental and modeling

Static and dynamic calibration data of the thin sensors used in order to measure contact pressure between the actuators and the skin are given. A review of contact pressure sensors is given as well.

Chapter 6: Modeling and control

Some circuits have ben identified and their dynamics modeled; a PID controller have been tuned in order to keep the contact force constant until unloading occurs and to come to the set point smoothly.

Chapter 7: Testing on the patients

Two different PLC controlled devices have been tested, giving both encouraging results as for the blood restoration.

2. Background

2.1. Why pneumatics

Why matching pneumatics benefits to soft actuators features? Both industrial and service robots can take advantage of adaptivity and safety that such systems exhibit.

As for industrial robots, in order to get fine positioning or tight clamping rigid grips are usually the elective choice. Sometimes the irregular geometry or peculiar mechanical features of the piece being handled make a lower bound on the stiffness and jerkiness of steel clamps. Or maybe the corrosive operating environment can make it risky using metal clamps, or too expensive as for the maintenance. In order to smoothen the effects of stress concentrators, a soft gripper exerting as much as an even force as possible could be a better choice. At the same time, rubber or plastic bladders are much less sensitive to corrosion and chemically aggressive conditions.

Manipulation of brittle objects, whether they are ice-cream cones or graphite electrodes, telescope mirrors or human skin, could be better achieved by means of bladder inflatable actuators.

In addition, such soft clamps dampen out vibrations (which is not necessarily an advantage as we will see lately), fit more easily in confined volumes and take the same shape of non-uniform surfaces.

Service robots interacting with animals or humans, on the other hand, need to be safe, clean, non harmful and, why not, lightweight and friendly. They have to be designed and controlled to accomplish such features.

In one word, compliance is the feature allowing for such features to be achieved.

In order to fulfill the requirement of faster operating speed a lower inertia is mostly sought for.

2.2. Prosthetics

Chronic venous insufficiency of the lower extremities is a condition caused by abnormalities of the venous wall and valves that leads to obstruction or reflux of blood flow in the veins.

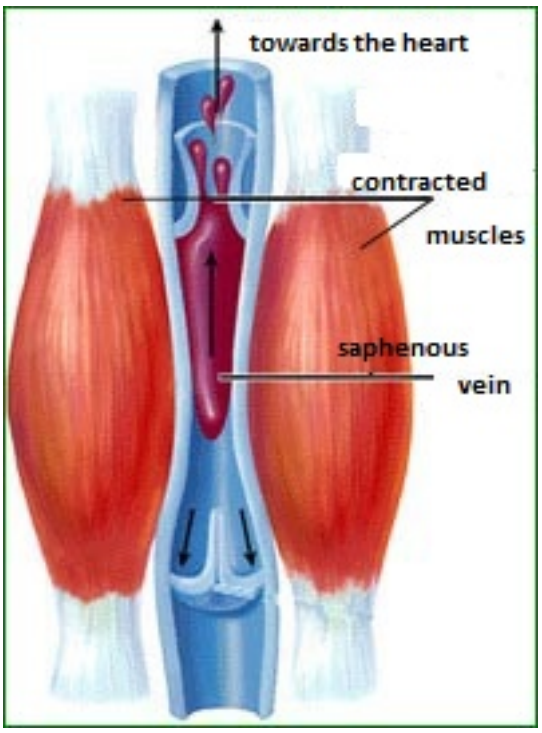

Figure 2.1 Calf compression helps check valves action on the saphenous vein flow towards the heart

Pneumatic compression has been long used for treatment of chronic venous insufficiency (Berliner, Ozbilgin, & Zarin, 2003). In the literature a wide acknowledgement of the compression as a necessary part of all treatments for chronic venous insufficiency and venous ulcers is found.

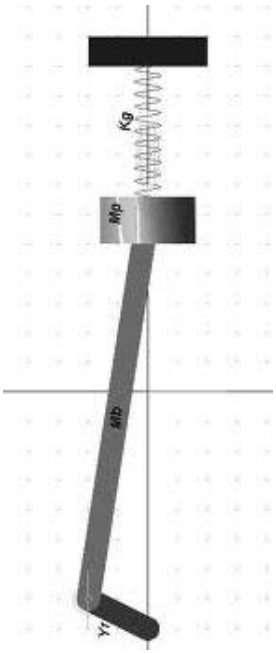

Figure 2.2 Compression on the foot sole, together with the ankle rotation, mimics a crank pushing a piston up onto the calf.

Compression is commonly provided with stockings. Some authors state that pneumatic compression therapy may be necessary if edema fails to resolve with compression bandages.

Prophylaxis to prevent deep venous thrombosis formation includes anticoagulation and physical methods such as intermittent pneumatic compression devices. In high-risk surgical patients, the use of anticoagulants may be contraindicated: whereas, physical methods have been proven effective.

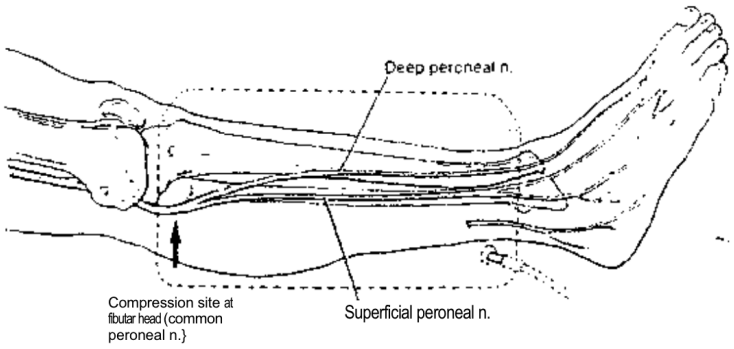

Fig. 2.3 Compression of the common peroneal nerve at the fibular head (arrow) by an inflated pneumatic leg sleeve

The most common side effects of intermittent pneumatic compression devices use are discomfort, warmth, and sweating beneath the vinyl leg sleeves. Complications associated with a related pneumatic compression device, namely sequential pneumatic compression devices have been reported. These complications include peroneal nerve palsy and pressure necrosis of the thigh. Neither of these complications has been associated with IPCD use.

Pneumatically powered orthoses meant as an aid for ambulation have been studied and tuned by several research groups lately.

Some results of this research can be found in (Manuello Bertetto, Meili et al., 2012, Manuello Bertetto, Meili et al., 2011, Concu, Manuello Bertetto, Meili et al., in press)

2.3. Tactile sensors

Tactile sensors are a key component in robotic applications requiring human-robot interaction. Surface force or pressure transducers are used both for simple qualitative touch sensing, thus requiring a simple binary output, and for quantitative continuous gauging of contact pressure through analog voltage signals.

Pressure sensors allow for feedback controlling the system or safety monitoring to

prevent harm to the user or damage of the device. A large class of service robots is (Hollinger & Wanderley, 2006; Vecchi et al., 2000) meant for biomedical applications or care purposes as artificial hands, gait orthoses or rehabilitation and wellness devices in general.

A few commercial, low cost force sensors are available on the market (Hollinger & Wanderley, 2006; Vecchi et al., 2000) and for some of them the producer doesn't guarantee an acceptable repeatability, not to mention linear or hysteresis free response. Many authors have studied such sensors' behavior (Castro & Cliquet, 1997; Freschi et al., 2000; Otto, Brown, & Callaghan, 1999.; Vidal-Verdu, Estı´balitz, Castellanos-Ramos, Navas-Gonzàlez, Macicior, Sikora, 2010). Sensors come in many sizes and shapes, given their prior requirement not to be thick or intrusive, and they work based on a few different principles, being them capacitive or piezoresistive, being too bulky elastic load cells. As for the shape/size issue, thin sensors' dimensions span from a few millimeters, allowing for point contact measurements i.e. for artificial fingers or point-wise, spherical-ended tools, to large arrays of tenth of centimeters side for larger contact areas, i.e. for stress distribution under the plantar sole or over the dorsal area or between soil and foundations (Palmer, Rourke, Olson, Nathaniel A., Abdoun, Ha, & Rourke, 2009; Shaw, Davis, Collins, & Carney, 2009) for civil engineering applications.

Our main target in considering these piezoresistive sensors was a soft-robot application, i.e. a deformable pneumatic device intended to boost leg circulation of paraplegic patients by applying an intermittent massage and at the same time imposing passive ankle dorsiflexion (Manuello Bertetto, Meili, Concu, & Crisafulli,

2012). Measuring the contact force between the actuator and the patients skin should give reliable and quick response in order to tune contact pressure. Thin-film sensors to be mounted under the actuator inner surface are eligible for this task, thus need to be tested and characterized.

The FlexiForce® sensors from Tekscan Inc., Boston, MA, US seemed to us a good commercial and affordable offer (Manuello Bertetto, Meili, 2012) for measuring small forces, also given their short response time (<5 μs). Good frequency response in the low- frequency band of our interest (0.5÷1 Hz, meaning the gait frequency, is required.

2.4. Modeling

Several approaches have been proposed for modeling the pneumatic actuators. The analysis of pneumatic actuators requires a combination of thermodynamics, fluid dynamics and the dynamics of the motion. For constructing a mathematical model, three major considerations are involved (French et al., 1988): 1) the determination of the mass flow rates; 2) the determination of the pressure, volume and temperature of the air inside the actuator; 3) the determination of the dynamics of the load. Identification techniques are also used for finding the mathematical model of the pneumatic actuators. Accurate model of pneumatic actuator is an important condition both for control design and for optimizing its mechanical behavior. (Sorli et al., 1999) presented two different formulations to model a pneumatic actuator, composed of an actuator and a digital valve. In the first one an air thermodynamic transformation was assumed and the simulation was carried out in the Matlab-Simulink environment, while in the second one also the energy equation was

introduced, so that the thermic exchange between the chambers and the external ambient was considered. A detailed mathematical model of dual action pneumatic actuators controlled with proportional spool valves was developed by (Edmond et al., 2001). Effects of nonlinear flow through the valve, air compressibility in cylinder chambers, leakage between chambers, end of stroke inactive volume, and time delay and attenuation in the pneumatic lines were carefully considered. System identification, numerical simulation and model validation experiments were conducted for two types of air cylinders and different connecting tubes length, showing very good agreement. This mathematical model will be used in the development of high performance nonlinear force controllers, with applications in teleoperation, haptic interfaces, and robotics. For modeling a pulse width modulation (PWM) based pneumatic systems a state space averaging approach was presented by (Eric et al., 2002). This provided the analytic machinery necessary to remove the discontinuities associated with switching and results in a model tractable to standard nonlinear control design techniques. The control of a single degree of freedom pneumatic positioning system illustrated this technique experimentally. (Arcangelo et al., 2005) presented an extensive set of experiments and a related mathematical model investigating the dynamics of pneumatic actuators controlled by on-off solenoid valves, whose opening and closing time response is based on a pulse width modulation (PWM) technique. The experimental set-up consists of both commercial electronics and circuits appropriately realized where particular needs are required. As well as providing a highly repeatable set of measurements, valuable for future comparisons, the experimental investigation also provided an appropriate base aimed at testing the performances of the analytical model. The analytical-

experimental comparisons showed the ability of the theoretical model to provide an accurate mean expectation of the position of the actuator less than about 2 mm. Such a capability of the model was tested for several operating and initial conditions during the first five cycles. The presented theoretical model dealing with non-linear dynamics phenomena whose behavior is highly transient should be considered an attempt aimed at providing a valuable tool for designing control strategies without the need for expensive physical models. (Shu et al., 2005) presented a methodology for deriving a nonlinear dynamic model for a pneumatic servo system. The model includes cylinder dynamics, payload motion, friction and valve characteristics. Methods for estimating the model parameters from simple experiments were also described. Experimental results demonstrating the ability of the model to predict the measured piston position and cylinder chamber pressure were included. (Qinghua et al., 2006) established the dynamic model of FPA (flexible pneumatic actuator), which is a new type of actuators, proposed in Zhejiang University of Technology. The primary factors, which affect the dynamic properties of FPA, are the mass flow of air and the volume of FPA chamber. Simulation results of inflating and deflating process of FPA indicated that the section area of air connector of FPA is proportional to the mass flow of air and affects the dynamic properties greatly. The dynamic response of FPA is rapid, completed within 15 milliseconds. (Carducci et al., 2006) validated a complete mathematical model of a pneumatic actuator driven by two on/off two ways valves (with Pulse Width Modulation technique) by tuning a number of geometric and functional characteristics and parameters by means of non-linear optimization algorithms. The experimental data were obtained driving the on/off valves with five different duty cycles: 10, 25, 50, 75 and 90% over a period of 20 ms

and measuring the actuator position with a potentiometer. In particular experimental apparatus was realized in order to measure valve coefficients in all operative conditions. (Xue et al., 2007) presented a dynamic model and a design method for an accurate self-tuning pressure regulator for pneumatic pressure load systems that have some special characteristics such as being nonlinear and time varying. A mathematical model was derived, which consists of a chamber continuity equation, an orifice flow equation and a force balance equation of the spool.

3. Flexible pneumatic systems

3.1. A review

3.1.1. Historical background

Design and development of flexible pneumatic actuators (FPA) have been much investigated in the last decades, for multiple purposes: health equipment, home care mechanisms and accessories, mimics of human tactile and sensing properties. Pneumatics generally represents a safe, fast and mainly inexpensive energy source. When it comes to coupling with soft actuators it reveals itself to be suitable for human interaction, either in active or passive fashion, yet lacking of that precision, both in force or pressure and position, it gives if stiff steel actuators (typically cylinders) are used. The advantages of such inflatable soft devices range from being clean and light-weight to exerting the required relatively small forces and pressures harmlessly on e.g. a patient skin or a flower or fruit to be picked, to being ideally given any geometrical configuration or shape. As for forces, either tensile or compressive, several layouts, briefly inspected in the following, provide pushing, pulling, bending and twisting features, as well as axial symmetric momentum. Also multi-DOF systems are achievable.

A useful classification of Flexible Fluidic Actuators can be made according to their operating principle, or the kind of force they are creating. Here we differentiate between designs that use expansion, contraction or bending directions to drive a system.

The FPA muscles were extensively studied and used in numerous non-conventional applications, (Schulte, 1961; Chou and Hannaford, 1994; Pack et al., 1997). A great

effort was made to propose and fabricate novel types of flexible pneumatic actuators (FPA) as well, in order to improve the pull capabilities of the muscle (Ferraresi et al., 1999). A few works on the modeling of pneumatic muscles have been presented (Hirai et al., 2000; Chou and Hannaford, 1996; Raparelli et al., 1999; Gorissen et al., 2011; Manuello Bertetto and Ruggiu, 2004). Many researchers have studied a particular type of flexible actuator powered by pressurized fluid, namely flexible Pneumatic Balloon Actuators (PBA's) introduced by Schwörer et al. (1998), Konishi et al. (2001) and others (Abe et al. 2007; Lu and Kim, 2009). For a more thorough state of the art of flexible fluid actuators, we refer to two recently published review papers (De Volder and Reynaerts, 2010). The operation of these actuators is based on the same mechanism as the joints of certain insects such as spiders (Schwörer et al., 1998; Parry and Brown, 1959; Zentner et al., 2000). Essentially, these actuators comprise two flexible layers with different bending stiffness which are bonded together at the edges to form a balloon. Because of this asymmetrical stiffness, the actuator bends when pressurized, thus generating the actuation motion. The asymmetric bending stiffness can be achieved using for instance different layer thicknesses or different Young's moduli (Jeong and Konishi, 2000). A promising research activity in the robotics community is the development of devices attempting to imitate biological forms that are based on flexible structures and often fluid-powered. Numerous examples are to be found either as manipulators, actuators, grippers and hands or mobile robots. For each of these robotics areas, several relevant advantages may be stressed when using flexible structures over traditional robots. Manipulators as well as grippers or flexible hands can operate with delicate objects without causing any damage because of their

compliance. Furthermore, robot hands can approximate the manipulation skills and grip force of the human hand when using fluidic actuators (Schultz et al., 2001; Dohta et al., 2001; Kwak and Lee, 2009). These types of structures have significant potential for improved performance over traditional manipulators in the areas of obstacle avoidance and manipulation (Hannan and Walzer, 2001). Moreover, these manipulators have the inherent ability to conform to environmental constraints on contact. Flexible manipulators can boast a drastic simplification in design over traditional devices while still being hyper-redundant in number of degrees of freedom (Ferraresi et al., 1997). No heavy motors and transmission boxes are required since only static sealing, with no relative motion, is used. Thus these devices appear to be well suited for operation in clean rooms and food and agriculture industries since they require no lubricants and wear particles are not released. A common inspiration from biology guides researchers in developing fluidic muscles or actuators. A large number of applications, from the human inspired muscle through angular or revolute actuators, can be found in recent literature (Daerden et al., 2001; Hirai et al., 2000; Noritsuguet al., 2000; Margineanu et al., 2008, Rodrigo et al., 2008). The striking characteristic of these motors is the high ratio between actuation force and weight. However, the robotic area where fluidic flexible structure devices are probably more widespread is that of mobile robots. There are several prototypes based on a flexible structure driven by fluid, which are capable of working in unstructured or even hostile environments. By exploiting the absence of electrical power, these robots can operate with radioactivity or in presence of electromagnetic fields. Some flexible robots have been built for navigating through pipes (Slatkin and Burdick, 1995), swimming (Sfakiotakis et al.,

2001) and climbing (Manuello Bertetto and Ruggiu, 2002). Despite the several advantages mentioned, a strong shortcoming in using these devices is their control strategy. Fluidic flexible robots require sophisticated controls in order to reach accurate and repeatable positioning. Furthermore, their dynamic modeling has to struggle with their deformable structure and unconventional actuations. An extended bibliography can be found concerning the issue of flexible robot modeling (Yoshikama and Hosoda, 1996; Ding and Selig, 2003). However, experimental applications are often limited to simple cases. Many approximate models, i.e. finite elements, Myklestad's method, the Ding-Holzer method and the screw theory have been proposed to overcome the difficulty of applying the distributed parameter approach. However, models of robots with continuum structures have rarely been dealt with (O'Brien and Lane, 2001, Leitman and Villaggio, 2006). In any case, much interest has been shown this kind of actuators, in particular for recovering the fundamental functions of paraplegic subjects.

The biomechanical research community recently evaluated the possibility of replacing the striate muscle pump on limb veins with the application of mechanical actuators to legs, thus restoring end diastolic filling pressure of ventricles. In this occurrence, a cardiac output compensation would occur and aerobic capacity would be restored in these patients.

In spinal cord injured (SCI) individuals there is a partial loss of nervous control over circulation, and this fact may explain some of the altered circulatory responses to effort occurring in SCI persons (Dela et al., 2003; Hopman, 1994; Jacobset al., 2002). The absence of peripheral vasoconstriction below the level of the spinal lesion and

the lower stroke volume (SV) increment compared to able-bodied subjects are well known phenomena during physical activity in SCI patients (Crisafulli et al., 2009).

The inability of SCI patients to increase venous return during exercise has been reported several times and has been associated with a disturbed redistribution of blood due to the lack of sympathetic-mediated vasoconstriction below the level of the spinal cord lesion (Davis et al., 1990; Hopman, 1994; Jacobs et al., 2002; Davis, 1990). This fact impairs venous return and cardiac filling and in part explains the low SV during exercise shown by these patients (Crisafulli et al., 2007).

Some studies employing antigravity suits found that this kind of device could increase peak oxygen uptake and decrease heart rate in relation to workload during arm crank exercise. Moreover, subjects with SCI demonstrated a significantly higher SV with the application of a pneumatic device capable of inducing lower body positive pressure, while able body individuals' performance was unaffected by this kind of intervention. These studies suggest that for individuals with SCI, the use of devices that increase venous return to the heart could augment exercise capacity by preventing the redistribution of blood to the lower extremities (Bazzi et al., 1996; Pitetti et al., 1994).

Intermittent Pneumatic Compression (IPC) (Hills et al., 1972) has been adopted since early 1970s by using inflatable leggings to prevent vascular diseases such deep vein thrombosis, blood clots and ulcers. Such stockings come in many shapes, both full-leg or half leg, segmented or not-segmented, sequentially inflated or not, and cuffs applied to thigh and calf may cover the whole length from knee to hip and all the shank long or may leave particular portions, such as the fibular head, unloaded so as not to inflate over it causing undesired compression of peroneal nerve (Lachmann et

al., 1992). The last consideration suggests not to use too wide devices but to apply a local compression instead. Medical devices that are also quite common, but of simpler design, are “military anti-shock trousers”, also known as “pneumatic anti-shock garments”, which consist of a few section sleeves applying pressure both over each leg and the pelvic section.

3.1.2. Classification based on operating principle

A useful classification of Flexible Fluidic Actuators can be made according to their operating principle, or the kind of force they are producing. Here we differentiate between designs that use expansion, contraction or bending directions to drive a system.

3.1.2.1. Expansion actuators

These systems are either bellow-type actuators or rolling lobe-type actuators. Examples of the latter type go back to the 19th century. These air springs have been made from the start for lifting applications or damping elements, used for example for rescue operations. Bellow-type actuators can drive or dampen tilt motions up to 30° without friction, being the only actuation element. Size can range from tenth down to a couple of centimeters.

Another large group are expansion actuators that work as rotary drive elements. (Sigmon, 1976) describes a solution where the structural integrity is created by the stiff housing and the torque is created by an internal bellow-type actuator (Figure 3.2(a)) The design proposed in (Johnston, 1965) describes a bellow-type actuator suitable for linear or rotary motions as well as single chamber actuators (Figure 3.2(b)-(d)). The proposed materials for the bellow include rubbers as well as metals.

In (Bicchi, A. & Tonietti, G., 2004) a very interesting design is introduced, regarding a patent on fabrication techniques used in the tire industry and describes a layered membrane design with several reinforcement layers (Figure 3.2(e), (f)). The actuator has a layered structure, being the layers reinforced. Anyway, standard materials such as ordinary water hoses are made of are often used. Such actuators can be coupled with controllable electrical actuators to make the most of both technologies.

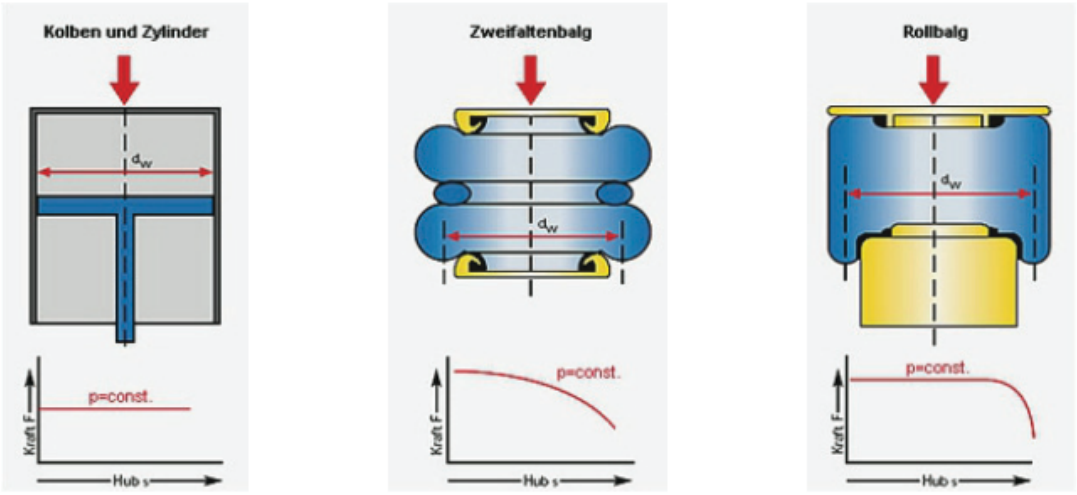

(a) Conventional Cylinder (b) Bellow-Type Actuator (c) Rolling Lobe-Type Actuator

Figure 3.1. Comparison of different kinds of expansion actuators (ContiTech AG, 2011; in (Gaiser et al., 2012)).

(DeLepeleire, 1974) discusses the stress distribution in the membrane of a rotary actuator and requirements for achieving low bending stiffness and high tensile strength. Another approach is described in (Fuchs, 1994). Here the drive element consists of a mono-material system. The whole drive is fabricated in one step (Figure 3.2(g)).

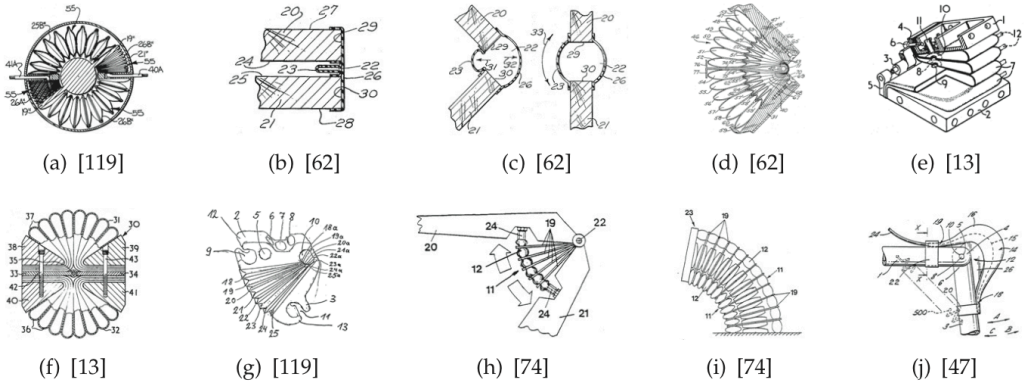

(a) [119] (b) [62] (c) [62] (d) [62] (e) [13]

(f) [13] (g) [119] (h) [74] (i) [74] (j) [47]

Figure 3.2. Radial Cross-Section View of Different Fluidic "Expansion" Drives (Gaiser et al., 2012)

While the presented concepts are designed to operate with pressures in the range of $0 - 20$ *bar* the development in (Larsson, 1988) is operated with pressures up to 200 *bar*. The actuator set-up allows both, linear and rotary actuation (Figure 3.2(h), (i)). The focus in these works lies on heavy-duty machinery but rotary drives or trunk-like structures are discussed for robotic applications as well. Detailed concepts regarding layered fiber reinforcements in the shell are introduced.

While the previous example requires complex knowledge and technology to produce an individually shaped membrane, other examples implement standard materials for flexible fluidic actuators. In (Ivlev, 2009; Marette, 1961; Schulz, 2004b) a design is proposed that uses bulky materials such as ordinary water hoses to form the actuator. Figure 3.2(j) shows one set-up of this FLEXATOR muscle. Subsequent developments applied the FLEXATOR technology to the fields of rehabilitation (Prior et al. 1993) and horticultural robotics (Tillett et al., 1994). The works of (Prior et al., 1993) introduced a unique approach that came to be known as "hybrid actuation" (Shin et al., 2009). Here the powerful fluidic actuators are combined with precisely controllable electrical actuators in a parallel configuration.

3.1.2.2. Bending actuators

Bending actuators generate bending motion when pressurized, allowing manipulation of objects in adaptive and compliant way. Basically, they can be vacuum or pressure operated. (Staines, 1962) presented vacuum operated and (Baer 1967, 1975) pressure operated conceptual solutions for this problem (Figure 3.3(a) and 3.3(b)).

The work by (Orndorff, 1971) and (Ewing, 1973) as well as (Andorf et al., 1976) introduce designs where bending occurs due to “anisotropic membrane stiffness”. (Craig et al., 1989) point out that these types of actuators can be folded to reduce shipping volume especially for space applications. Figures 3.3(c)-3.3(e) show the different designs. Bending actuators designed with multi-lumen hoses are represented by the work of (Suzumori et al., 1992, 1995, 1996, 2007) shown in Figure 3.3(f). Radial reinforcements inhibit radial expansion so that the operating pressure is 1.4−4 bar. There are a large variety of trunk-like bending actuators that create bending motion by adding structural constraints. A few examples are shown in Figures 3.4(a)-(c). Monolithic bending actuators represent the last group in this section. Different research groups have been working on this topic during the last years (Ilievski et al., 2011; Koishi et al., 2001; Zentner et al., 2007). These actuators are single material devices and mainly fabricated in one step. Operating pressures are mostly < 1 bar. Some prototypes are shown in Figure 3.4(d)-(e).

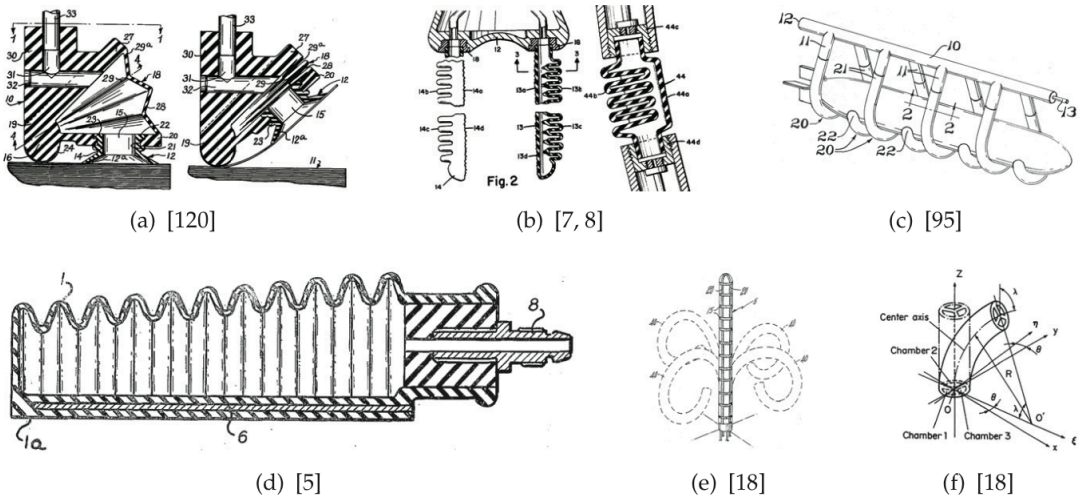

(a) [120] (b) [7, 8] (c) [95]

(d) [5] (e) [18] (f) [18]

Figure 3.3. Bending Actuators (Gaiser et al., 2012)

Another type is that of multi-chamber tubes exhibiting as many bending degrees of freedom as the lumen hoses they are made of, having axial and radial stiffness constrained by stiff reinforcement.

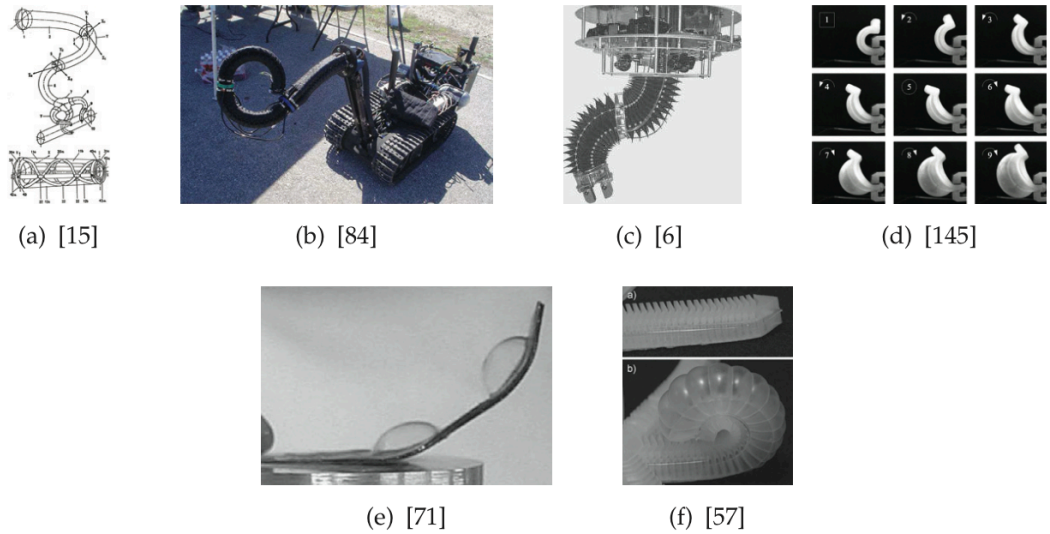

(a) [15] (b) [84] (c) [6] (d) [145]

(e) [71] (f) [57]

Figure 3.4. Trunk-Like Bending Actuators and Monolithic Bending Actuators (Gaiser et al., 2012)

3.1.2.3. Contraction actuators

Very promising technology since many decades, these actuators produce a tensile

force when pressure is applied. Both consist of an elastomeric membrane wrapped with elastic fibers. They can be divided into two main groups: The first group includes actuators that generate a tensile force due to “Anisotropic Membrane Stiffness”. (Daerden & Lefeber, 2000) described some of those actuators in their review article. These actuators increase in surface area when pressurized. The axial contraction is coupled to a radial expansion in which some of the energy is used for membrane deformation. Generally Joseph L. McKibben is said to be the inventor of the most popular design, often referred to as “McKibben Muscle”. However, earlier patents describe the same design. In 1929 (Dimitri Sensaud de Lavaud, 1929) introduced a fluidic muscle as shown in Figure 3.5(a). This early work was later followed up by the patents of (Morin, 1953) and (Woods, 1957), where the design and characteristics of the fluidic muscle were described in detail. The actuators consist of a highly elastic inner membrane that is covered with a helically wound fiber reinforcement like a braided fiber hose (Figure 3.5(b)). When pressurized the fiber angles change until the critical fiber angle of $\vartheta = 54,4^{\circ}$ is reached (Figure 3.5(c)) (Woods, 1957).

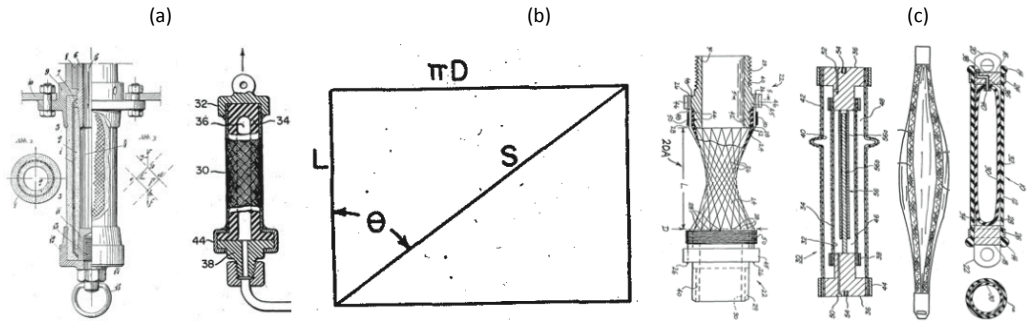

(a) (de Lavaud, 1929) (b) (Woods, 1957) (c) geometric correlation (d) (Sigmon, 1976) (e) (Negishi, 1991) (f) (g) between fiber angle ϑ and (Lewis,1974; Monroe,1994) muscle diameter *D*

Figure 3.5. Different Fluidic Muscles (Gaiser et al., 2012)

In (Paynter, 1988b) describes a variation of this type of fluidic actuator. The “hyperboloid muscle” is equivalent to a prestretched fluidic muscle, which extends the range of motion (figure 3(d)). Other set-ups are discussed in (Paynter, 1974; Paynter, 1988a).

Commercially available fluidic actuators were introduced by Bridgestone Corporation, Japan, FESTO AG&Co. KG, Germany, and Shadow Robot Company, UK. Bridgestone introduced a single-acting (Takagi, 1986) and a antagonistic (Negishi, 1991) actuator design (Figure 3.5(e)) but soon stopped their activities in the field. With operating pressures up to 2 *bar* and a fatigue life of 67, 000 load cycles these actuators weren’t really competitive.

Nowadays FESTO offers the biggest portfolio of fluidic muscles. Operating pressures are 0 − 8 *bar* in connection with a fatigue life of more than 10, 000 load cycles depending on the load case. (Lewis, 1974) and (Monroe, 1994) proposed a design with only axially fiber reinforcements. Thus actuation is connected with a radial stretch of the pure rubber sections between the axial fiber strands (Figure 3.5(f),(g)).

The second group of “Contraction” actuators generates the force due to **“**Vectored Structural Degrees of Freedom”. These actuator designs try to raise efficiency and to minimize the hysteresis compared to the first group of actuators. Ideally there is no strain of the membrane and almost no internal friction. When pressurized these actuators increase in volume while maintaining the same surface area. (Yarlott, 1972) proposed a folded structure that unfolds when pressurized and thus contracts (Figure 3.6(a))

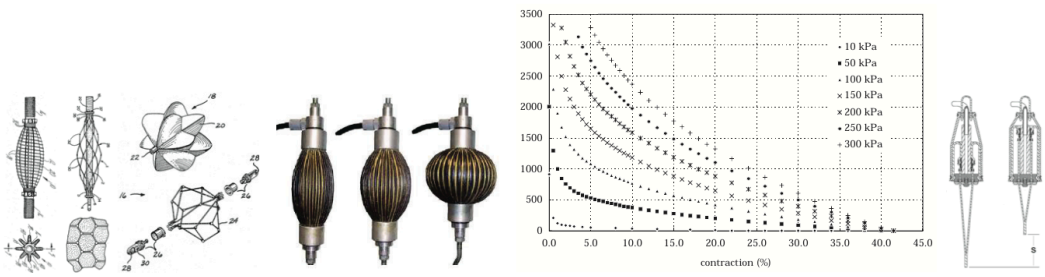

(a) [143] (b) [73] (c) [58] (d) [19] (e) [21] (f) [25]

Figure 3.6. Some FFAs based on "Vectored Structural Degrees of Freedom" (Gaiser et al., 2012)

3.2. Our balloon actuators

We are using and testing some commercial sphygmomanometer cuffs that make very efficient and promising toroidal balloon actuators. They are actually very interesting because of their inextensibility and axial symmetrical shape, i.e. both mechanical and geometrical properties.

We'll give a look to the cyclic inflating-deflating behavior as a first thing, and we'll try to state some law for the pressure as a function of the volume, to be used into the constitutive equations.

3.3. Actuators characterization

3.3.1. The actuator cyclic behavior

A sample of the acquired circuit pressure values is shown in Figure 3.7.

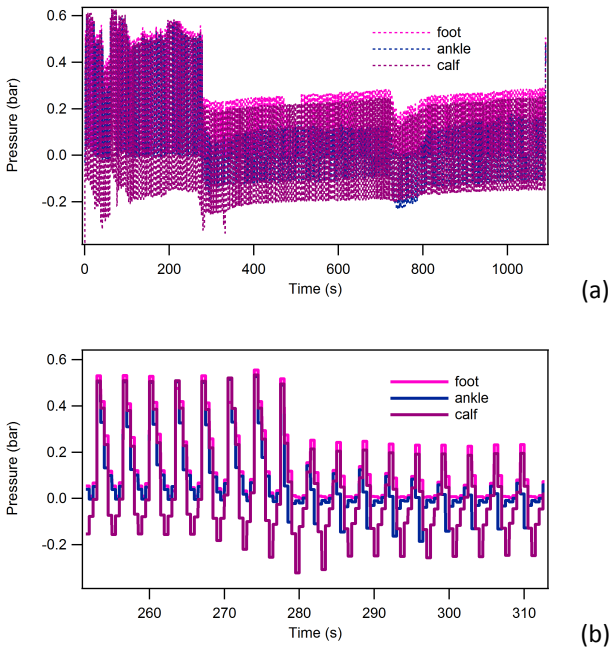

Figure 3.7. Air pressure vs. time just upstream of each cuff bladder: (a) global trend and (b) detail: pressure oscillations are almost synchronous.

The shown trend highlights some circuit features: first, ejector efficiency, which during deflation brings about a negative relative pressure mostly visible in the calf bladder curve, is stressed with increasing operating pressure, finally overcoming the inflating action and resulting in a minor average effective value; second, the three bladder pressure peak values appear to be in phase even though the solenoid valve on-off law shown in Fig. 3.7 gives out-of-phase commands to them. This phase coupling can be explained by the role of the common branch for air ejecting as well as with the very slow circuit dynamics due to the large air volumes; third, a much less steep slope of pressure rate at valves opening was achieved thanks to the unidirectional flow regulators, resulting in a ramp instead of a step impulse; it is to be noted that their check valve prevents air from flowing back in the inlet pipe.

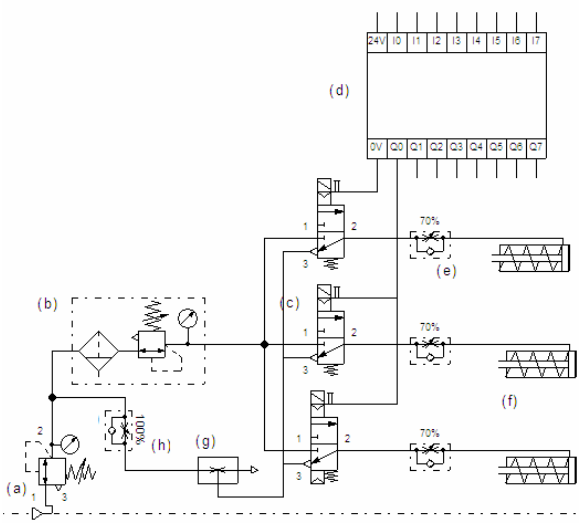

Figure 3.8. The pneumatic circuit.

3.3.2. Some engineering hypotheses

Power consumption of the system, being negligible the piezometric and dynamic energy losses along the circuit piping, is mainly P_e to ascribe to the ejectors' action and to a lesser extent P_i due to bladder inflation. Deformation energy, spent for the actuator to perform its action on patient's leg, is not accounted for here.

- P_e is the work done by the ejectors, whose flow rate at the feeding pressure of 2 *bar* is 30 *l*/min: it is about 250 *W*.
- P_i is the pressure power needed for inflating the 6 actuators in a T=3.5 *s* time period, assuming volume and pressure change in time as shown in Fig. 3.8 (a), (b) so that *p*-*V* cycle shape is approximately as depicted in Fig. 3.8 (c): bladder volume increases at constant zero relative pressure (isobaric compression), faster than decreasing when deflating, then is kept constant by the rigid cuff (isovolumic compression), then slowly decreases; the work done

on the system can thus be given by the rectangular area below the graph; it is one order of magnitude smaller than P_e .

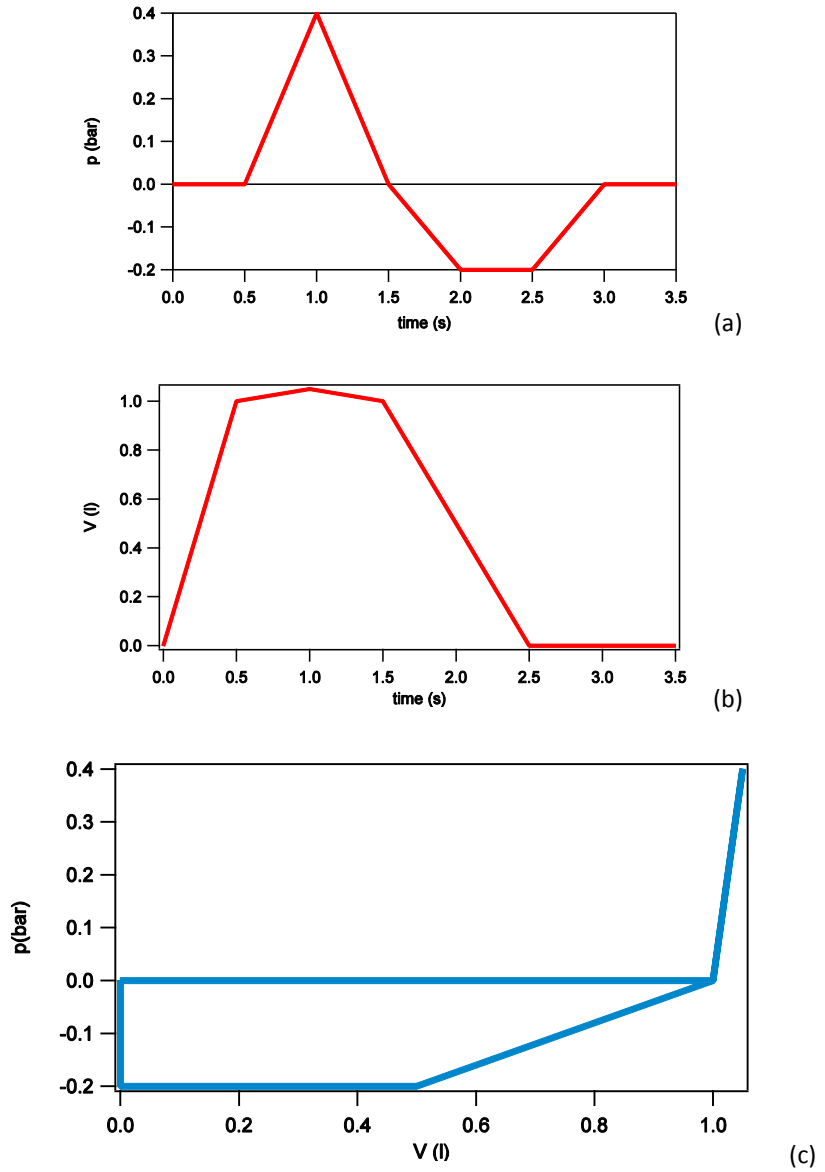

Figure 3.9 (a) bladder pressure is initially at atmospheric level while inflating, rapidly increases as maximum volume is reached, i.e. when the actuating action is exerted, then reduces to a negative relative value to finally become zero; (b) bladder volume goes from zero to its maximum capacity, then while the cuff slightly stretches due to internal pressure it performs the leg massage, and goes back to zero when air is sucked out by the ejectors; (c) the corresponding pressure-volume graph, where expansion at atmospheric pressure is followed by a sudden rise of internal pressure and eventually by the outflow in vacuum conditions.

We can see that the system requires very low power.

3.3.3. P-V behavior: experimental data

We needed an experimental setup to state a pressure-volume relationship for our bladder actuators. Instead of measuring the contact force we applied a hydrostatic load all around the actuator surface, as shown in Figures 3.10 and 3.11. A tank, suspended to a load cell, was progressively filled in with the water coming from a larger tank containing an inflated-deflated actuator: two large enough pipes --to avoid internal flow resistance leading to a pressure drop— were connecting the two tanks. The calibration curve of the load cell, i.e. its output voltage as a function of the water volume (or weight, given the density) is shown in Figure 3.11.

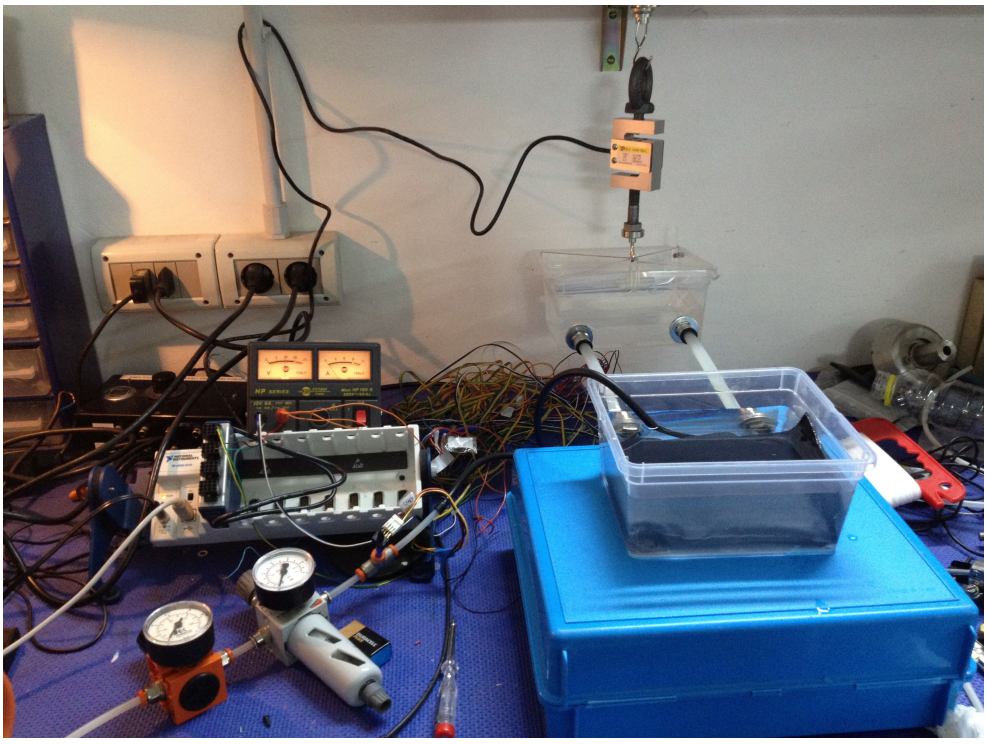

Figure 3.10 The progressively inflating bladder will slowly push the surrounding water into the suspended small tank (front view).

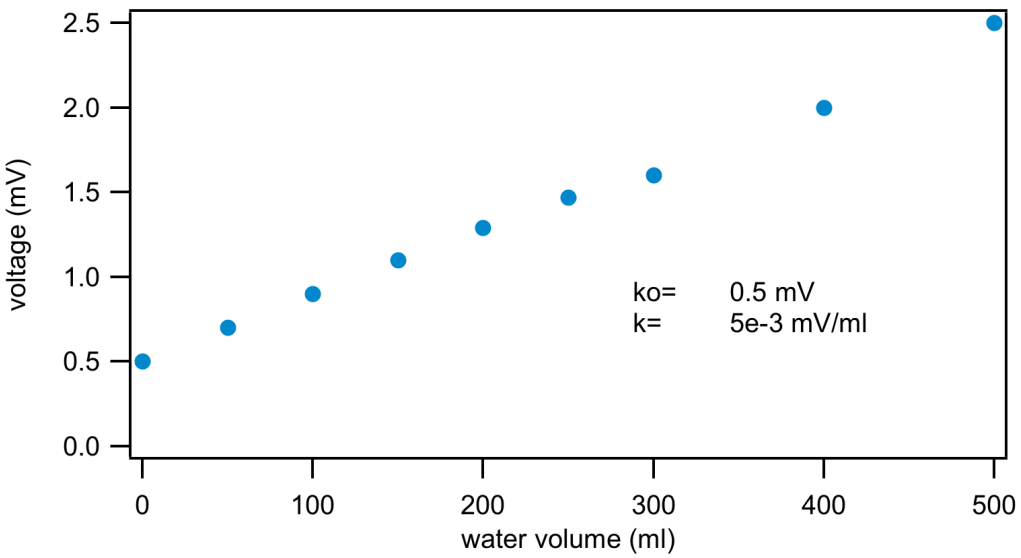

Figure 3.11 The load cell calibration curve

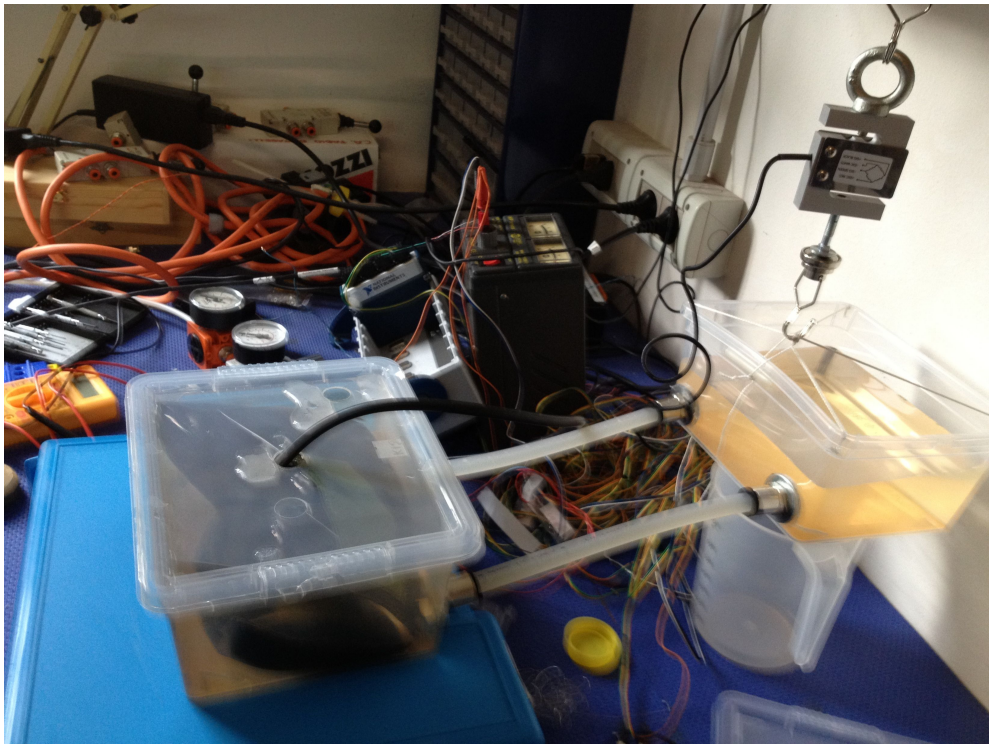

Figure 3.12 As the actuator gets inflated, a top lid prevents it from floating; meanwhile, the water flows into the gauged small tank (side view).

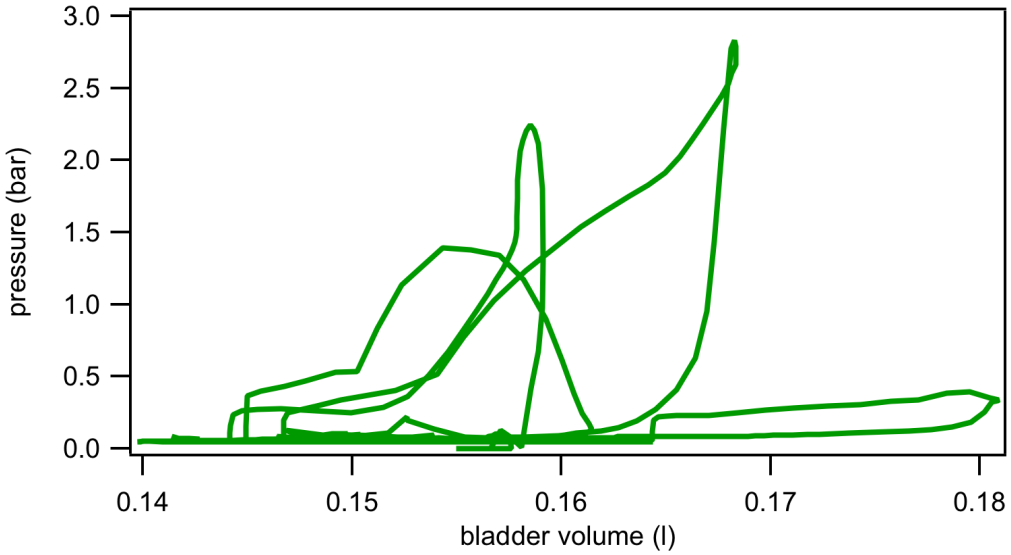

Figure 3.13 The pressure inside the actuator as a function of its volume, as obtained with the setup in Figure 3.8, 3.9.

The experimental and computed curves shapes are in fact very similar, i.e. the assumptions made in 3.3.2 suit very well to the mechanical behavior of our system. Below in Fig. 3.14 experimental and computed trends for pressure and volume of an inflated balloon actuator are compared.

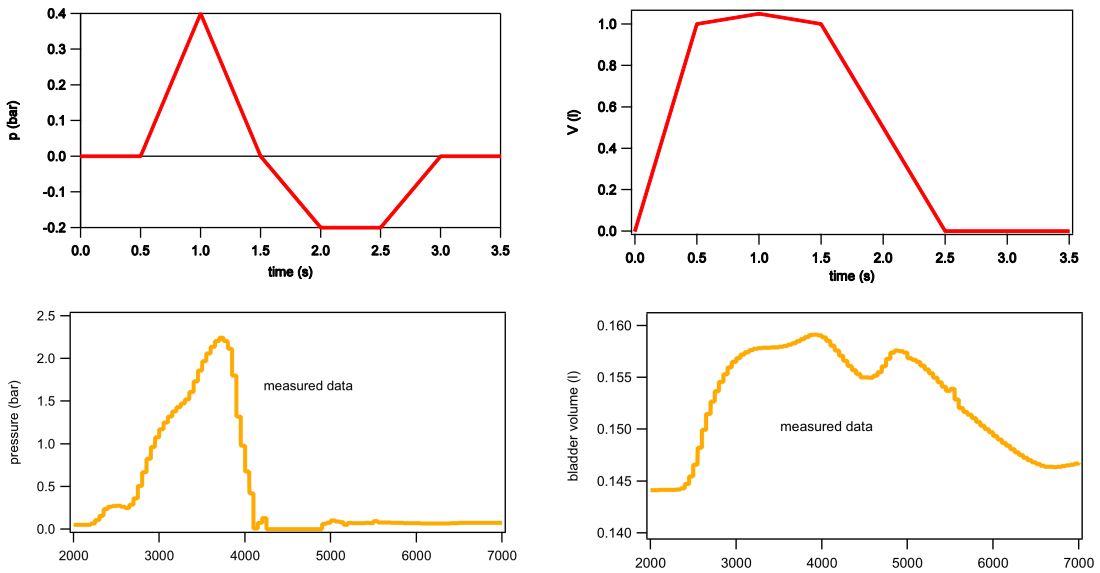

Figure 3.14 The computed (red) and measured (yellow) curves for both pressure (a) and volume (b) for our actuators are quite similar in shape and trend.

They are almost perfectly matching except for the values, being slightly different the geometry.

The whole cycle shows almost the same shape as well as in in Figure 3.12 below.

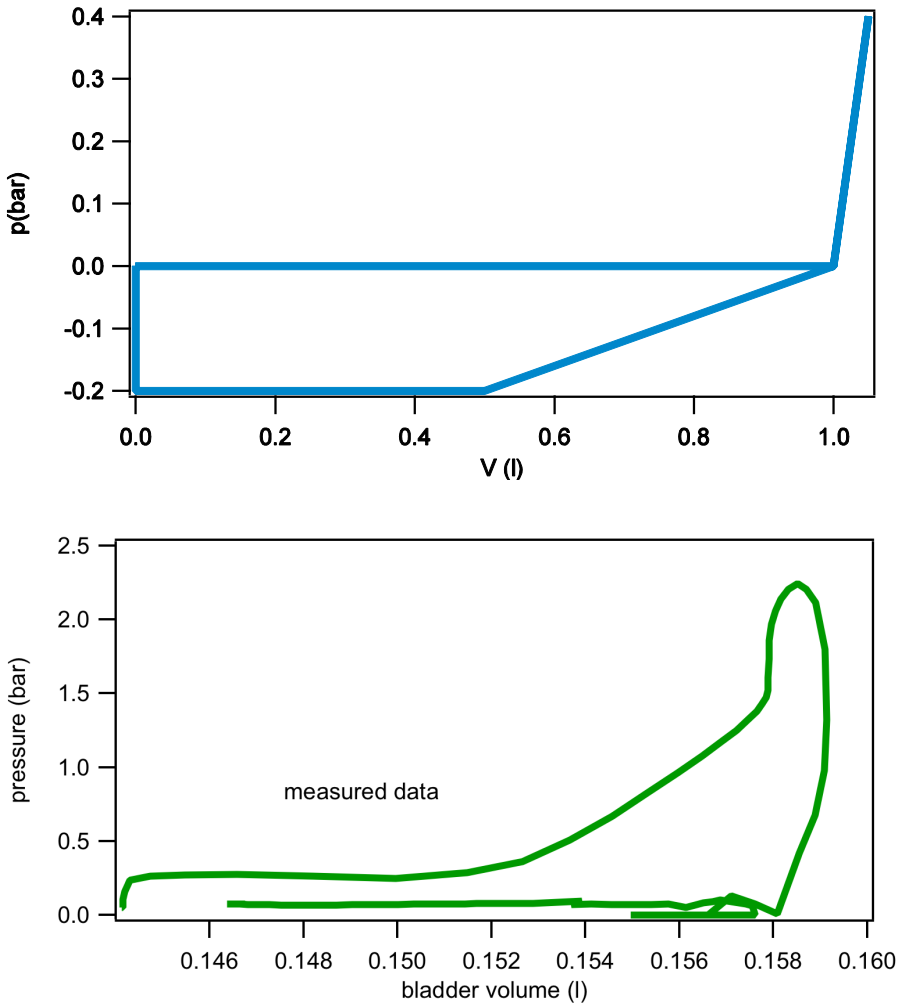

Figure 3.15 The computed (blue) and measured (green) curves of a pressure loading-unloading cycle for a bladder cuff actuator are quite similar in shape and trend.

3.3.4. P-V behavior: conclusions

We can state that our engineering hypotheses in 3.3.2 were good, as the results are almost perfectly overlapping with the measured curves. This experimental, empirical p-V law can thus be introduced into the constitutive equations.

4. Preliminary experimental

A first calf-plantar sequential pneumatic compression device, consisting of three sensorized and PLC-controlled chambers has been first designed and implemented. It performed a massage on the calf surface and on the foot sole at a given controlled pressure level and frequency and, in addition, carried out the ankle passive movement.

Preliminary tests were performed on patients, using a commercial apparatus normally devoted to lymphatic drainage massage. In testing the mechatronic apparatus under real working conditions three air pressure transducers were used to feedback control the actuation system and the pressure trends in the actuator chambers during massage are here reported

4.1. Tests on patients under incremental effort

A preliminary study was performed to verify the effectiveness of compression on patients' legs in restoring circulation efficiency, identifying the minimum threshold of pressure values to be applied to the lower limbs and the sizes of the muscle areas to be involved in the actuators action. After this study the force and pulse trends as a function of time to be applied on different areas of the limbs where the actuators were to be assembled were identified.

To this end a commercial device, normally devoted to lymphatic drainage massage, was used. This device, shown in Figure 4.1, consists of a sheath/boot with four sleeve sectors assembled in sequence from foot to thigh, each independently supplied with compressed air, to perform a sequential inflation. The sectors are indicated in Figure 4.2 as Ch#n.

In this way, peristaltic compression, having a rostral-caudate trend corresponding to a pressure wave from foot to thigh, is implemented. The pressure level is about 50 mm Hg; this level is higher than the venous pressure in the lower limbs, which typically varies in a range from 10 to 20 mm Hg, as the air pressure inside the pressurized chambers can be significantly higher than that transmitted to the veins, here not detected. The time period of pressure increment in each chamber is about 15-20 s, so the peristaltic cycle has a period of about 1 min.

Figure 4.1: The peristaltic device on a leg of a paraplegic patient.

The preliminary tests were performed on eleven patients.

The volume variation of the cardiac chambers was detected by the bi-dimensional echocardiography shown in Figure 4.3. Similarly, the volume oscillation of the

cardiac chambers was detected in the same patient, without the peristaltic device, comparing the test results in the two different conditions.

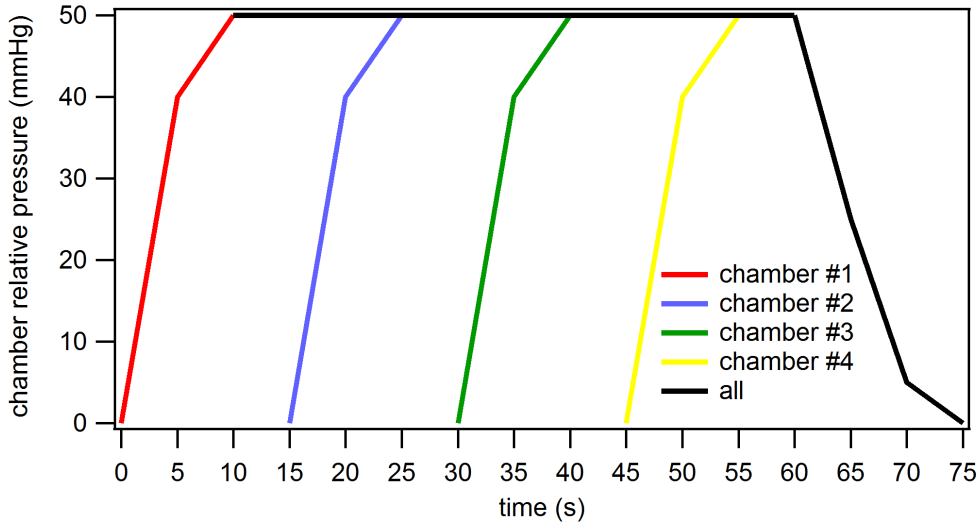

Figure 4.2: The pressure trend in time air-supplying the four chambers of the boot.

The volume oscillations of cardiac chambers are higher when the peristaltic device is applied to the legs of the patient during the incremental effort test compared to incremental effort testing without it.

Each boot consists of four chambers; they are air-supplied in a peristaltic way, as represented in the graph in Figure 4.2 The chambers, from the lower one around the foot to the upper one on the thigh, are inflated in turn after 15 s each. The chambers are then deflated altogether and after 3 s the cycle starts again. Thus the device is cycle-powered approximately every 75 s. The maximum pressure value in the chambers is 50 mmHg.

A paraplegic patient is then given an incremental effort test by means of an arm-ergometer, as shown in Figure 4.3.

bi-dimensional echocardiography

Figure 4.3: A patient having a bi-dimensional echocardiogram during an incremental effort test. He is using an arm ergometer and is wearing a peristaltic device.

During this test peristaltic devices were applied to the patient's legs. The arm ergometer load, applied by an electromagnetic brake, is imposed at 30% of the maximal effort, which was detected for each patient from a previous test: the ergometer load changes for each patient as a function (30%) of their respective maximum tolerable load. The hemodynamic parameters are shown in Table 4.1, where the mean values for the eleven patients are reported. In particular, the effectiveness of applying pressure on the legs to recover circulation efficiency is shown by the increment of the end diastolic volume and the cardiac output (grayed fields in Table 4.1. This confirms that the pressure action on the legs is capable of supporting the heart action. Both parameters are a measure of the heart activity: cardiac output is the blood flow pumped by the heart, and the higher the flow, the more the ventricular volume increases. The first two parameters are also related, as

cardiac output is a function of heart rate and stroke volume, being the heart rate the number of heart beats per minute. It is to be noted how heart rate decreases as pressure is applied to the legs, which is a symptom of heart relief.

In Table 4.1 the measured parameters are shown, both with and without the ergometer load and combining the results obtained using the boot or not. The values corresponding to the condition “without the ergometer load” and “without pressure on leg” as well, i.e. those on the first column are to be taken as reference values at rest.

Table 4.1: Four hemodynamic parameters showing (highlighted values in particular) how the patients cardiac function improves when having pressure applied on their legs.

	without the ergometer load		*imposing the ergometer load*	
Hemodynamic parameter	**without pressure on leg**	**with pressure on leg**	**without pressure on leg**	**with pressure on leg**
HR(bpm) heart rate	**88.3**	**85.8**	**114.2**	**110.3**
SV(ml) stroke volume	**65.1**	**63.7**	**72.1**	**85.7**
CO (ml/min) cardiac output	**5752.3**	**5478.6**	**8284.6**	**9457.8**
EDV(ml) end diastolic volume	**141.5**	**157.9**	**180.4**	**226.5**

4.2. The blood pressure recovery device

The development and use of robotic systems for rehabilitation is a widely investigated topic and many such devices are commercially available to meet the needs of different therapies.

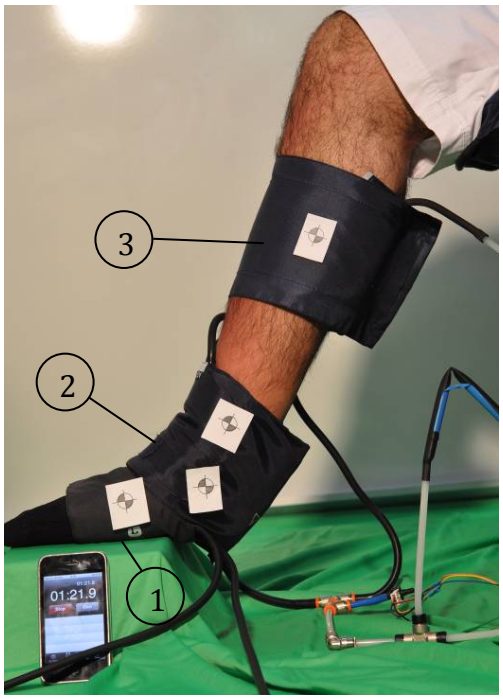

Figure 4.4: The blood pressure recovery device.

The purpose of this research is to produce a device that will combine two different functions: to produce a distributed pressure action and passively move limbs in a controlled way. The use of external aid devices (static, manually operated or motorized) exerting the pressure action with the aim of improving the return of blood and lymph from the circulatory periphery to central systems has been adopted for a long time.

In Figure 4.4 the device put on by a patient is represented. Three balloon actuators can be seen: the first one acts (1) on the foot sole to recover the pressure coming from the soil during the gait; the second one (2) performs ankle rotation in a sagittal plane; the third one (3) radially compresses the calf and simulates a pumping action from the gastrocnemius muscle on the leg veins to simulate walking.

In Figure 4.5 the scheme of one of the circuits supplying each of the three balloon actuators is shown. On the right hand side a photograph of the circuit is shown.

The compressed air comes from the supply (1) and is processed within the FRL (Filter, Pressure Reducer, Lubricator) group. The compressed air flow is then controlled by the electrovalve (3) and drives the balloon actuator (4), here represented as a single-effect cylinder. The regulator valves (5) allow the speed control of the balloon actuation. The pressure switch (6) gives a signal for commutation of the electrovalve (3) to avoid reaching too high a pressure level in the actuator (4) with danger to the patient. To have an easier actuator exhausting phase during the actuation cycle the environment is depressurized downstream of the valve by the vacuum generator ejector (7), supplied through the flow regulator (8). In the photograph the preliminary circuit used for driving one balloon actuator can be seen. The system is closed-loop controlled by a PLC basic unit, namely a SIEMENS LOGO 24 RC, provided with two digital I/O modules of the DM8 24 model and DM16 24 model.

A NI cDAQ-9172 CompactDAQ chassis (Figure 4.6), equipped with a NI9219 4-Channel, 24-Bit, analog input module, was used to read pressure data coming from three 0-15 psi Honeywell 24PC Series transducers.

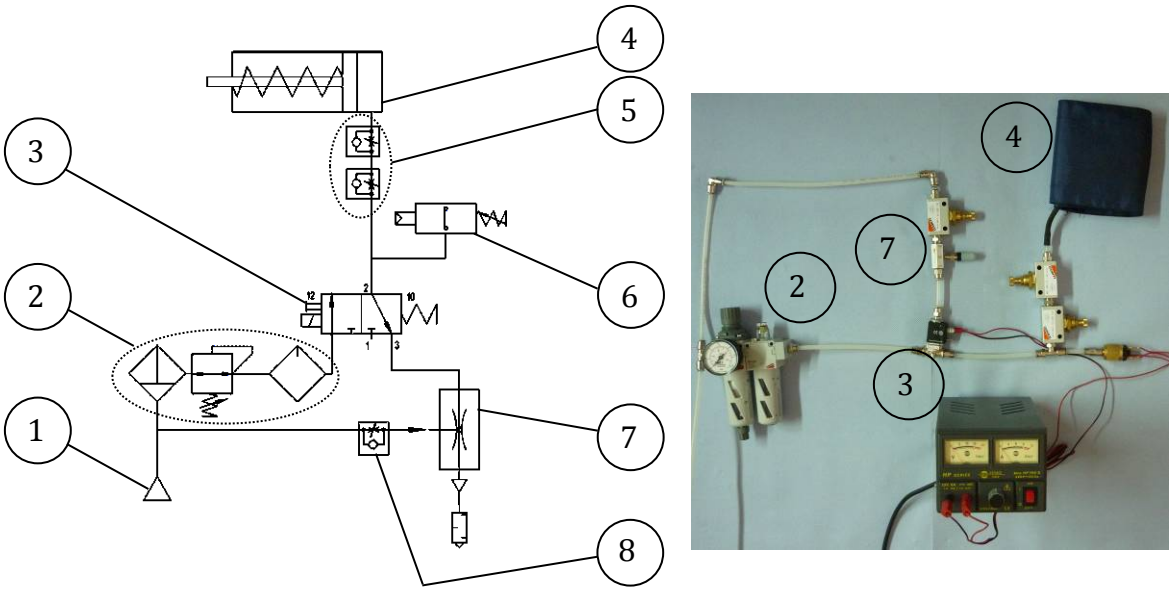

Figure 4.5: One of the three circuits supplying the balloon actuators of the blood pressure recovery device.

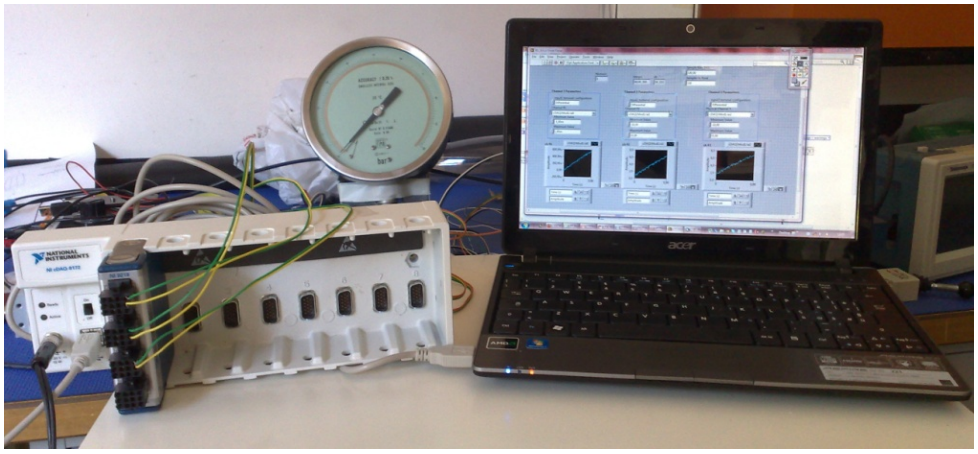

Figure 4.6: The pressure acquisition system.

The pressure trend of the three balloon actuators, each detected by a pressure transducer assembled on the supply circuit near the actuator supply port, is referred to in Figure 4.7.

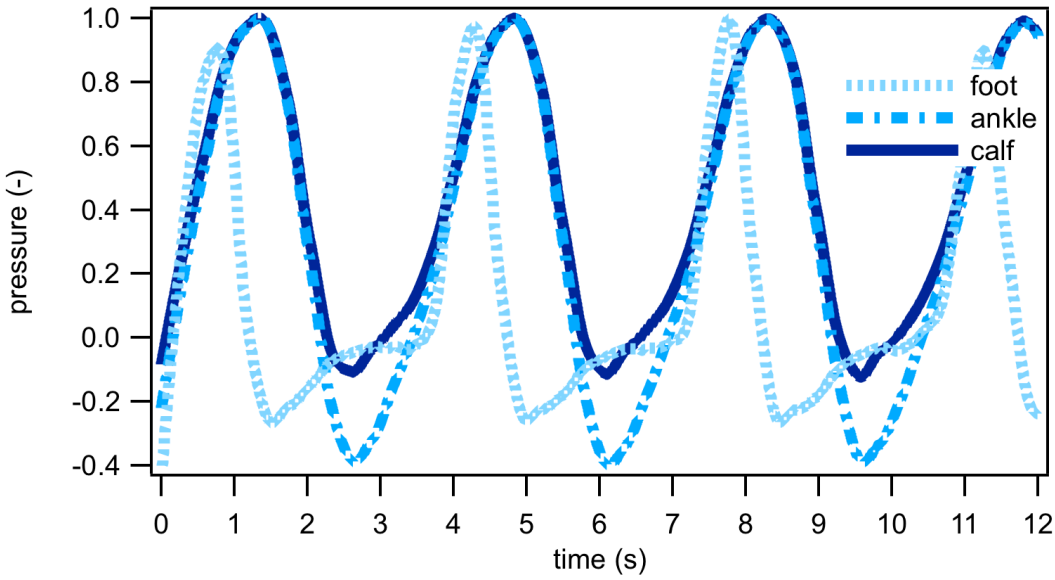

Figure 4.7: Pressure trends in the three balloon actuators.

The dotted curve plots the pressure trend vs. time in the actuator acting on the foot sole; the dot-dashed and the solid ones represent, in turn, the pressure in the actuator performing the ankle rotation and in the actuator producing radial compression of the calf. Frequency represented here is 0.25 Hz, as for a healthy person walking slowly. Pressure peaks on different leg segments have been chosen so as not to overlap since that appears to bring better results, but a more systematic approach can be taken in the future to give some numerical values.

Figure 4.8 shows a histogram of relative changes of blood flow taken on a sample of patients who were classified based on their Body Mass Index (BMI), which is the percent rate between body fat and total weight. Flow was measured both on the vena cava at the abdomen level and on the ascending aorta just downstream of the

aortic valve. Both flow changes decrease as BMI increases, showing how the presence of body fat could vanish the efficacy of the treatment.

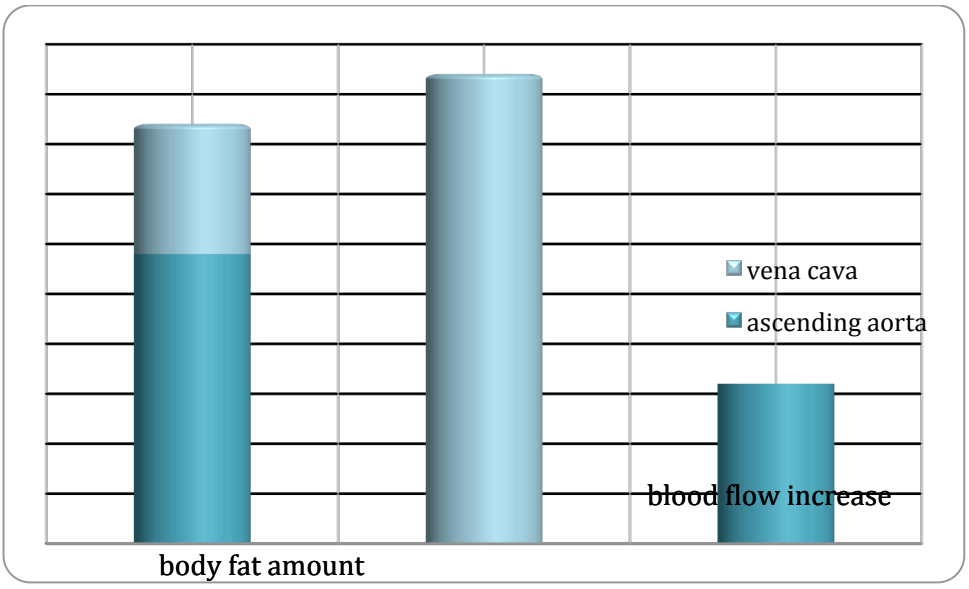

Figure 4.8: Blood flow boosted by the pneumatic actuator, displayed as a function of BMI.

4.3. Preliminary results

The effectiveness of mechanical action on leg muscles of paraplegic patients in restoring end diastolic filling pressure of ventricles was assessed using a commercial device: cardiac output compensation and aerobic capacity improvement was echocardiographically monitored on these patients during incremental effort tests.

To this purpose the device was set up to apply to the patient's leg a pulsing pressure reaching levels and having a trend suitable for restoring circulation efficiency. The device was then tested and the pressure trends in the actuator chambers are reported in this paper. Massage was performed at a given frequency approximating the human pace. In future works the device will be tested on patients following authorization of formal clinical trials.

5 Contact experimental and modeling

In order to feedback the contact pressure, a proper and widespread sensorization has to be set up as well.

This section presents first the state-of the-art of robotic tactile sensing technologies and analyzes the present state of research in the area tactile sensing. Various tactile sensing technologies have been discussed under three categories: (1) transduction methods; (2) structures that generate a signal on touch; and (3) new materials that intrinsically convert mechanical stimulus on touch into usable signals. The tactile sensing technologies are explained along with their merits and demerits. The working principles of various methods have been explained and selected implementations are presented.

Afterwards, the sensors adopted in our research are described and examined, and details are given about static and dynamic characterization.

Finally, results of a comparison between the measured data and a FE model are given.

5.1. Contact sensors

Although in the present work we are interested in contact pressure measuring, a more widespread review of tactile sensing technologies in robotics will be given.

Tactile sensing has been a component of robotics for roughly as long as artificial vision and auditory sense modalities. Tactile sensing began to develop in the 1970s—albeit at a slower pace, when compared with the development of other sense modalities. Early surveys on the state of tactile sensing show a wide diversity in the types of sensing device that were developed in the 1980s (Harmon, 1982; Nicholls, &

Lee, 1989). Early works on tactile sensing focused on the creation of sensor devices using new transduction techniques and a large number of experimental devices and prototypes were built and reported in the literature. Particular attention was given to the development of tactile sensing arrays for the object recognition (Hillis, 1982). The creation of multifingered robotic hands, in late 1980s, increased the interest in tactile sensing for robotic manipulation and thus started appearing works utilizing tactile sensing in real-time control of manipulation (Dario, & de Rossi, 1985; Howe, & Kutkoski, 1993; Jacobsen, McCammon, & Biggers, 1988; Howe, 1994). The new applications demanded features such as mechanical flexibility and conformability and accordingly new designs and materials for tactile sensing received attention.

Table 5.1 The classification of various Tactile Sensing technologies (Dahiya & Valle, 2013)

Transduction Medium/Method	**Material**	**Sensor Structure**
Resistive	Composites Carbon Nano	Microelectromechanical systems
Capacitive Optical Magnetic	Tubes (CNT) Conductive	(MEMS)
Ultrasonic Piezoelectric	Polymers Force Sensing	Plastic MEMS POSFET Extended
Electrorheological	Resistors	Gate Transistors
Magnetorheological	Pressure Sensitive Ink	Organic Field Effect Transistors
Electrochemical	Conductive Gels	(OFET) Flexible Printed Circuit
	Conductive Fibers and	Boards (PCB) Mechanical
	Yarns	Switches
	Piezo-/pyroelectric	
	Materials	
	Photoelastic Materials	

While the development of tactile sensors for robotic fingertips and hands continued, the application areas such as motion planning in unstructured environment brought whole body sensing to the fore. As a result, many sensitive skin design projects were

undertaken in the late 1980s and 1990s (Cheung, & Lumelski, 1989; Cheung, & Lumelski, 1992; Um, Stankovic, Giles, Hammond, & Lumelsky, 1998).

The application domain of robotics has been continuously increasing and the new generation of robots nowadays includes social robots, rehabilitation and assistive robots, biorobots, medical robots and humanoids. Compared to the human controlled industrial robots, operating in “No-Humans” working zones, these new generation robots are characterized by close interaction with environment (including humans) and autonomous learning. In addition to the standard manipulation and exploration tasks, the new generation robots are also expected to interact safely. Tactile sensors distribution over the entire body is indispensable to build service robots that can co-exist with humans for support and enhancement of human life. The full-body tactile sensor could generate more tactile information than in the case where only joint force and moment are measured. As a result, nowadays there is an increased interest in developing large area or whole body tactile sensing structures that allow a robot to safely carry out a task while maintaining physical contact (Mukai, Onishi, Odashima, Hirano, & Luo , 2008; Dahiya, Metta, Valle, & Sandini, 2008).

Analyzing the present state of research in the area tactile sensing, three strategies emerge for the development of tactile sensing units in robots (Dahiya, Metta, Cannata, & Valle, 2011): (1) developing sensors based on various methods of transduction; (2) development of structures that generate a signal on touch; and (3) the use of new materials that intrinsically convert mechanical stimulus on touch into usable signals. This classification of tactile sensing technologies is given in Table 5.1

and explained in this chapter along with their merits and demerits. The working principles of various methods have been explained and selected implementations are presented. Quite often the tactile sensing schemes belong to one or more aforementioned strategies, which is also reflected by some of the implementation presented in this chapter. The overview presented here also takes into consideration the reviews on the state of research in tactile sensing reported in literature from time to time.

5.1.1. Resistive sensors

Resistive tactile sensors utilize the change in resistance of the sensing material for detection and measurement of contact forces. The degree to which resistance of any sensing material changes depends on: (a) the contact location (e.g. potentiometer type); (b) the contact force or contact pressure (e.g. piezoresistance, and elastoresistance). Accordingly, the resistive tactile sensors can be grouped in two categories.

Resistive sensors based on the first type, are either made of two-dimensional grid of sensing elements or composed of two flexible sheets coated with a resistive material (with finite resistivity, typically on the order of 100 Ω/sq.) placed on top of each other and separated by air, microspheres, insulating fabric etc., as shown in Figure 5.1 (a). Accordingly, former arrangement is termed as discrete resistive touch sensing and latter as analog resistive touch sensing. The scheme of analog resistive touch sensing, in typical 4-wire configuration, is shown in Figure 5.1(a)–(f). During operation, a uniform, unidirectional voltage gradient is applied to the first sheet, as shown in Figure 5.1(b). When the two sheets are pressed together the second sheet

serves like the slider in a linear potentiometer and measures the voltage as distance along the first sheet, thus providing the X coordinate. When this contact coordinate has been acquired, the uniform voltage gradient is applied to the second sheet to ascertain the Y coordinate. The complete method of ascertaining contact location is given in Figure 5.1(b)–(f). As voltage V_x or V_y is applied over the X or Y plane and the voltage V_{xout} or V_{yout} measured at any of the analog high impedance (Hi-Z) terminals is approximately given by:

$$V_{xout} = \frac{Rx2}{Rx1 + Rx2} Vx$$

$$V_{yout} = \frac{Ry2}{Ry1 + Ry2} Vx$$

proportional to the X or Y coordinate of contact point. Both the sampling of the two voltages and the subsequent calculations are very simple and the operation occurs instantaneously, registering the exact touch location as contact is made.

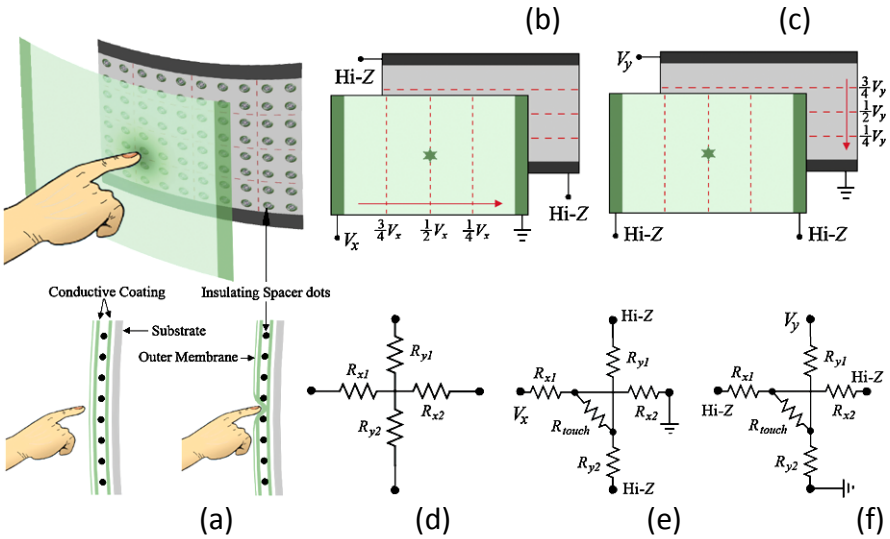

Figure 5.1 (**a**) The scheme of analog resistive touch sensing; (**b**) X coordinate measurement: Voltage gradient applied across the front sheet and voltage measured at any of the Hi-*Z* terminals of back sheet; (**c**) Y coordinate measurement: Voltage gradient applied across the back sheet and voltage measured at any of the Hi-*Z* terminals of front sheet; (**d**) Circuit configuration under untouched condition; (**e**) Circuit configuration for measuring X coordinate; (**f**) Circuit configuration for measuring Y coordinate (Dahiya & Valle, 2013)

In addition to the contact location, the touch pressure (or Z axis measurement) can also be measured by relating pressure to the resistance (Svyatoslav, 2004). Analog resistive touch sensing technology typically results in high resolution (4096 × 4096 DPI or higher) and high response speed (10 msec or higher), thus providing fast and accurate touch control. However, the approach results in detection of only one contact location. While suitable for the touch screens of appliances such as personal digital assistants (PDAs), and as generic pointing devices for instruments, the analog resistive sensing technology has limited utility for robotic applications where simultaneous multiple contacts are often observed. With some design modifications the multiple contacts can be measured and hence analog resistive sensing technology can be adapted for robotic applications. Among others, the hybrid resistive tactile sensing (Zhang, & So, 2002) is one such technique that allows measurement of multiple contact points. Hybrid resistive sensing is a combination of the analog resistive and the array touch sensing technologies. It also involves two sheets of

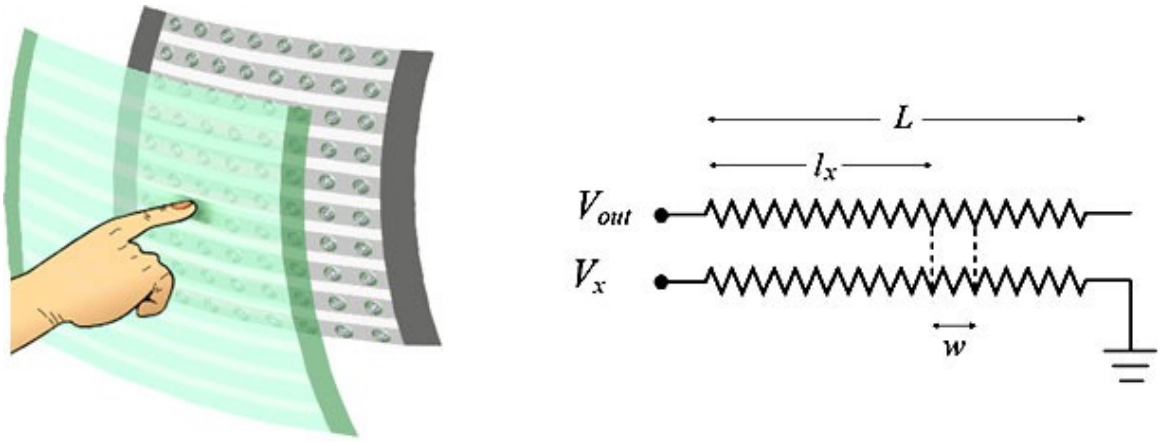

Figure 5.2 The scheme and equivalent circuit diagram of hybrid analog resistive touch sensing (Dahiya & Valle, 2013)

conductive materials, one on top of the other. However, one or both sheets are divided into multiple strips aligned along their lengths. One such scheme, with both sheets divided into multiple strips, is shown in Figure 5.2. In this way, the configuration looks like one-dimensional arrays of stripped analog resistive sensors described earlier and the contacts can be sensed along different strips separately. The sensor measurement, along a strip, depends on both the location and the length of con- tact along each strip. Following a simple circuit analysis, the output of the sensor equivalent shown in Figure 5.2 can be obtained as:

$$V_{out} = \frac{l_x + w/2}{L - w/2} V_{ref}$$

Where V_{ref} is the reference voltage applied across the sheet, w is the contact width, l_x is the contact distance from one of the ends as shown in Figure 5.2, and L is the length of the strip. Because the sensor is discretized in one direction, each scanning of the sensor produces a set of at least n measurements from which the contact shape is to be reconstructed. In comparison with the n^2 operations needed with a conventional matrix sensor configuration, the number of measurements, and hence the scanning time, is much lower in case of hybrid resistive tactile sensing. The number of measurements in each scanning will, however, become $2n$ if two measurements are made for each contact point—as in analog resistive touch sensing described earlier. Similarly, the scheme discussed above requires a minimum of $n + 2$ connectors/wires (one for the V_{ref} , one for common ground, and n for the sensing the individual strips) against 2n (without MUX) needed with a conventional matrix sensor configuration.

Piezoresistive touch sensors are made of materials whose resistance changes with force/pressure. Touch sensing system using this mode of transduction have been used in anthropomorphic hands (Weiss, & Worn, 2004). Piezoresistive tactile sensing is also popular among the MEMS based and silicon based tactile sensors (Beebe, Hsieh, Denton, &. Radwin , 1995; Wolffenbuttel, & L.Regtien, 1991; Kane, Cutkosky, & Kovacs, 2000). Some examples of piezoresistive sensors are given in Figure 5.3. These examples also include the sensors that are based on MEMS approach. The MEMS based tactile sensors are described later in the section on tactile sensing structures.

Recently, the piezoresistive tactile sensors have been realized using materials such as conductive rubber, conductive polymers, conductive gels, conductive fibers and yarns, force sensing resistors (FSR), and pressure sensitive ink etc. Sometimes, the changes in resistance of a conductive elastomer or foam are also termed as elastoresistance or elastoresistivity. However, for simplicity, the term piezoresistance is used here.

5.1.2. Capacitive sensors

The capacitive measurement methods have been used for a long time in many applications to measure physical values like distance, pressure, liquid level, acceleration, humidity, and material composition etc. The newer applications, widely using capacitive touch technology, include human–machine interfaces applications such as laptop track pads, computer displays, mobile phones and other portable devices. The capacitive measurement methods are also widely used in many MEMS based touch sensing arrays such as those for high resolution tactile imaging of

fingerprints. The technique has also been employed in robotics to detect contacts over large areas of a robot's body.

At the heart of any capacitive sensing system is a set of conductors that inter- act with electric fields. Typically, the capacitive sensors are the plate capacitors (Figure 5.4), consisting of two identical and parallel metal plates or electrodes of area A separated by a distance d with a flexible spacer (usually, silicone or air) of relative dielectric constant ε_r . The basic principle behind working of a capacitive sensor is detection of the change in capacitance when something or someone approaches or touches the sensor. The capacitance of a parallel-plate type capacitor (Figure 5.4) is given as:

$$C = 4\pi\, \varepsilon_r \varepsilon_0\, \frac{A}{d} + C_f$$

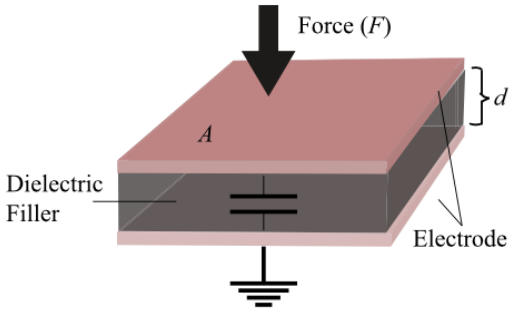

Figure 5.4 A parallel plate capacitor consisting of tow parallel plates of area A, separated by a flexible insulator of relative dielectric constant ε_r . The thickness of the dielectric film is d (Dahiya & Valle, 2013)

where ε_0 is the (electric) permittivity of a vacuum, and C_f is the contribution from edges of the electrode (which tend to store more charge than the rest of the

electrode). Typically, $A \gg d^2$ in all designs for tactile sensors, therefore, the C_f term is negligible. The distance between the electrodes is usually lower, as the inverse relation between capacitance and gap between electrodes is highly non-linear and the sensitivity drops significantly with larger gaps.

When a force is applied on the capacitive sensors, it changes the distance between the plates or the effective area—resulting in the changed capacitance. The normal force changes the distance between the plates while tangential force changes the effective area between the plates. The capacitive sensors are thus capable of detecting touch by sensing the applied normal or tangential forces; however, they are not efficient enough to distinguish these two types of forces. The change in capacitance is eventually converted into a change in voltage by using an appropriate circuit and a measure of the applied force is obtained. The capacitive sensors therefore convert the physical input signal to the output signal in two steps: firstly, by transducing a physical quantity into a change of electric capacitance; then, by measuring and converting the capacitive signal into an electric output signal.

5.1.3. Optical sensors

The optical mode of transduction (Figure 5.5) is another alternative for the tactile sensing in robotics. In simple terms, the optical sensing involves “injecting” light into a medium (generally, soft and deformable) and measuring the change in the amount or the pattern of light when force is applied. Depending on how the amount or pattern of light is detected, the tactile sensors based on optical mode of transduction can be grouped into two categories:

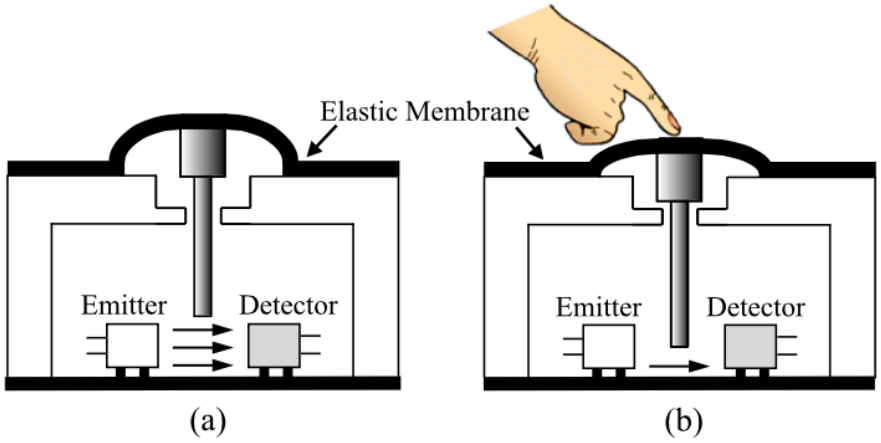

Figure 5.5 (**a**) The optical transducer before applying the force or before contact; (**b**) The opaque pin moves downward after contact and blocks the block path of light between *emitter* and *detector*, thereby reducing the intensity of light received by *detector* (Dahiya & Valle, 2013)

1. The *extrinsic* optical sensors, where the physical stimulus interacts with the light external to the primary light path.

2. The *intrinsic* optical sensors, where the optical phase, intensity, or polarization of transmitted light are modulated without interrupting the optical path.

Sometimes, optical fibers are directly used as the transducers in the design of tactile sensors. Therefore, this could also be considered as the third category of optical sensors.

5.1.4. Magnetism based sensors

The touch or tactile sensors based on magnetic transduction are developed using two approaches. Firstly, the sensors measuring the applied force led change in the magnetic flux using either the Hall effect or magnetoresistance. Second, the sensors measuring the change in the magnetic coupling or change in the inductance of a coil

as a result of applied force or pressure. A few tactile sensors using these approaches have been reported in literature (Nelson, Van Dover, Jin, Hackwood, & Beni, 1982).

5.1.5. Ultrasonic based sensors

The ultrasonic transduction for tactile sensing is one of the methods where mechanical transduction is decoupled from electrical transduction. A typical ultrasonic sensing arrangement, shown in Figure 5.6, involves a thin rubber covering that is deformed when an object presses into it. The amount of this deformation depends upon the magnitude of the force applied to the object and the stiffness of the rubber. Underneath this rubber covering are ultrasonic transmitters and receivers. The ultrasonic transmitters launch a small ultrasonic pulse of a few megahertz into the rubber pad. This pulse then propagates through the pad and is reflected from the ex- posed surface of the rubber. The reflected or echo pulse is received by the receiver, which is usually the same element that launched it. The round-trip travel or transit time is proportional to the thickness of the rubber pad overlying a particular tactile element. Therefore, by measuring the change in the round-trip travel or transit time (i.e. $t_1 - t_2$) of the pulse, it is possible to measure parameters like change in the thickness of the rubber pad (i.e. $d_1 - d_2$) and hence the applied force. The operation of the sensor can be expressed as:

$$d_1 - d_2 = \frac{1}{2} c\,(t_1 - t_2)$$

$$F = k(d_1 - d_2) = 1/2\, k(t_1 - t_2)$$

where F is the compressing force, c is the speed of propagation of the ultrasonic

wave in the rubber covering, and k is the rubber stiffness. Typically, the ultrasonic pulse transit times through the pad and back are on the order of few microseconds and changes in pad thickness of a few microns can therefore be detected. The strength of the echo pulse depends upon the acoustic properties of the rubber pad and the material contacting the pad.

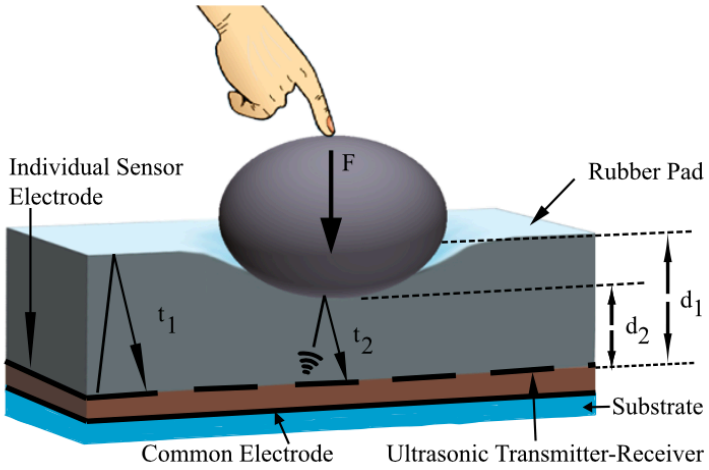

Figure 5.6 Working principle of an ultrasonic tactile sensor (Dahiya & Valle, 2013)

The resonant frequencies of the piezoelectric materials change when they come in contact with the objects having different acoustic impedances (Dahiya, Valle, Metta, & Lorenzelli, 2007; Dahiya, Valle, & Lorenzelli, 2009). The change in resonance frequency of the sensor, in accordance with the contact object's acoustic impedance, is also sometimes used to detect contact parameters. The change in resonance frequency has been used for detecting hardness and/or softness of objects (Omata, Murayama, & Constantinou, 2004) and to detect force/pressure (Krishna, & Rajanna, 2004). Simple and elastic tactile sensors utilizing acoustic resonance frequency to detect contact parameters like principal stress, friction, and

slip are also described in (Shinoda, Matsumoto, & Ando, 1997; Nakamura, & Shinoda, 1997). The ultrasonic-based tactile sensors have fast dynamic response and good force resolution. However, many such sensors use materials like lead zirconate titanate (PZT), which are difficult to process in miniaturized circuits.

5.1.6. Piezoelectric sensors

The piezoelectric transducers generate charge/voltage proportional to the applied force/pressure. They are also able to generate force due to applied electrical in- put. They can therefore be used both as sensors and actuators—the property that makes them 'Smart Materials'. The mechanical and electrical transductions are coupled in case of piezoelectric sensors.

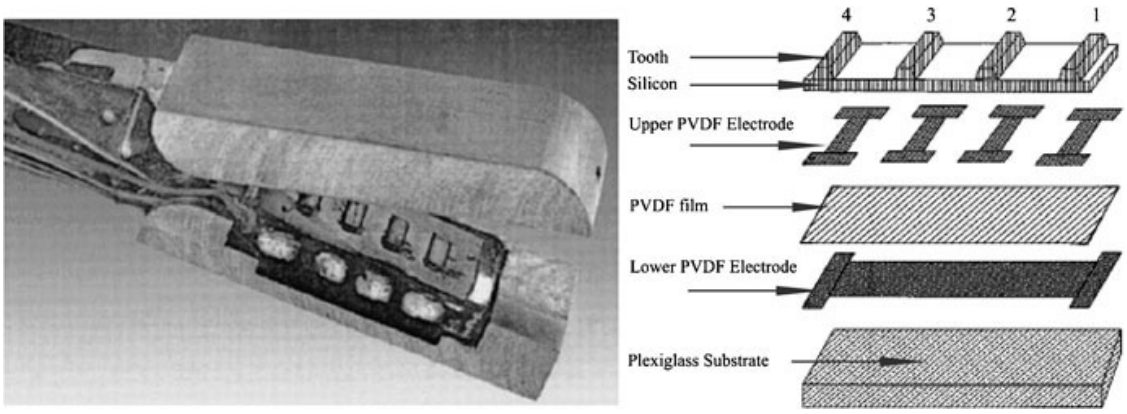

Figure 5.7 An endoscopic grasper prototype integrated with the piezoelectric tactile sensor. The photograph (*left*) of the endoscopic grasper prototype and (*right*) the expanded view of the piezoelectric polymer PVDF based tactile sensor unit (with permission, from Dargahi, Parameswaran, & Payandeh, ©(2000) IEEE) (Dahiya & Valle, 2013)

A typical piezoelectric tactile sensor element has the same construction as the

capacitance-based sensors (Figure 5.4), where the dielectric material is piezoelectric with thickness t and area A. The piezoelectric material deforms by Δt on touching with contact force F to generate charges +Q and −Q at the two electrodes. As the element is also a capacitor, the induced charge leads to a potential V across the tactile element, as given by:

$$V = \frac{Q}{C} \approx \frac{dF}{C} = \frac{dt}{4\pi\varepsilon\varepsilon_r A} F$$

The piezoelectric sensors are highly sensitive with high voltage outputs even to small dynamic contact deformations. If a load is maintained, then the sensor output decays to zero. Therefore, these sensors are most suited for sensing dynamic forces. The sensing elements do not require power supply for its operation, and hence the sensors using piezoelectric transduction are reliable and efficient in terms of power consumption. Depending on the design of the sensor, different modes (longitudinal, transversal and shear) can be used to load the piezoelectric element. The tactile sensors based on piezoelectric transduction exhibit high sensitivity, a large dynamic range, a wide bandwidth with good linearity, and a high signal-to-noise ratio (SNR). The piezoelectric materials often used in tactile sensing schemes are described later in the section on tactile sensing materials.

5.1.7. Electrorheological sensors

Some gels or electrorheological (ER) fluids have the ability to transform from a liquid to a plastic state, in milliseconds, on application of a strong electric field across them. This is known as the electrorheologic effect. The fluid viscosity of the ER fluid

is proportional to the applied field strength. The ER fluids are a suspension of a dielectric solid or polymeric particles (the dispersed phase) in an insulating base oil (the continuous phase), which under normal conditions behaves as a Newtonian fluid. Examples of ER fluids include, silicone oil with $Na_{12}Al_{12}Si_{12}O_{48}$, and a nematic liquid crystalline (LC) E7 mixed with lithium polymethacrylate (LiPMA) (Taylor, Pollet, Hosseini-Sianaki, & Varley, 1998). A widely accepted description of the electrorheologic effect states that the dielectric solid particles in the fluid become polarized and form microstructures (chains or clusters) under the presence of an electric field. Whereas a majority of applications use the ER fluids in shear mode, they are subjected to both shear and squeeze in case of tactile arrays. A tactile actuator and a matching sensor, based on the aforementioned principle, is reported by Voyles et al. (Voyles, Fedder, & Khosla, 1996). The actuator–sensor pair has male–female symmetry for the purpose of remote monitoring of touch sensing. The fingertip-shaped sensor detects contact events on its external surface using a gel layer as a dielectric in capacitive sensing, while the similarly shaped actuator recreates the remotely sensed tactile events on its internal surface by changing the solidity of areas of the gel in contact with the human operator. The ER fluid based robotic fingers have also been reported in literature (Kenaley, & Cutkosky, 1989). The ER fluids are attractive because they are controlled electrically, which is convenient as there are no moving parts. They require little power (although voltages can be very high) and they can be made very compact. In fact, the smaller the dimensions, the higher the field strengths and the stronger the ER effect. These characteristics make ER fluids attractive for the haptic interfaces.

5.1.8. Magnetorheological sensors

Similar to the ER effect, discussed above, there exists magnetorheological (MR) effect whereby the MR fluids exhibit rapid, reversible and significant changes in their rheological (mechanical) properties while subjected to an external magnetic field (Taylor, Pollet, Hosseini-Sianaki, & Varley, 1998). The MR fluids are suspensions of micron sized ferromagnetic particles dispersed in different proportions of a variety of non ferromagnetic fluids. As with ER fluids, the MR fluids are also in liquid state without external stimuli. While MR fluids are subject to amagnetic field, they behave as solid gels, typically becoming similar in consistency with dried-up toothpaste. In recent years, MR fluid based haptic displays and haptic interfaces have been investigated by some researchers. Carlson and Koester have developed a prototype of portable hand and wrist rehabilitation device based on MR fluid (Carlson, & Koester, 2001). MR fluids have also been used to construct tactile and haptic displays to replicate perceived biological tissue compliance (Scilingo, Sgambelluri, DeRossi, & Bicchi, 2003; Liu, Davidson, Taylor, Ngu, & Zarraga, 2005). The challenges of producing strong magnetic fields over large surface areas, however, limit the application of MR fluid sensors. From discussion above it may be noticed that tactile sensors based on nearly all possible modes of transduction exist. Some of the least explored transduction methods not explained above include, electrochemical and acoustics methods. The advantages and disadvantages of some of the frequently used tactile sensing methods are summarized in Table 5.2. Some of these methods combine mechanical and electrical transduction (e.g. capacitive, resistive, and ferroelectric) and some other do not have such coupling (e.g. optical, ultrasonic, and magnetic). The main problem with coupled mechanical–electrical transduction

schemes is the difficulty in optimizing one form of transduction without compromising the other. This is simply because there is no material with just the right combination of mechanical and electrical at- tributes. By separating the mechanical and electrical transduction in the sensor, both forms of transduction can be optimized without compromising the other. Consider for instance, the elastic material typically used in the sensor covering can be chosen for the most appropriate combination of stiffness, resistance to abrasion, tearing, oxidation, chemicals and other environmental factors. Since the rubber covering simply overlies the sensor, it can be replaced when it is worn or damaged or when different rubber characteristics are required; such as less stiffness to provide higher force sensitivity.

5.2. Characterization

Service robots meant for human interaction need to simulate touch sensitivity, or contact force is to be known for control purposes, therefore tactile sensors are a key component in robotic applications requiring human-robot interaction. For better integration and effective utilization of tactile data, the tactile sensing schemes are required to be conformable. Surface force or pressure transducers are used both for simple qualitative touch sensing, thus requiring a simple binary output, and for quantitative continuous gauging of contact pressure through analog voltage signals. Measurements have thus to be quick, reliable and have a good frequency response in the required band. Moreover, minimal dimensions are required, as well as an evenly responsive contact surface. We chose at first a commercial contact force sensor which exhibits all of these features: minimal overall dimensions, uniform

measuring area, customizable range and certified linearity, no drift and hysteresis or good frequency response features. Prior calibration has to be performed under non-perturbed conditions, so as to take into account of different constraints applied by the facing surfaces. Here our static and dynamic calibration results are presented along with the peculiarities we came across. We also compared its output to a commercial capacitive buzzer's. We wanted to assess if the sensors would exhibit linear behavior, no drift nor hysteresis as stated by the manufacturer. The sensors should offer uniform sensitivity over the sensing area, so matching section weights can be used to load them for static calibration. Besides this simple method, we also used hydrostatic pressure in a sealed chamber, getting rid of errors uncertainties coming from loading over the edges or from point loading. This method also allows for dynamic testing, as impulse loading or different frequency pressure waves can be applied to the sensors. Calibration curves will be presented in different loading conditions, focusing our attention on loading velocity and frequency. Although sensor gain exhibits remarkable changes after repeated loading, its smooth and continuous output makes us think it can still be put in a feedback chain.

With the intention of performing preliminary experiments with tactile sensing, they were chosen as a good compromise between price and performance.

5.2.1. Sensors properties

The Tekscan FlexiForce® sensor is made of two polyester sheets patterned with piezoresistive ink electrodes (see Figure 5.8).

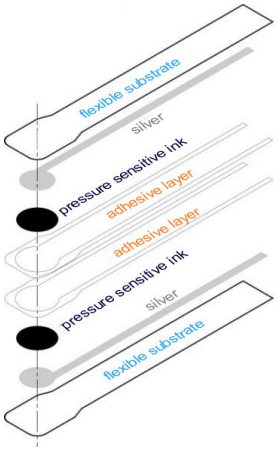

Figure 5.8 Sensor construction.

The sensor acts as a force-sensing resistor in an electrical circuit. The lower the load, the higher the resistance. When a force is applied to the sensor, this resistance decreases.

Figure 5.9 The amplifier based on the suggested op-amp drive circuit.

As the manufacturer suggests, we used a custom op-amp drive circuit (see Figure 5.9) following the given scheme to produce a linear voltage output between 0÷10 volts and allowing for DC power supplying eight sensors at once, being in turn fed at 5 V through a USB cable.

The A201 model we are studying has a 9.53 mm diameter sensing area, and a 0÷4.4 N force range. These piezoresistive sensors are guaranteed for a linear output, acceptable repeatability and low hysteresis (see Table 5.1).

Table 5.2 – FlexiForce® A201 data sheet

Linearity (Error)	< ±3%
Repeatability	< ± 2.5% of Full Scale
Hysteresis	< 4.5% of Full Scale
Drift	< 5% per Logarithmic Time Scale
Response time	< 5µs

5.2.2. Static calibration

Two methods were adopted: dead weights laying in the sensors surface, and hydrostatic air pressure in a sealed container. For applying loads on the sensors surface a plastic shim (Figure 5.10) was placed between the sensing area and the weight bottom when contact areas would not match, and to uniformly distribute loading when the contact surface was not smooth, thus avoiding kinks or stress concentrations. Of course such care cannot be taken in actual applications.

Figure 5.10 The shim used to evenly distribute the load.

A pressure vessel (a sealed bottle, see Figure 5.12) was used to test the sensors using hydrostatic pressure, thus getting rid of all those issues tied to stress distribution, and should give as clean output values as possible.

5.2.2.1. Drift

Four increasing weights were laid over the sensor surface for 2 hours each to assess drift, and pressure values were continuously monitored and recorded by means of a NI cDAQ-9172 CompactDAQ chassis, equipped with a 9219 4-Channel, 24-Bit, analog input module A sample of acquired data is shown in Figure 5.11. Loading conditions changes are not associated to the gap in output voltage values.

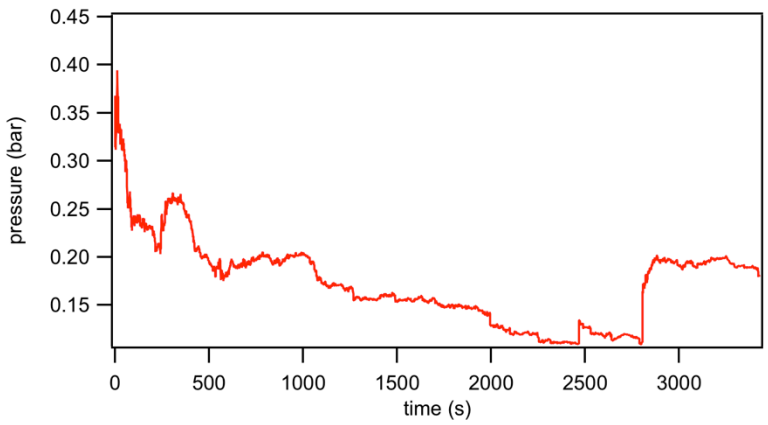

Figure 5.11 An example of the drift trend in about one hour time

5.2.2.2 Hydrostatic pressure loading

Static loading curves, some of them followed by unloading, were all recorded at the same velocity, about the same as the one adopted in working conditions, and after the conditioning procedure suggested by the manufacturer: each sensor was repeatedly loaded and unloaded at about 110% full scale, and tested almost immediately not to lose conditioning effects.

It is to be noted how each curve is smooth and how they are perfectly scaled to each other although they do not match.

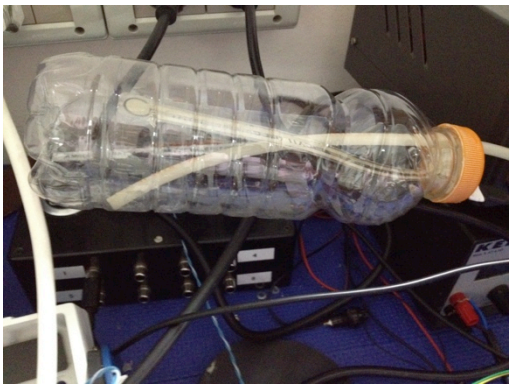

Figure 5.12 The sealed plastic bottle used for hydrostatic pressure testing.

Nevertheless, it doesn't seem that repeatability can be achieved anyhow in spite of not changing the testing conditions.

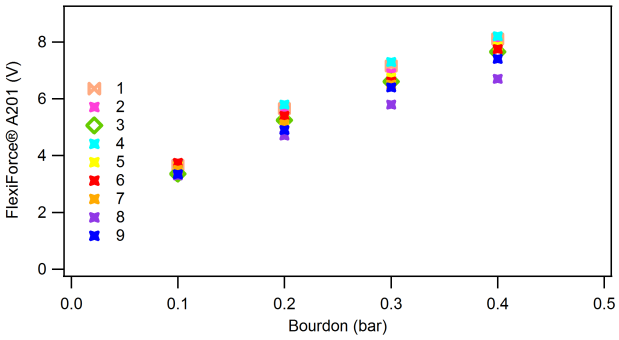

Figure 5.13 Static-loading curves (sensor voltage output vs. high-precision Bourdon gauge): the gain is not related to the loading sequence.

Moreover, the test sequence is not related to the gain increasing or decreasing.

As for linearity, in Figure 5.14 are shown two rectified calibration curves and their coefficients. The power law $p=(V/12)^{\wedge 2}$ seems to give better fitting here.

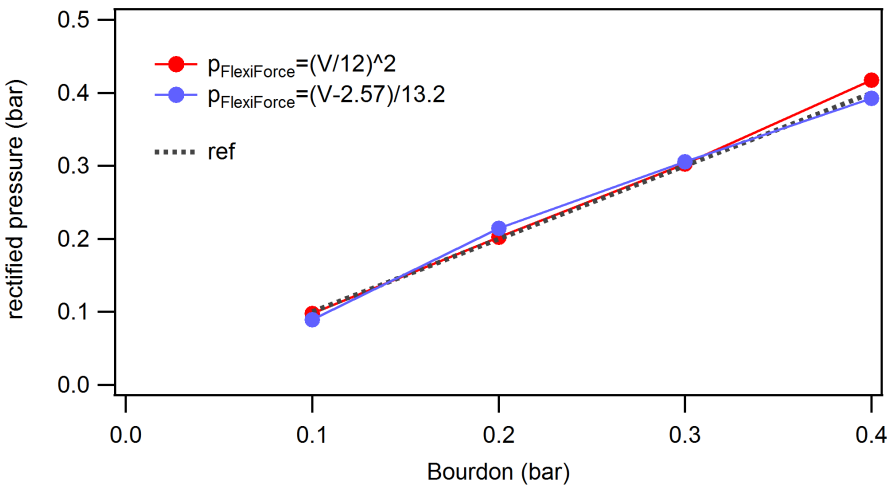

Figure 5.14 Calibration curves for one piezoresistive sensor.

A piezo buzzer (Figures 5.15, 5.16, 5.17) was also tested as comparison.

Figure 5.15 A piezo buzzer.

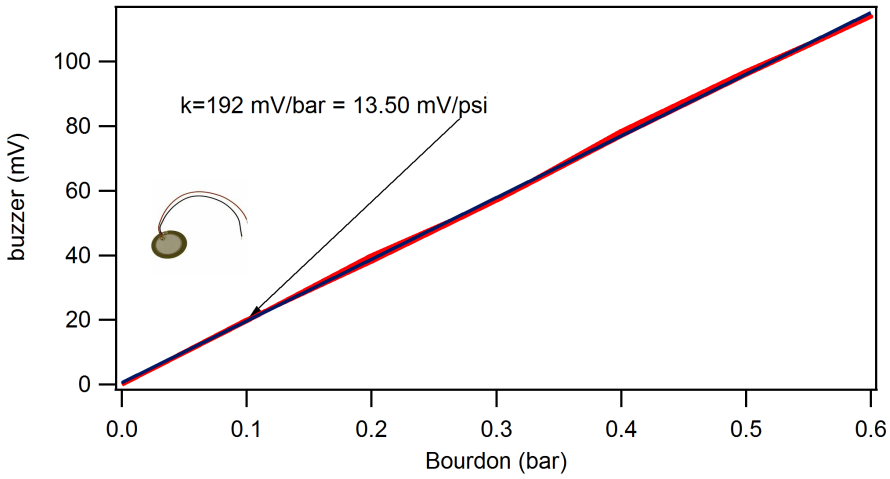

Figure 5.16 Calibration curves for the piezo buzzer.

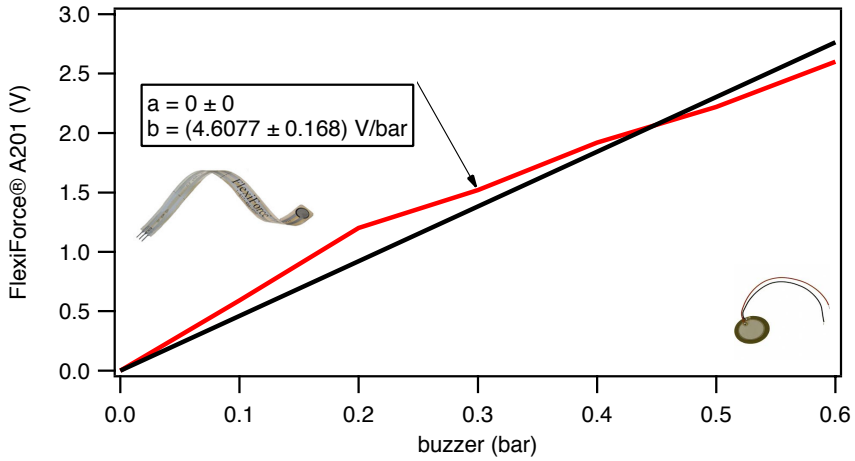

Figure 5.17 FlexiForce force sensor vs. piezo buzzer.

5.3. Dynamic calibration

5.3.1. Purpose

We wanted to assess the loss of calibration occurring over multiple loading cycles, if any, as static loading and drift curves suggest. This would minimize the sensor utility for repeated, long-term load measurements not to speak of feedback controlling the system.

A preliminary loading-unloading curve is shown in Figure 5.18. During the test the sensor behaves in a satisfactory and reliable way, without any appreciable response changes.

5.3.2. Sine wave loading

The sensor was cycle-loaded at low frequencies by means of one of the two analog outputs (16-bit, 833 kS/s) of a NI-6221 USB module piloting at 0÷10 V DC a Norgren VP10 E/P converter with an air consumption of 0.85 Nl/min and a response time less than 0.5 s for 10-90% step change. Experimental setup is shown in Figure 5.18.

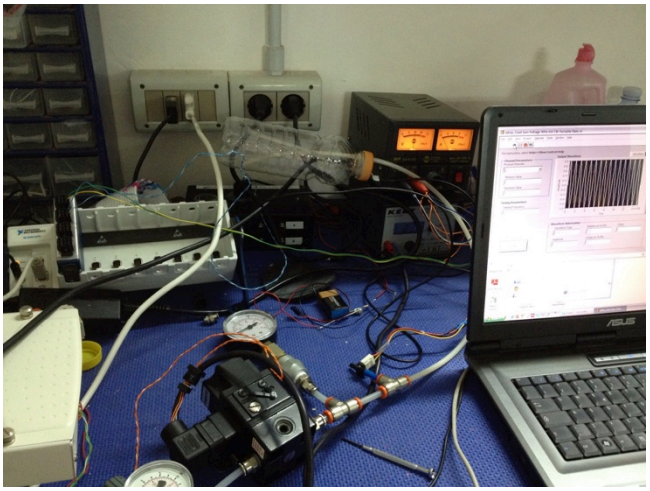

Figure 5.18 Experimental setup

The proportional valve was power supplied at 24 V DC. A few loading conditions were chosen to assess the sensors performance: pressure was imposed to oscillate around a mean value of 0.5 bar at frequencies of 0.5 Hz and 1 Hz, and 0.2 bar amplitude (0.4÷0.6 bar). Air pressure was also monitored upstream of the container by means of a 0-15 psi Honeywell 24 PC Series piezo-resistive differential pressure gauge with 15 mV/psi sensitivity.

The green curves in Figure 5.19a, 5.19b below give the line pressure measured by the transducer, while the blue ones are the output of the thin-film sensor inside the

pressure bottle. They do not match in amplitude nor in global trend, generally overestimating the measured pressure.

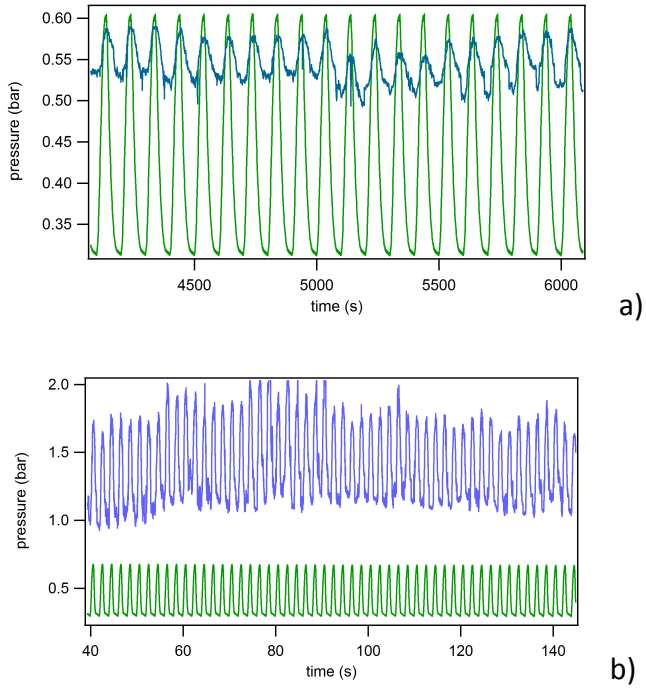

Figure 5.19 The line pressure measured by the transducer (green) vs the output of the thin-film sensor inside the pressure bottle (blue).

5.3.3. Contact testing

In Figure 5.20 below a power function calibration is given for a loading-unloading curve in the 0÷0.4 bar range.

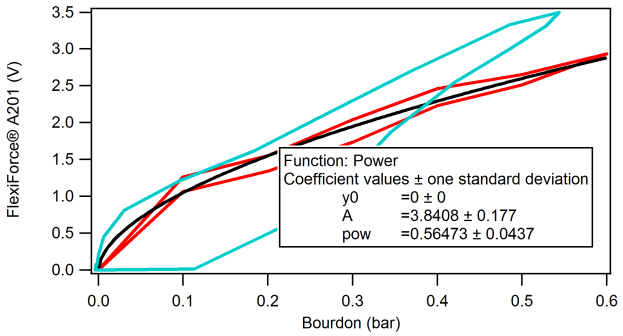

Figure 5.20 Power function calibration coefficients for a loading-unloading curve. A cyclic contact measurement (in blue) is also shown for comparison.

The blue curve was obtained interposing the thin-film sensor between a plastic pipe and the inflatable actuator (a cuff-bladder system) of the device in [5]. In Figure 5.21 a cyclic loading-unloading curve was obtained by inflating-deflating the cuff. The black curve comes from testing the system on a arm. The red curve exhibits higher hysteresis.

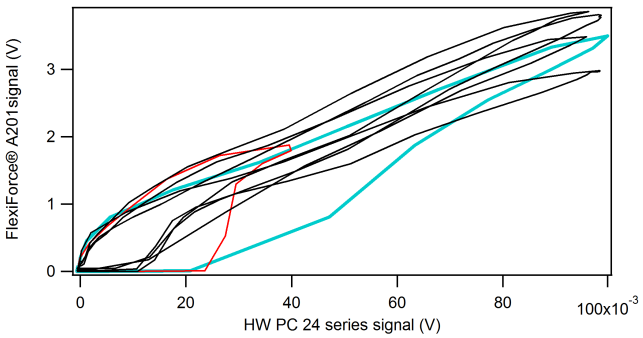

Figure 5.21 Qualitative trend of the measured pressure contact between a plastic tube and the cuff-bladder system in [9] (blue curve) and cyclic loading-unloading curves from contact pressure measurements between the same actuator as above and a human arm. Air pressure is given by the analog output of the Honeywell differential transducer.

5.4. Results

The drift curves doesn't seem to be satisfactory, as they present sudden gaps that cannot be foreseen or avoided, or simply don't give repeatable measures being measured pressure unchanged.

The static loading curves as well exhibit neither repeatability nor linearity. A question could be raised about the opportunity to use a linear or a power function to give the best fit. Both solutions are presented. The pressure range could lead towards one or the other.

As for low-frequency cyclic loading, the sensors' behavior doesn't seem to be reliable either, as unexpected and unjustified raises and drops of the output occur, still being it smooth.

5.5. Conclusions

These observations make us think that the studied thin-film piezoresistive sensors deserve a further systematic investigation, being their advantages in terms of size, smooth output, apparently good frequency response -in the band of use and investigation- and sensitivity still predominant on their poor repeatability, which could be rectified i.e. through on-the-fly tuning.

1. Circuit modeling and control

The control objective consists of the regulation of the contact force **f** so that

- it comes to the constant set point $\mathbf{f}_d$ smoothly and
- its value holds constant until unloading occurs

in order for the massage to be still effective without causing pain or distress or any cutoff to the blood flow, or for giving it the desired linear or oscillating law.

- **Model performance**

The results of modeling tasks are to be checked by approximation quality, and model complexity-interpretability. Most commonly, the approximation/prediction error is used as assessment criterion.

- **Control performance**

The standard riteria to assess the control performance include the step response, reference tracking, disturbance rejection behavior and the control effort (Belforte, Mauro, & Mattiazzo, 2004). This is analyzed for the nominal case and in some benchmark problems also with predefined structured model uncertainties. Such case is application-dependent. The step response is used to characterize the accuracy of the closed loop system.

From the control point of view, compliant pneumatic actuators represent a complex dynamic system of high nonlinearity. In contrast to conventional fluidic actuators, compliant pneumatic actuators possess some important properties, which are

essential with respect to modeling and control problems.

1.1. Different configurations

Different set up's, still significant to our purpose, were tested in order to dynamically identify them.

Figure 6.1 below shows the PLC driven circuit whose behavior we intend to model.

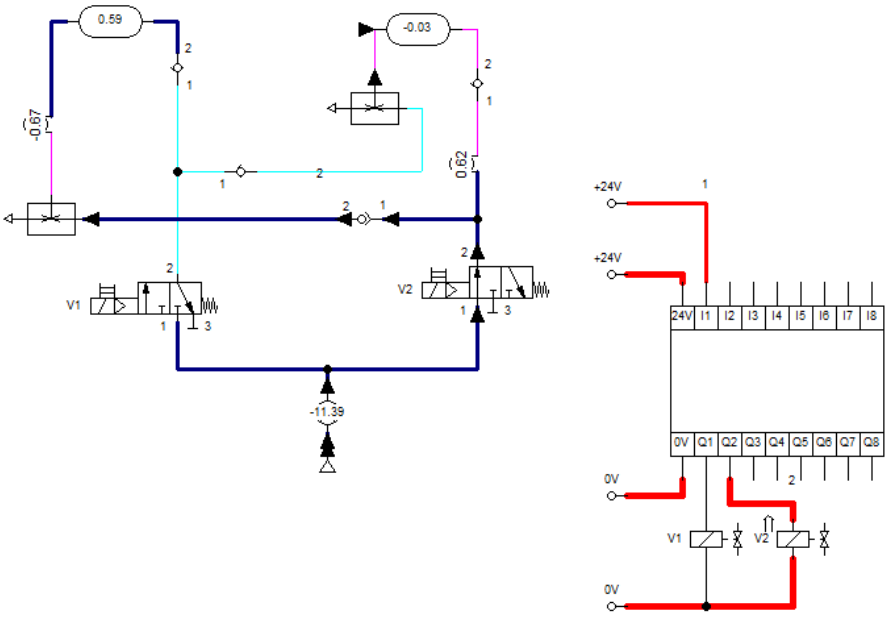

Fig. 6.1 FluidSIM® pneumatic scheme of the PLC driven double capacitor circuit

The following results are given for two different configurations, both of them voltage controlled, shown in Figure 6.2, 6.3.

A 3/2 valve distributes the flow in the circuit of Figure 6.1, feeding both the accumulator and the air ejector that is connected to the relief port 3. Downstream of that, a Norgren VP10 E/P converter voltage driven by one of the two analog outputs

(16-bit, 833 kS/s) of a NI-6221 USB module gives a 0÷10 V DC sine law to the feeding pressure.

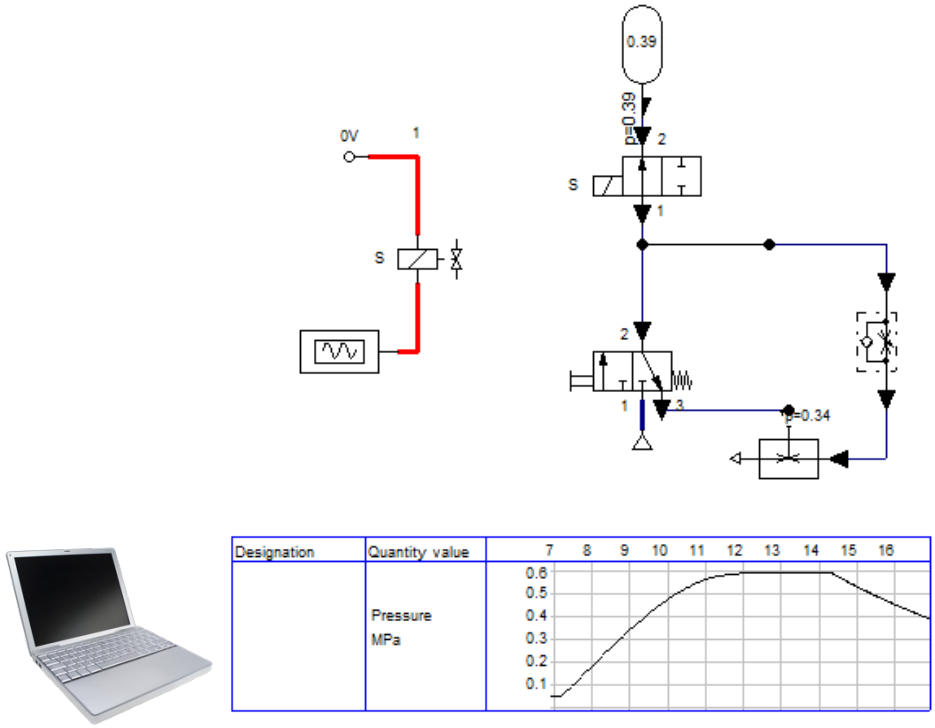

Fig. 6.2 FluidSIM® pneumatic scheme of the single-capacitor circuit including an E/P pressure regulator driven by a LabView controlled signal generator

A different circuit, shown below in Figure 6.3, includes two E/P pressure regulators upstream of each valve; air ejection is achieved by supplying both of them with a feeding circuit consisting of a 3/2 valve and an air ejector.

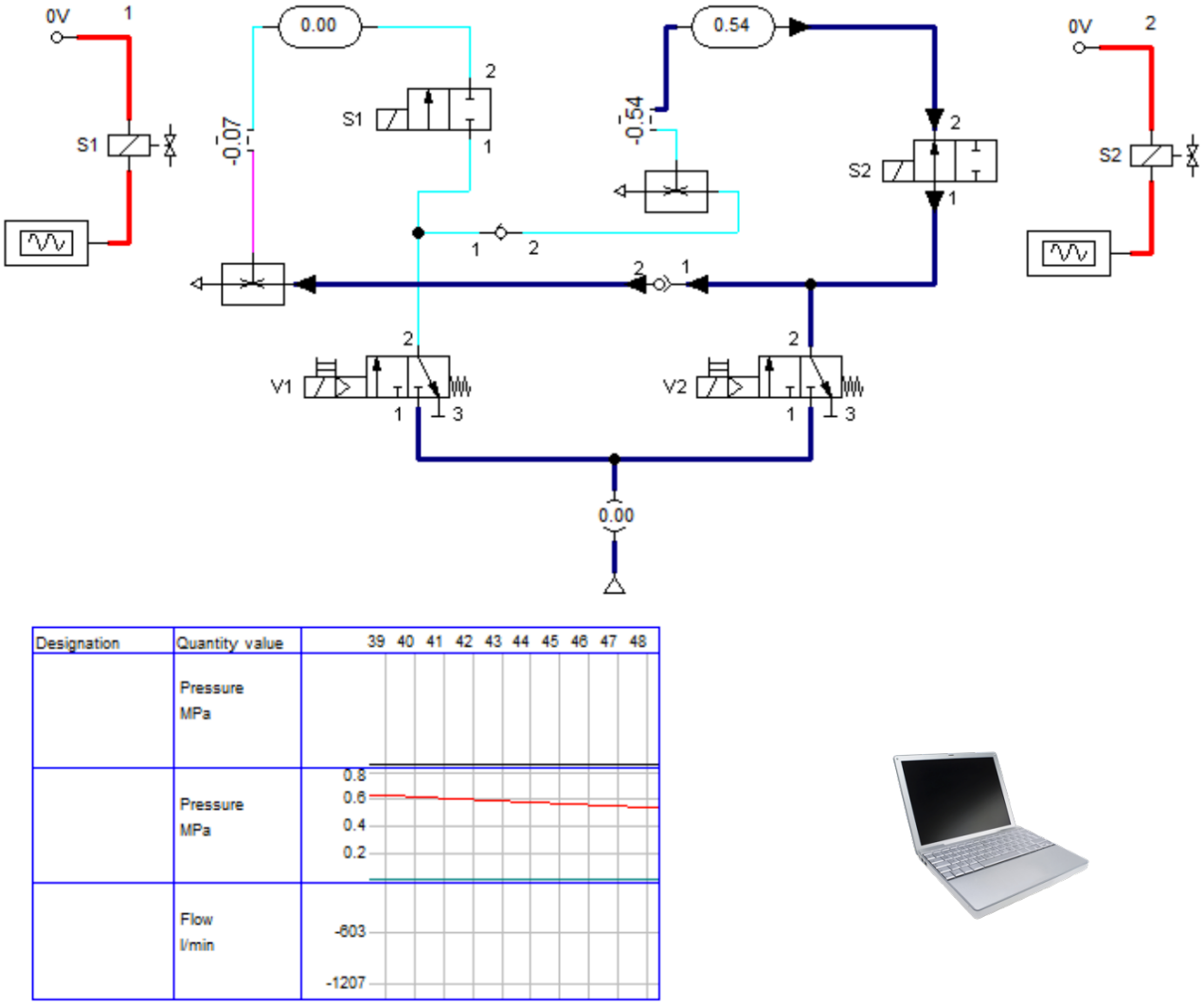

Fig. 6.3 FluidSIM® pneumatic scheme of a double-capacitor circuit including two E/P pressure regulators, both driven by a LabView controlled signal generator

6.2. Identification and modeling

Our pneumatic system can be modeled in the same manner as the electrical circuits with lumped parameters. Briefly reminding the analogy, we have:

- **energy storing components: the inductors.**

An inductor stores energy based on its inertial properties and due to the acceleration of electric charges or masses.

For a fluid flowing in a pipe a pressure drop is linked to the flow rate by the

$$\Delta p = L\dot{q}$$

Where L is the pneumatic inertance (like the electrical inductance) whose unity is Pa s^2/kg or m^{-1} and it can be shown to be equal to

$$L = \frac{\pi d^2}{4} l = A \cdot l$$

Longer or wider pipes (bigger length l or section A) cause the air to oscillate and the system to be of second order. For shorter pipes the inertial contribute can be neglected.

- **energy dissipating components: the fluid resistors**

Fluid resistors are components offering resistance to flow, such a sudden change of pipe section. Pressure drop is proportional to the mass velocity, i.e. the flow q, the same way as electrical resistance causes voltage drops proportional to the current or the viscous friction is proportional to the velocity (in a mechanical analogy such as that caused by a dashpot or a damper), although the relationship between Δp and q is non linear so that an exact analogy with the electrical resistance is not possible.

$$G = \frac{\Delta p}{q}$$

Fluid resistance *G* unity is Pa s/kg. G is used here, instead of the more common *R*, not to mistake it with the gas constant R.

- **energy-storing components: the accumulators**

In pneumatic systems both accumulators and large tanks can play this role.

Because air is a compressible fluid, a large volume of air embodies this compressibility effect, making thus a tank, whether it's rigid or not, act as an accumulator. A compliant actuator with no proper volume, as we will see later, makes it difficult to state a pressure-volume relationship.

We will therefore model our large volume actuators as equivalent capacitors due to the compressibility of the air. The capacitance is given by the

$$q = C\frac{dp}{dt}$$

where

$$C = \frac{\rho_i \cdot p}{k_v \cdot p_i} + \frac{V}{R \cdot T}\ ;\ C = \frac{\rho_i}{k_v} \cdot \left(\frac{p}{p_i}\right)^{\frac{1}{k}} + \frac{V}{a^2}$$

are the isotherm and adiabatic pneumatic capacitances of an elastic chamber, being

$$k_v = \frac{dp}{dV}; a = \sqrt{\frac{dp}{d\rho}}$$

the volume stiffness k_v and the sound velocity a.

Nonlinearity of the flow as a function of pressure is to be evaluated in order to properly model the actuator capacitance. An assumption can be made abo ut the transformation being slow enough to be considered isothermal ($n = 1.0$) or adiabatic with pressure rapidly changing which means there is no heat transfer in and out of the tank as the air is compressed and, as a result, small changes in temperature occur ($n = 1.4$), by deducing experimentally the polytrophic exponent n in the following

$$q = \left[\frac{\rho_i}{k_v} \cdot \left(\frac{p}{p_i}\right)^{\frac{1}{n}} + \frac{V}{n} \cdot \frac{\rho_i}{p_i}\left(\frac{p}{p_i}\right)^{\frac{1-n}{n}}\right] \cdot \frac{dp}{dt} = C \cdot \frac{dp}{dt}$$

The polytrophic capacitance C above, valid for an elastic tank, consist of two terms: the first one depends on the volume variation of the tank, the second one depends on air compressibility. Pneumatic capacitance, as seen, is always nonlinear.

Modeling: a closed-form equation

This is the most common way to represent a dynamic system.

A lumped-parameter modeling of the circuit can be based on deeming each component responsible for energy-storing and dissipating properties as well as inertial behavior.

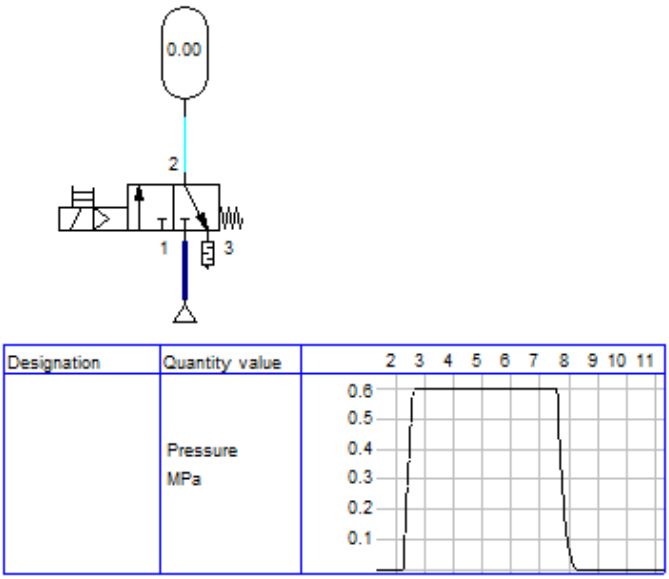

Fig. 6.4 Single accumulator simple RLC circuit

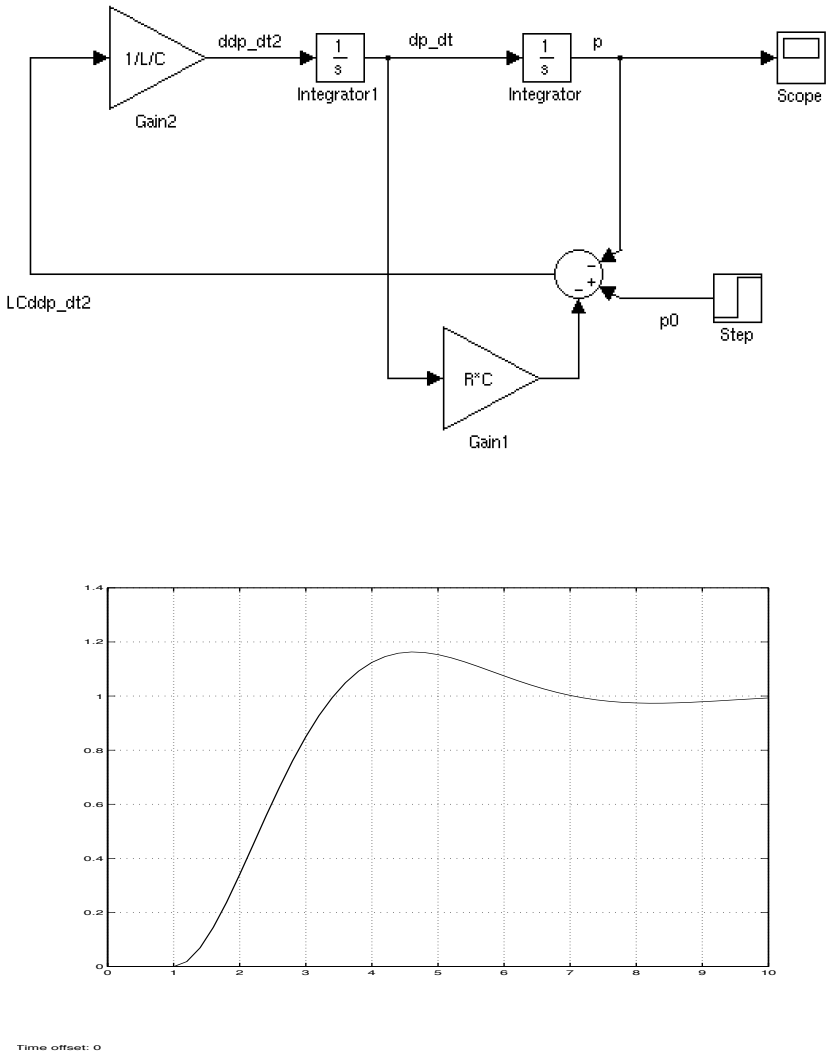

Fig. 6.5 Step response simulation for the open-loop circuit model in Figure 6.4

For the RLC circuit above a sound equation could be:

$$p(t) = L\frac{dq}{dt} - Rq - \frac{1}{C}\int q \cdot dt$$

$$p_1 = p_2 + RC\dot{p}_2 + LC\ddot{p}_2$$

Nonlinearities are most probably coming either from air compressibility and from the peculiar behavior of the inflatable balloons constrained by their fabric cuff.

Modeling: estimating and identifying object models

The system has been analyzed in both SISO (Single-Input Single-Output) and MIMO (Multiple-Input Multiple-Output) configuration. In Figure 6.6 analog data coming from the on-off opening valve law are shown, together with the pressure measured upstream of the balloon actuator. Some estimation results will be shown below. A first look at the data by means of System Identification Toolbox gave us some preliminary indication about data quality: the main outcome is the presence of a system integrator which can lead to instability. Nonlinearities in the data are worth being investigated, and that is what we did.

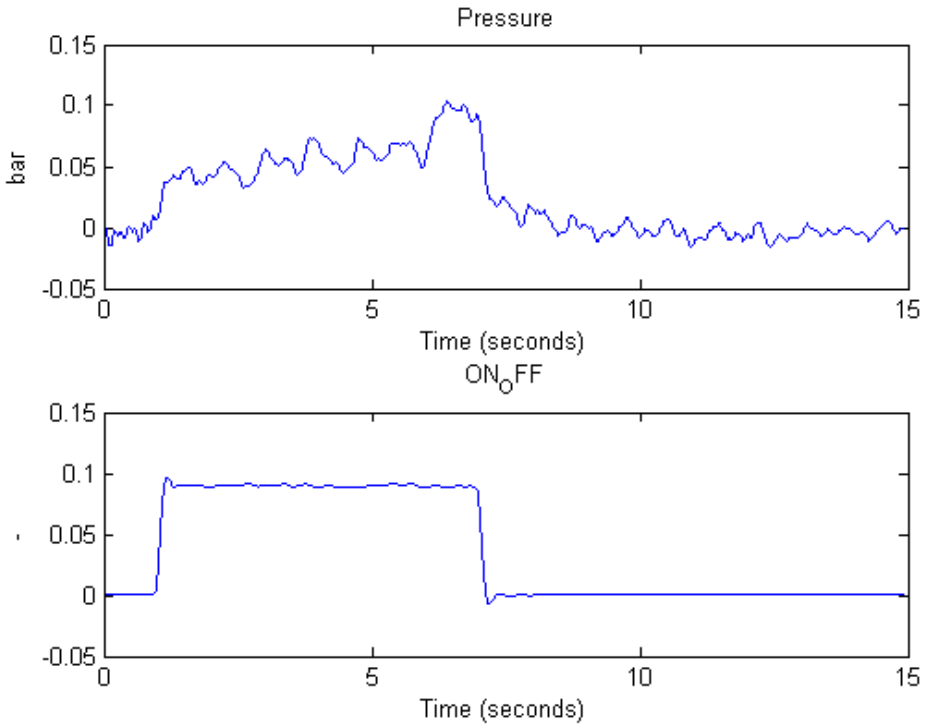

(a)

(b)

Fig. 6.6 A sample of the analog pressure data as a step response: pressure inside the balloon actuator (a) and on-off opening valve signal drawn from the PLC contact (b)

Modeling: Transfer function estimation

Measured input/output data gave us a first estimation of a transfer function *G*: a model order of 2 was chosen as a constraint.

$$G(s) = \frac{11.23s + 15.04}{s^2 + 23.37s + 20.16}$$

Modeling: estimating linear state-space models

Estimation of a continuous state-space model in the usual form

$$y' = Ax + Bu + Ke$$
$$y = Cx + Du + e$$

gave us the following coefficients

$$A = \begin{bmatrix} 0.8164 & -6.999 \\ 6.35 & -8.469 \end{bmatrix} \quad ; \quad B = \begin{bmatrix} 2.6 \\ 1.206 \end{bmatrix} \quad ; \quad C = \begin{bmatrix} 1.826 & -0.009194 \end{bmatrix} \quad ; \quad D = 0 \quad ;$$

$$K = \begin{bmatrix} 173.5 \\ -1.264\text{e+}04 \end{bmatrix}$$

with a fit to estimation data of 99.82%

Same process models were preliminary checked with different initial assumptions:

The model structure have been specified by selecting the number of real or complex poles, and whether to include a zero, delay, and integrator, afterwards displaying the resulting transfer function in the Process Models dialog box.

'P1D' process model, i.e. with 1 pole and a time delay

$$G(s) = \frac{K_p}{1 + T_{p1}s} e^{-T_d s} \quad ; \quad \begin{array}{l} \mathrm{K}_p = 0.73198 \\ \mathrm{T}_{p1} = 1.049 \\ \mathrm{T}_d = 0 \end{array}$$

At the same way, different linear models were tested (Ljung, 2003, *System Identification Toolbox User's Guide*):

'P2ZU' two poles and one zero, underdamped
'P0ID' an integrating (self-regulating) process, with time delay
'P2U' two poles, underdamped

Modeling: estimating nonlinear state-space models

An ARX model has been tested, i.e.

```
sys = idnlarx(LinModel,Nonlinearity)
```

as well as grey box models

```
sys = idnlgrey(FileName,Order,Parameters)
```

Validating models

The proper, usual way for validating models has been followed, i.e. splitting the recorded signal in two and using one half for estimate a model and the other for validating it on unseen before data.

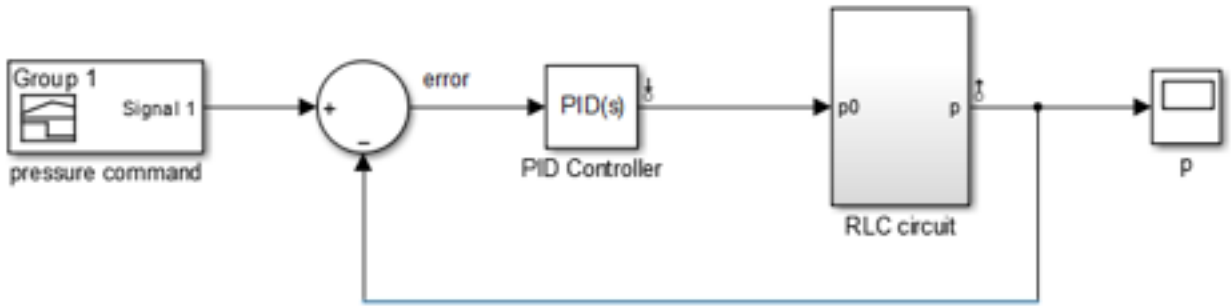

Fig. 6.7 PID controlling of the system in Figure 6.5

5. Clinical testing

Two main sets of measures are worth being presented, both carried on by means of the devices developed either at our Lab of Applied Mechanics and Robotics or in cooperation with the Mechanics and Aerospace Engineering of the Polytechnics of Turin.

We performed the tests jointly with the research équipe of physicians of the Laboratory of Sports Physiology at the Department of Medical Sciences - University of Cagliari.

5.1. Motivation

We considered paraplegic patients as the main target for a clinical use of our device; nonetheless, we tested those first on healthy subjects in order both not to risk of harming the patients, and to get a basis of results not perturbed by deficiencies that could not be of the same order and whose influence on the results is to be tested as well. The effects of applying different intermittent pressure patterns on patients' legs are highlighted and related to impedance cardiography measures of heart efficiency parameters. A preliminary explanation is given of the physiological processes involved in diastolic insufficiency leading to reduced aerobic capacity.

Moreover, healthy subjects are of research interest themselves as injuries occurring during workouts or when competing often mean several weeks of bed restrain, which can be quite a prejudice for endurance athletes, as they result in seriously compromising the competition performance due to a decrease of left ventricular end diastolic volume deriving from a reduction of training-induced ventricle hypertrophy.

7.2. Methods

7.2.1. Hemodynamic measurements

Heart efficiency parameters (in Fig. 7.1 impedance cardiography idea is explained) were continuously monitored using an impedance cardiograph (NCCOM 3, BoMed, Irvine, Calif., USA).

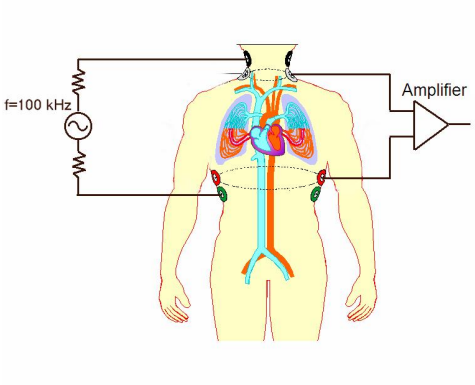

Fig. 7.1. Impedance cardiography heart efficiency measurements. By means of disposable electrodes a constant intensity electrical current circulates in the thorax. Changes in bioelectrical impedance (Zt) are detected. They are proportional to the left ventricle systolic flow.

NCCOM 3 was connected to the subject with eight spot electrodes: two pairs of sensing elements were placed in the lower thorax and cervical area at the base of the neck, while the current injecting pairs (2.5 mA, 70 kHz) were external to the sensing ones, above the cervical and below the thoracic pairs. NCCOM 3 analog traces of electrocardiogram (ECG), and the maximal Z_0 first derivative (dZ/dt) were stored using a digital chart recorder (ADInstruments, PowerLab 8sp, Castle Hill, Australia) for being processed getting SV, SV/DT and PEP/VET ratio. The processing procedure cannot be automatic but requires human interaction with knowledge of cardiodynamics to exclude signal errors and beat artifacts.

7.3. Testing procedure

7.3.1. Endurance athletes

The changes in thoracic electrical bioimpedance were assessed to indirectly evaluate (by an inverse correlation) the changes in left ventricle end diastolic volume, when mechanical actuators are acting on legs. Nineteen healthy male participants were admitted to the trials. Each participant, seated with his extensor and flexor leg muscles voluntarily relaxed, was submitted to the action of the mechatronic device, imposing pressure trends on the feet and legs.

7.3.2. Pneumatic actuators

Figure 7.2 shows one of the two semi-boots utilized to actuate compressions on subjects' legs. It consisted of 6 flexible pneumatic actuators (bladders) assembled into a rigid shell that is the structure of the boot. The device performs a definite massaging action on specific zones of the lower limb, according to particular time laws. Moreover, it meets anatomical requirements by generating distributed forces along the entire contact surface. Positive effects on the cardio-circulatory condition are expected on the basis of preliminary tests where suitable pressure distributions were imposed on defined lower limbs zones (Manuello Bertetto, Meili et al., 2012)

Pneumatic actuators are inflated by compressed air flowing through high performance miniaturized solenoid valves (Fig. 7.3). A portable PLC (Programmable Logic Controller) controls the device imposing the pressure trend in the flexible

actuators interacting with the participants.

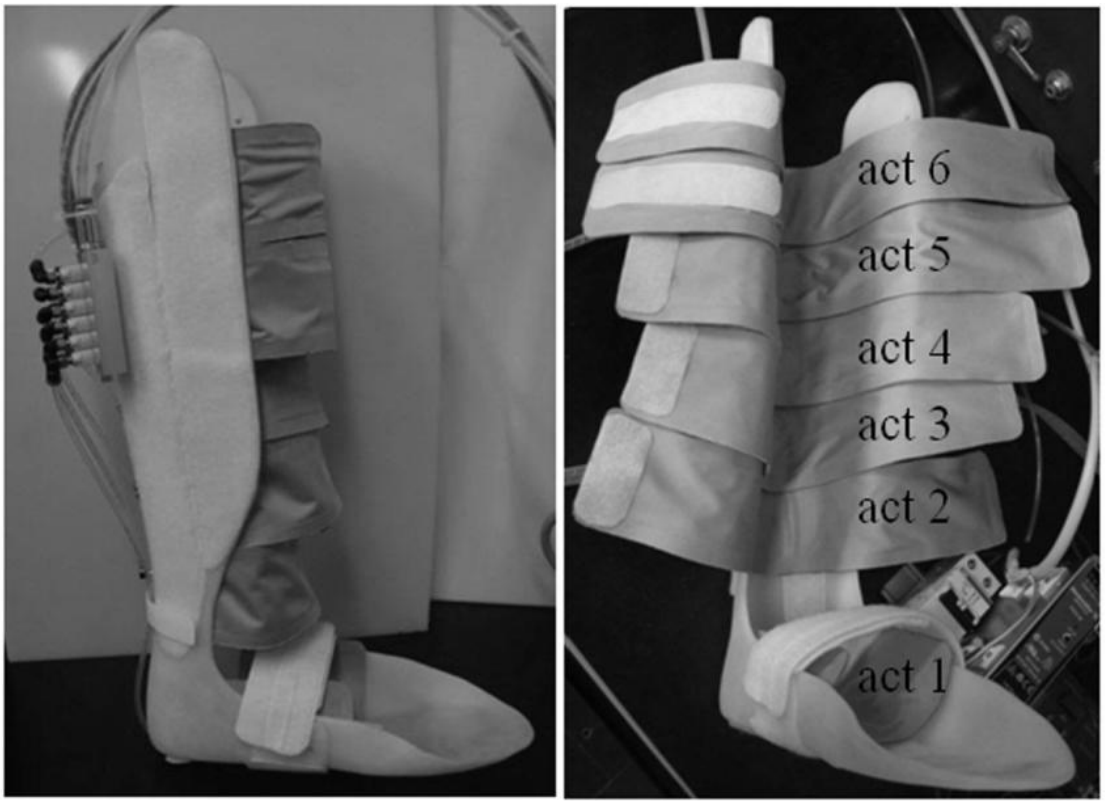

Fig. 7.2 Here represented one of the two anatomic boots with flexible pneumatic actuators. Each boot has six inflatable pneumatic actuators (bladders).

The PLC basic unit was a SIEMENS LOGO 24 RC, provided with two digital I/O modules of the DM8 24 model and DM16 24 model. Typical scheme of the circuit supplying each flexible actuator (Fig. 7.2) provided that compressed air coming from the supply (1) was treated by a FRL group (Filter, Regulator, Lubricator). The air flow was controlled by an electro valve (3) and supplied the actuator (4, here represented as a single-effect cylinder). The flow-regulators (5) regulated the dynamic response of the actuator at the expected condition. The pressure switch (6) commutates the electro-valve (3) when the actuator pressure reached a defined limit, to avoid an excessive pressure level that could be dangerous for the patients. The exhaust port of the valve was depressurized by the vacuum generator ejector (7), supplied

through the flow regulator (8) in order to facilitate the actuator deflation during the actuation cycle. To carry out an easier and faster actuator exhausting phase, during the actuation cycle, the exhaust port was depressurized downstream of the valve by a vacuum generator ejector

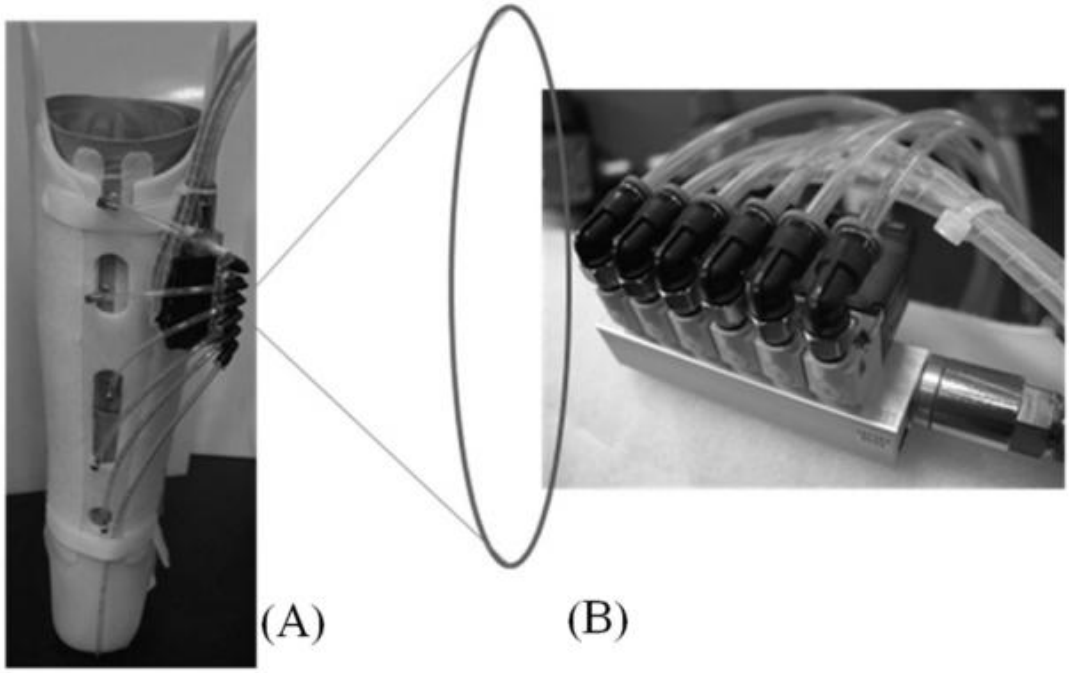

Fig. 7.3 The six high performance miniaturized solenoid micro-valves group controlling the air flow in the actuators, assembled on the boot structure (A) and shown in detail (B).

A NI cDAQ-9172 CompactDAQ chassis, equipped with a NI9219 4-Channel, 24-Bit, analog input module (National Instruments, Italy), was used to read pressure data coming from three 0-15 psi Honeywell 24PC series pressure transducers (Honeywell International Inc., USA) which acquired the air pressure driving the flexible actuator. The appropriate levels of air pressure were defined by preliminary tests, in order to preserve the comfort of the tested subject. It is to be noted that the operating pressure sensibly drops inside the flexible actuators, with respect to supply regulated pressure, reaching values one order of magnitude lower, due to the

system dynamics and the plant characteristics. Taking this into account, it was possible to impose, for each lower limb, compression protocols involving sequences of activation-deactivation following a peristaltic pressure, having a caudate-rostral trend. The logical scheme chosen in these experiments was to alternate the activation of the two sleeves to simulate the muscle action pattern during walking.

7.3.3. . Inflating tests design

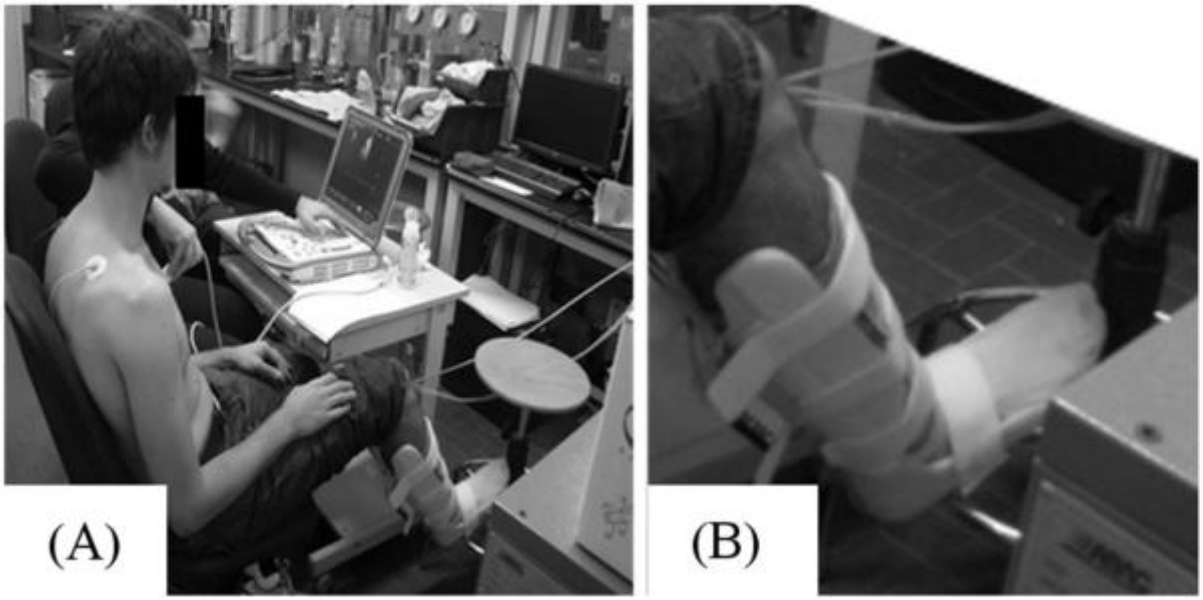

Fig. 7.4 The application of the mechatronic device to the athletes' legs is here represented (A). In situ mechanical actuator particulars can be seen in the expanded image (B).

Before monitoring the cardiovascular response during activation of the device, each participant was monitored for 3 min at rest to collect baseline values. Then, the mechatronic device was positioned on the legs of a seated participant, with his extensor and flexor leg muscles voluntarily relaxed (Fig. 7.4). Once the preparation was completed, all volunteers underwent a compression-relaxation cycle. As indicated in Fig. 7.2, the actuators were numbered starting from the foot plant

actuator (act1) up to the higher one (act6). The time interval activation for each actuator was of 3 s, with 1.5 s delay between each. The half-cycle for one boot lasted for 10.5 s, with a delay of 3 s between the two boots; thus the entire cycle including both boots was 27s (Fig. 7.5). The inflating relative pressure reached the maximum value of 0.3 bar. On each thigh an elastic containment stocking was worn to reduce venous distension coming from the increase of blood flow during mechanical actuation.

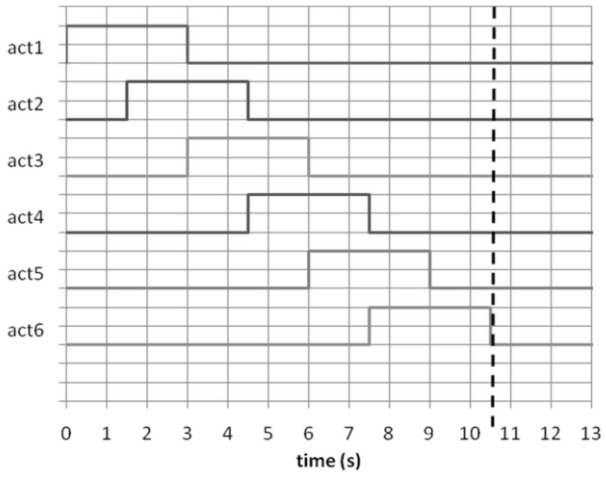

Fig. 7.5 The time sequence of the actuators command signals. Broken vertical line indicates the half-cycle end.

7.3.3. Hemodynamic assessment

Hemodynamic variables were monitored and recorded beat-to-beat by means of an impedance cardiography device (NCCOM 3, BoMed Inc., Irvine, USA) allowing for continuous non-invasive TEB assessment throughout all the phases of the protocol (Davies et al., 2000)

The impedance measuring device was connected to the participant by eight ECG disposable electrodes (Fig. 7.4). Two pairs were thoracic and cervical electrodes to

inject a constant current (2mA, 70kHz) from the generator (G), whereas two other pairs were sensing electrodes placed above the cervical and below the thoracic pairs and tied up the amplifier section (A) (Crisafulli et al., 2006). The electrical signals were acquired by a digital chart recorder (AD Instruments, PowerLab 8sp, Castle Hill, Australia) (Crisafulli et al., 2007). Beat-to-beat values of TEB at the end of cardiac diastole (Z_0) were acquired and Z_0 was utilized as an inverse index of LVEDV [16]. The rationale for this choice is shortly presented below. We can consider the electrical resistors that all together constitute an electrically equivalent model of the thorax: most of them are of solid consistence (muscles, bones, cartilages, vessels, connective tissue of lungs) and practically homogeneous and constant with time mass.

On the contrary, lung air content and thoracic liquids content are subjected to cyclical changes. So, changes in equivalent electrical impedance of the thorax, i.e. Z_0, can be referred to by a sinusoidal oscillation showing two harmonics: the main one corresponding to breathing phases and the secondary one, with a lesser amplitude, corresponding to cardiac cycle phases (Kubicek et al., 1966). By utilizing a common electronic band-pass filter the main respiratory harmonic of Z_0 can be excluded and, in this way, observed changes in Z_0 only depend on changes in intrathoracic liquids volume. These in turn depend on both blood volume within heart and thoracic vessel and on extra-vessel water volume. It is expected that, in a healthy subject, extra-vessel water volume does not change significantly, thus Z_0 ought to depend essentially on beat-to-beat variations of thoracic blood volume, which reaches its relative peak when ventricles get to end diastolic volume. Since blood is a more

current-conducting tissue, an increase in end diastolic volume induces a corresponding reduction in Z_0 (Bernstein et al., 2005).

During experimental sessions, Z_0 values were assessed for each subject just before beginning the test (Z_0-basal) and at the end of the test (Z_0-test). During tests ECG traces were assessed as well. By utilizing a commercial statistic program (MedCalc Software), assessed values of Z_0-basal were compared with Z_0-test values using the Students' t test for paired samples and a value of $P<0.05$ was considered as significant.

7.3.4. Results and discussion

As shown by the columns height in the graphs of Fig. 7.6, Z_0-test values showed a significant reduction (-1,3 %, $P < 0.0002$) with respect to Z_0-basal values.

On the basis of the well known Frank-Starling Law, increases in LVEDV reaches to a corresponding increase of stroke volume. This very important, training induced, hemodynamic adaptation is the key to adapting, in a more efficient way, the cardiac output in response to the oxygen demand from aerobic, ATP-producing cellular mechanisms inside the muscle fibers of endurance athletes. In a recent paper by (Waring et al., 2012) it was found that, in adult rats submitted to a mainly aerobic exercise training schedule on motorized treadmill (30 min/day, 4 days/week for 4 weeks, 55-60% VO_2-max), the heart responded with hypertrophy of pre-existing myocytes as well as with newly formed smaller cardiomyocytes accompanied by neo-angiogenesis. Due to aerobic exercise training, in the same animals the adult-resident endogenous cardiac stem/progenitor cells showed an increased expression

of transcription factors which are indicative of their commitment on both cardiomyocytes and capillary lineages. Moreover, these exercised animals showed, versus sedentary ones, an up-regulation of Insulin-like growth factor-1, neuregulin-1 and bone morphogenic protein-10. Interestingly, all these regulating molecules posses well known growing activity on their target cells. So, molecular and cellular basis of endurance depending on increase of LVEDV seem to be sufficiently explainable.

Concerning detraining effects on cardiac function, in a paper by (Kemi et al., 2004) in which adult rats performed interval training 1h/day, 5day/week, on a 25° inclined treadmill, for 10 weeks (exercise intervals alternated between 8 minutes at about 85% of VO_2max and 2 minutes at about 50%.), exercise detraining has been suggested as the main responsible condition for cellular mechanisms underlying aerobic fitness decrease to reduced cardiomyocyte dimension. In fact, these Authors found that after 4 weeks of detraining both cardiomyocyte width and cardiac weight regressed towards pre-training values as well as fractional shortening and Ca^{2+} sensitivity. It is interesting to underline that, as the consequence of the detraining-induced morphologic and functional decline, a loss of the VO_2max, with respect to its value reached at the top of previous training, was also induced.

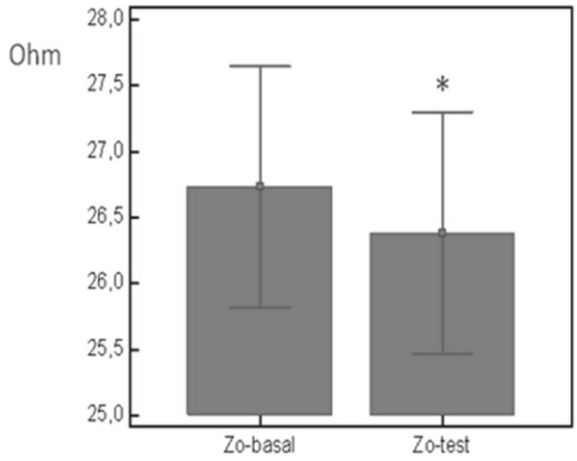

Fig. 7.6 Columns represent mean values of the thoracic electrical impedance (Ohm) respectively before legs compression session (Z_0-basal) and just at the end of the compression session (Z_0-test). Vertical bar in each column

7.3.2. Motion-impaired patients

A group of people with different levels of legs motion impairment, whose proper informed consent was obtained, underwent two cycles of rhythmic leg massages. Feeding air pressure upstream of the system was tuned using the air service unit, and set at 1.5 *bar* at first, then raised to 2.0 *bar* . Pressure levels were chosen so as not to result uncomfortable for the tested subject and about blood pressure values as well. Circuit pressure upstream of each bladder was measured on one leg by means of three 0-15 psi Honeywell 24 PC series piezo-resistive differential pressure gauges with 15 mV/psi sensitivity, one for each cuff, and acquired by means of a NI cDAQ-9172 CompactDAQ chassis equipped with a NI9219 4-channel, 24-bit, analog input module. Operating pressure sensibly drops inside the bladders, reaching values about one order of magnitude smaller than supply values.

7.3.2.1. The device

A system, built by applying three sphygmomanometer cuffs connected to an air supply circuit was used to intermittently compress each leg: one was to massage the patient's foot sole, one his ankle and one his calf. A branch of the two symmetrical twin circuits is shown in figure 7.8.

A sample of acquired circuit pressure values is shown in Fig. 7.7.

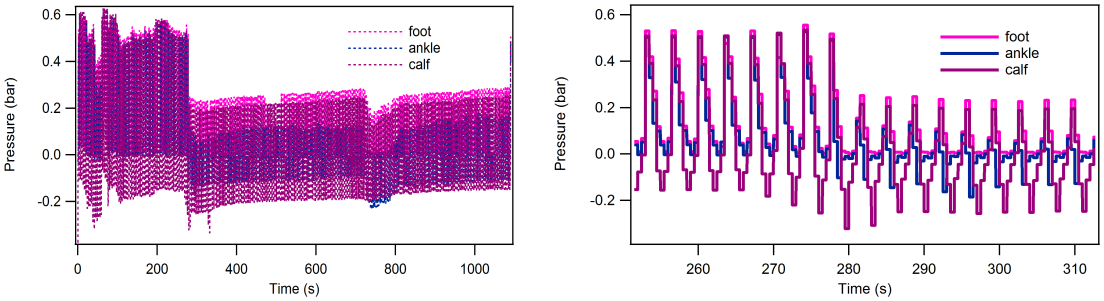

Fig. 7.7. Air pressure vs. time just upstream of each cuff bladder: (a) global trend and (b) detail.

The shown trend highlights some circuit features: first, ejector efficiency, which during deflation brings about a negative relative pressure mostly visible in the calf bladder curve, is stressed with increasing operating pressure, finally overcoming the inflating action and resulting in a minor average effective value; second, the three bladder pressure peak values appear to be in phase even though the solenoid valve on-off law shown in Fig. 7.10 gives out-of-phase commands to them. This can be explained with the very slow circuit dynamics due to the large air volumes; third, a much less steep slope of pressure rate was achieved thanks to the unidirectional flow regulators; it is to be noted that their check valve prevents air from flowing back in the inlet pipe.

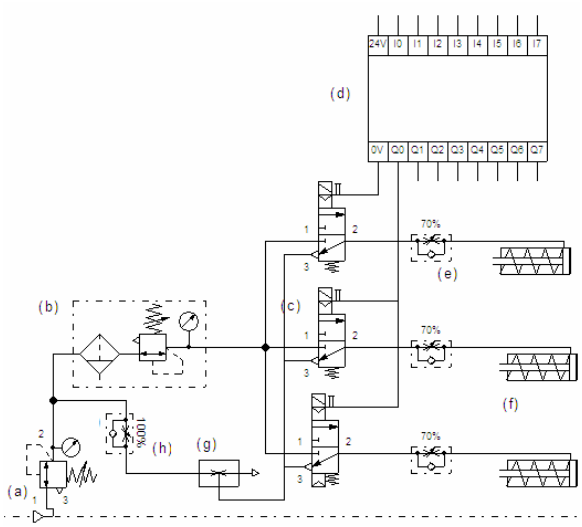

Fig. 7.8. The pneumatic circuit.

Downstream of the air supply (a) an air service unit (b) allows the fine-tuning of the supply pressure as well as filtering the inlet air. Six electro-operated pneumatic flow control solenoid 3/2 valves (c) are piloted by a PLC (d) so as to intermittently inflate the cuffs' bladders (f). Upstream of each bladder an in-line unidirectional flow control regulator (e) to help in smoothing the inflow pressure change thus allowing free outflow. In both the outflow branches collecting way 1 of each valve an in-line Venturi ejector (g) helps deflation, fed by a flow regulator working as a check valve so as not to allow outflow along the checked line

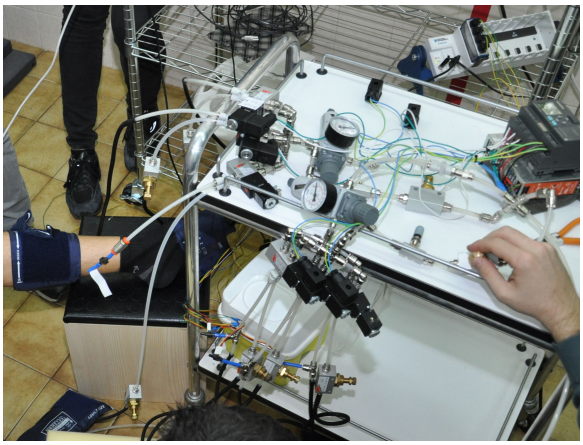

Fig. 7.9. The device under working conditions.

Activation was performed with the foot and calf cuffs in 4 min time segments at about 0.3 Hz frequency (3.5 s period) meaning this a slowly walking person's pace (half a period each step); the on-off timing diagram imposed by the PLC on the solenoids is shown in Fig. 7.10.

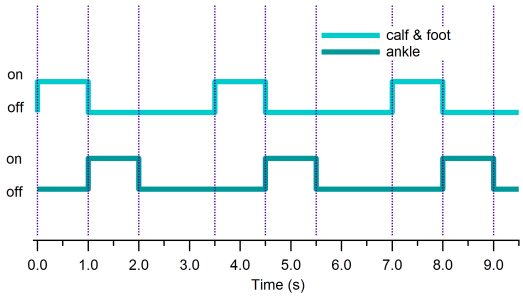

Fig. 7.10. Timing diagram of the electro-valves' on-off law imposed by the PLC.

In Figs. 7.11 to 7.13 the two typical extreme behaviors (i.e. Group 1 and Group 2) for hemodynamic adjustments observed within the tested group are shown and compared.

7.3.2.2. Some clinical remarks

In a normobaric and normoxic environment (i.e. at sea level) oxygen delivery (OD) for an organism having normal hemoglobin values depends on cardiac output (CO, l/min). This is driven, in turn, by the oscillations of hemodynamic variables such as ventricular preload (VP), i.e. the end-diastolic ventricular volume, and myocardial contractility (MC), i.e. the systolic ventricular pressure rate. Both changes in VP and CO lead to an increase in ventricular ejection per stroke (SV, stroke volume). Since heart rate (HR) is constant, this increases CO both in a heterometric (VP) and homeometric (MC) way, finally augmenting the OD.

Impedance cardiography (IC) makes it possible to noninvasively measure VP indicators such as the diastolic filling rate SV/DT (DT diastolic time) and MC indicators, e.g. the PEP/VET (ventricular pre-ejection time/ventricular ejection time) ratio, whose inverse is proportional to intraventricular pressure increment (Concu and Marcello, 1993).

A reduction of the hemodynamic response, which is mainly caused by diastolic deficit, has been detected in paraplegic patients during metaboreflex stimulation. This deficit was, in turn, connected to a VP decrease probably depending on lower limb loss of tonus caused by spinal injury (Crisafulli et al., 2009). In these patients the muscle pump, which would normally compress the larger veins, is lacking mostly at the sural triceps level, whereas in normal subjects it boosts intravenous pressure. Since the subject is in an orthostatic position, the muscle pumping action together with the residual *vis a tergo* counteracts the hydrostatic pressure exerted by the blood column between heart and feet, thus allowing both regular cardiac diastolic flow and VP. Crisafulli et al. showed that the normal activation of hemodynamic adjustments as a response to simulating physical exercise with both a neurophysiological and biochemical metaboreflex stimulation (Crisafulli et al., 2003) was not sufficient since no SV increment was caused and there was no VP and MC ~~to~~ increase either. All this means a chronic diastolic insufficiency for paraplegic patients which leads to an insufficient SV based on its heterometric auto-regulation mechanism, leading in turn to inadequate CO response and then to OD deficiency. Such a condition worsens the life quality of patients as it reduces their oxygen availability.

7.3.2.3. Hemodynamic measurements

In Figs. 7.11 to 7.13 hemodynamic variables are related to applied intermittent massage at different pressures. The two typical extreme average behaviors (i.e. Group 1 and Group 2) for hemodynamic adjustments observed within the tested subjects are shown and compared.

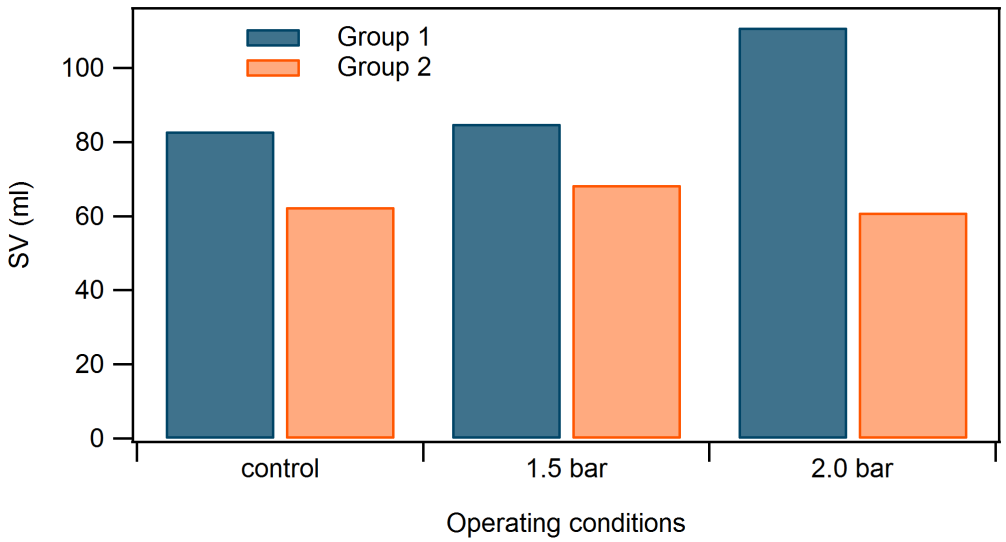

Fig. 7.11. Opposite trends of Stroke Volume (SV) values at different supply pressures: beyond the threshold level the desired effect vanishes for Group 2 subjects.

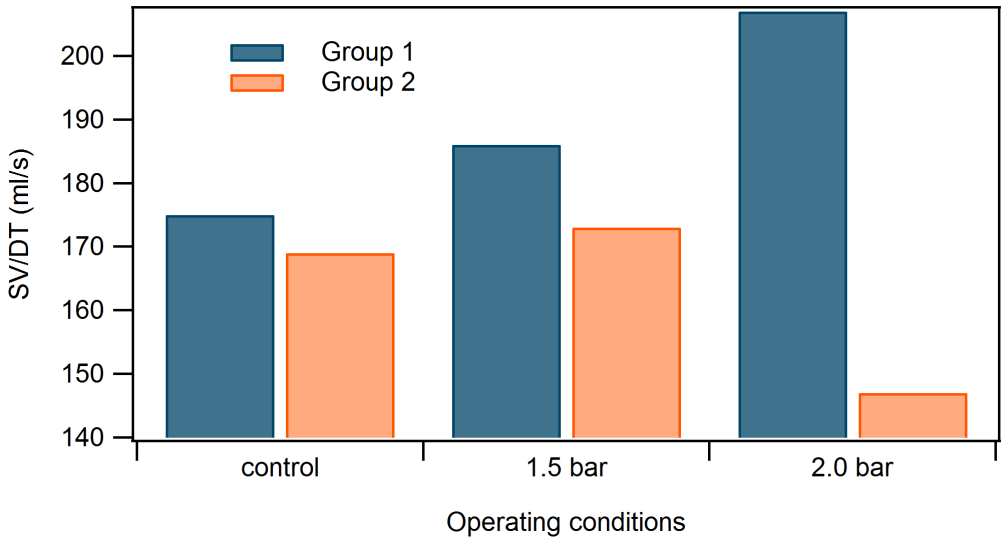

Fig. 7.12. Diastolic filling rate (SV/DT) in the same conditions as in Figs. 7.11, 7.13: expected effects are visible for Group2 people only below the threshold level.

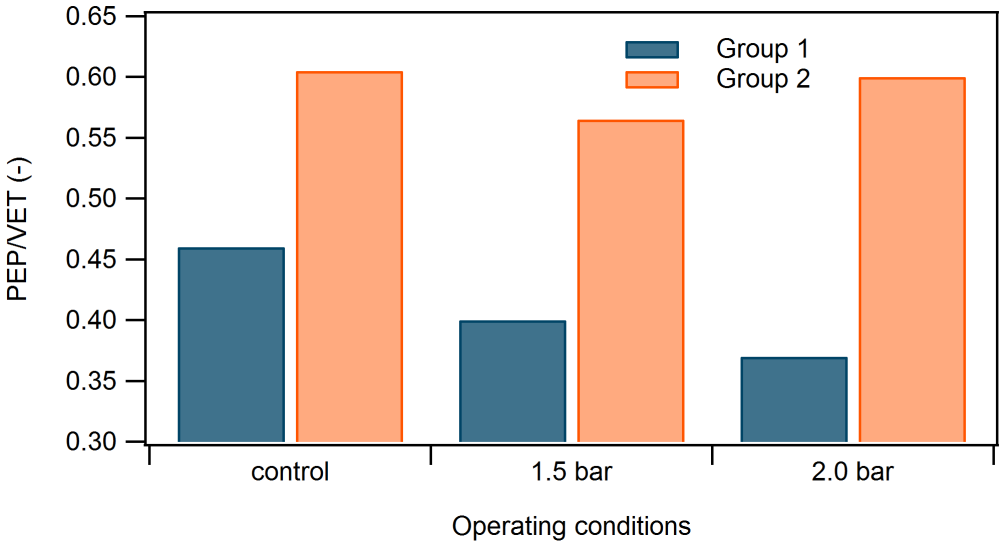

Fig. 7.13: PEP/VET index decreases as expected as a function of applied pressure for Group 1 subjects, showing an inverse trend for too high a pressure value for Group 2 subjects.

The trends of measured indexes for Group 1 subjects are discussed in the following, and compared to correspondent ones for Group 2. In Fig. 7.11 SV values before testing (control) and during device performance are displayed. Actuation was exerted at 1.5 *bar* and 2.0 *bar* upstream of the system: the trend for Group 1 is an increase up to 30% of the control value.

In Figure 7.12 it is clearly seen that these SV increments, caused by the rhythmic foot-calf compression, are tied to the progressive, pressure-dependent increase in diastolic filling rate SV/DT: this hemodynamic variable, describing VP, has a steeper increase reaching 20% at 2.0 *bar*.

Figure 7.13 shows the PEP/VET ratio (which decreases with MC) going for Group 1 rapidly reducing to about a 20% its control value at 2.0 *bar* supply pressure.

Going back to Figure 7.11 above for Group 2 we observe an opposite behavior: the graph shows that after inducing an SV increment by supplying the system at 1.5 *bar*, a reverse trend is conversely observed when supplying at 2.0 *bar*: SV has a negative drop, to less than the control value.

This behavior is consistent with the one shown in Fig. 7.12, where SV/DT slightly increases at 1.5 *bar*, decreasing then at 2.0 *bar* actuation, according to the SV trend as above, except (as it should be) for the reverse slope.

Considering that intraventricular pressure rate depends upon pre-systole stretching degree of myocardic fibers (according to the Frank-Starling mechanism, aka Maestrini law of the heart) we can also explain the PEP/VET reduction (Fig. 7.13) as myocardic fiber length reaching its relative maximum with MC increasing as well, whereas for less stretched fibers (i.e. 2.0 *bar*) PEP/VET reduces roughly to its control value.

7.3.2.4. Discussion

We focused our attention on how such alternate massaging systems can really produce heart efficiency besides the general comfort that makes their diffusion so widespread.

Our observations lead us to believe that the system is effective in increasing both ventricular preload and its resulting ventricular ejection. Nevertheless, the relationship between SV and the pressure pattern imposed by the foot-calf system appears to be a truly complex one and definitely linked to the morpho-functional peculiarities of the subjects. In very simple words, it appears that beyond a threshold

set for each subject the squeezing action acts in a way opposite to the desired one, resulting in a grip holding blood flow and preventing it from restoring end diastolic filling pressure of ventricles, thus improving cardiac output. Detection of each subject's threshold would then be needed before setting operating pressure. By compressing a wider area, for example using two adjacent calf cuffs, may also be helpful in distributing the action on the leg surface.

For this reason, how pressure is to be applied, at which levels, frequency and locations on the legs is still to be investigated.

Another branch of investigation will be the dynamic behavior of the circuit, which must be known and predictable in order to model pressure laws tailoring them to the patients' needs.

8. Conclusions

The results of testing the soft pneumatic devices developed in the framework of this thesis, and the wider research activity as well are very encouraging.

In all tested subjects the monitored hemodynamic variables, significant for heart efficiency (stroke volume, stroke volume rate and ventricular pre-ejection time/ventricular ejection time), underwent positive trends when intermittent massage was applied at increasing feeding pressure.

The tested devices, applying the imposed rythmic massage laws, appear to be effective in altering the chosen hemodynamic parameters drawn by impedance cardiography data. Feeding pressure tuning has been performed to highlight the proper maximum pressure threshold for each subject, and fed back to the proportional valves inserted into the circuit.

As for the design point of view, both small sequential actuators and large, compliant ones are very effective in having their job done. The former are easier to inflate and deflate without introducing too many elements in the circuit. On the other end they need an exoskeleton to constrain their expansion. The bigger ones are stand-alone devices requiring some more design caution and offer a good engineering versatility as for geometry and circuit design.

Some possible future developments are outlined below:

- closing the loop through an EMG signal, or any bio-feedback that can account for pain or discomfort;
- testing of different contact sensors…
- … or designing of an ad hoc one
- modeling the contact surface actuator-skin that can be helpful in predicting or setting any pre-tension threshold;
- pneumatic controlling (PWM)
- tuning of the control system

References

A.M.Taylor, D.M.Pollet, A.Hosseini-Sianaki, C.J.Varley, Advances in an electrorheological fluid based tactile array. Displays **18**, 135–141 (1998)

Abe, R., Takemura, K., Edamura, K. & Yokota, S. (2007). Concept of a micro finger using electro-conjugate fluid and fabrication of a large model prototype. *Sens. Actuators A*, 136:629-637.

AD7147: CapTouch™ (2008). Available at: http://www.analog.com

Alexandru, S., P. Gheorghe and C. Bogdan, 2006. Aspects regarding the neuroadaptive control structure properties application to the nonlinear pneumatic servo system benchmark, Electrotechnics, Electronics, Automatic Control, Informatics, 82-86.

Ali, H. I., Bahari, S., Noor, B. M., Bashi, S. M. & Marhaban, M. H. A Review of Pneumatic Actuators (Modeling and Control). *Aust. J. Basic Appl. Sci.* **3,** 440–454 (2009).

Ali, H. I., Bahari, S., Noor, B. M., Bashi, S. M. & Marhaban, M. H. A Review of Pneumatic Actuators (Modeling and Control). Aust. J. Basic Appl. Sci. 3, 440–454 (2009).

Andorf, P., Franz, D., Lieb, A., Upper, G. & Guttropf,W. (1976). Robot finger. URL: http://www.freepatentsonline.com/3981528.html, R. L. (1971). Gripping device. URL: http://www.freepatentsonline.com/3601442.html

Anitescu, M., Hart, G. D. (2007) Solving Nonconvex Problems of Multibody Dynamics with Joints, Contact, and Small Friction by Successive Convex Relaxation, *Mechanics Based Design of Structures and Machines* 31(3)

Apicella, M., Cogswell, J., Ghobrial, K., Kelly, S. & Peacock, T. The Thin Scale : Phase II Design Team frequently to monitor their weight and general health . Current scales are rigid and bulky , piezoresistive sensors in a silicone enclosure . sensors on the market capable of measuring large forces . These piezoresist.

Arcangelo, M., I.G. Nicola and G. Angelo, 2005. Experimenting and modeling the dynamics of pneumatic actuators controlled by the pulse width modulation (PWM) technique, Mechatronics, 15: 859-881.

Artusi, M. *et al.* Electroactive Elastomeric Actuators for the Implementation of a Deformable Spherical Rover. *IEEE/ASME Trans. MECHATRONICS* **16,** 50–57 (2011).

Artusi, M., Potz, M., Aristizabal, J., Menon, C., Cocuzza, S. & Debei, S. Electroactive Elastomeric Actuators for the Implementation of a Deformable Spherical Rover. *IEEE/ASME Trans. MECHATRONICS* **16,** 50–57 (2011).

Artusi, M., Potz, M., Aristizabal, J., Menon, C., Cocuzza, S. & Debei, S. Electroactive Elastomeric Actuators for the Implementation of a Deformable Spherical Rover. *IEEE/ASME Trans. MECHATRONICS* **16,** 50–57 (2011).

Available at:http://www.soton.ac.uk/~rmc1/robotics/artactile.htm

B. Chang, A. Chew, N. Naghshineh and C. Menon 2012. A spatial bending fluidic actuator: fabrication and quasi-static characteristics, *Smart Materials and Structures,* Vol. **21, pp.** 1-7

B.J. Kane, M.R. Cutkosky, G.T.A. Kovacs, A traction stress sensor array for use in high-resolution robotic tactile imaging. J. Microelectromech. Syst. **9**(4), 425–434 (2000)

B.V.Jayawant, Tactile sensing in robotics.J.Phys.E,Sci.Instrum.**22**,684–692(1989)

Baer, J. I. (1967). Material handling apparatus and the like. URL: http://www.freepatentsonline.com/3343864.html

Baer, J. I. (1975). Fluid motor and material handling apparatus and the like utilizing same. URL: http://www.freepatentsonline.com/RE28663.html

Baiden, D. & Ivlev, O. Human-robot-interaction control for orthoses with pneumatic soft-actuators--concept and initial trails. *IEEE Int. Conf. Rehabil. Robot.* **2013,** 6650353 (2013).

Balasubramanian, S., Huang, H., Member, S., He, J. & Member, S. Quantification of Dynamic Property of Pneumatic Muscle Actuator. in *Eng. Med. Biol. Soc. 2006. EMBS '06. 28th Annu. Int. Conf. IEEE* 2734–2737 (2006). doi:10.1109/IEMBS.2006.259536

Balasubramanian, S., Huang, H., Member, S., He, J. & Member, S. Quantification of Dynamic Property of Pneumatic Muscle Actuator. in *Engineering in Medicine and Biology Society, 2006. EMBS '06. 28th Annual International Conference of the IEEE* 2734–2737 (2006). doi:10.1109/IEMBS.2006.259536

Balasubramanian, S., Huang, H., Member, S., He, J. & Member, S. Quantification of Dynamic Property of Pneumatic Muscle Actuator. in *Engineering in Medicine and Biology Society, 2006. EMBS '06. 28th Annual International Conference of the IEEE* 2734–2737 (2006). doi:10.1109/IEMBS.2006.259536

Bazzi-Grossin, C., Bonnin, P., Bailliart, O., Bazzi, H., A. Kedra, W. & Martineaud, J. P. (1996). Maximal exercise in spinal cord injured subjects: effects of an antigravity suit. *Sci Sports, 11*, 173-179.

Bazzi-Grossin, C., P. Bonnin, O. Bailliart, H. Bazzi, W. A. Kedra, and J.P. Martineaud 1996. Maximal exercise in spinal cord injured subjects: effects of an antigravity suit. *Sci Sports*, Vol. 11, pp.173-179.

Belforte G. (2005) Manuale di Pneumatica, Tecniche Nuove

Belforte G., Manuello Bertetto A., Mazza L., (1998) Pneumatica – Corso completo, Tecniche Nuove

Belforte, G., Mauro, S. & Mattiazzo, G. A method for increasing the dynamic performance of pneumatic servosystems with digital valves. *Mechatronics* **14,** 1105–1120 (2004).

Berliner, E., Ozbilgin, B. & Zarin, D. a. A systematic review of pneumatic compression for treatment of chronic venous insufficiency and venous ulcers. *J. Vasc. Surg. Off. Publ. Soc. Vasc. Surg. (and) Int. Soc. Cardiovasc. Surgery, North Am. Chapter* **37,** 539–44 (2003).

Bertetto, A. M. & Ruggiu, M. In-pipe inch-worm pneumatic flexible robot. in *Adv. Intell.* Mechatronics*, 2001. Proceedings. 2001 IEEE/ASME Int. Conf.* 1226–1231 (2001).

Bertetto, A. M. & Ruggiu, M. In-pipe inch-worm pneumatic flexible robot. in *Advanced Intelligent Mechatronics, 2001. Proceedings. 2001 IEEE/ASME International Conference on* 1226–1231 (2001).

Bertetto, A. M. & Ruggiu, M. In-pipe inch-worm pneumatic flexible robot. in *Advanced Intelligent Mechatronics, 2001. Proceedings. 2001 IEEE/ASME International Conference on* 1226–1231 (2001).

Beyl, P. *et al.* Compliant Actuation in New Robotic Applications. in *Proc. NCTAM06 -- 7th* Natl*. Congr. Theor. Appl. Mech.* (2006).

Beyl, P., Vanderborght, B., Ham, R. Van, Damme, M. Van, Versluys, R. & Lefeber, D. Compliant Actuation in New Robotic Applications. in *Proceedings of the NCTAM06 -- 7th National Congress on Theoretical and Applied Mechanics* (2006).

Bicchi, A. & Tonietti, G. (2004). Fast and "soft-arm" tactics (robot arm design), Robotics Automation Magazine, IEEE 11(2): 22 – 33.

Bird, P.J., 1985. Development in the design and control of pneumatic linear actuators, European Conference on Electrics versus Hydraulics versus Pneumatics, Inst. of Mechanical Engineers, London, In Mechanical Engineering, 77-83.

Birglen, L. & Gosselin, C. M. Fuzzy Enhanced Control of an Underactuated Finger Using Tactile and Position Sensors. *Proc. 2005 IEEE Int. Conf. Robot. Autom.* 2320–2325 doi:10.1109/ROBOT.2005.1570459

Bowns, D.E., and R.L. Ballard, 1972. Digital computational for the analysis of pneumatic actuator systems, Proc. Inst. Mech. Engrs, 186(73): 881-888.

Burrows, C.R. and C.R. Webb, 1970. Further study of a low pressure on-off pneumatic servomechanism, Proc. Inst. Mech. Engrs, 184(45): 849-859.

C. Lebosse, P. Renaud, B. Bayle, and M. de M. Modeling and Evaluation of Low-Cost Force Sensors. *IEEE Trans. Robot.* **27,** 815–822 (2011).

C.Domenici, D.DeRossi, A stress-component-selective tactile sensor array.Sens.Actuators A, Phys. **13**, 97–100 (1992)

Camerota, A. J. (MD; F. F. Intermittent pneumatic compression improves healing of venous leg ulcers.

Camerota, A. J. (MD; F. F., Vibuhuti Chouan, P. & Russel, H. N. The Fibrinolytic Effects of Intermittent Pneumatic Compression. *Ann. Surg.* **226,** 306–314 (1997).

Canghoon, K., H.C. Jae and H. Daehie, 2008. Coordination control of an active pneumatic deburring tool, Robotics and Computer-Integrated Manufacturing, 24: 462-471.

Carducci, G., N.I. Giannoccaro, A. Messina and G. Rollo, 2006. Identification of viscous friction coefficients for a pneumatic system model using optimization methods, Mathematics and Computers Simulation, 71, 385-394

Castro, M. C. & Cliquet, A. A low-cost instrumented glove for monitoring forces during object manipulation. *IEEE Trans. Rehabil. Eng.* **5,** 140–7 (1997).

Chang, B., Chew, A., Naghshineh, N. & Menon, C. A spatial bending fluidic actuator: fabrication and quasi-static characteristics. *Smart Mater. Struct.* **21,** 045008 (2012).

Chang, B., Chew, A., Naghshineh, N. & Menon, C. A spatial bending fluidic actuator: fabrication and quasi-static characteristics. *Smart Mater. Struct.* **21,** 045008 (2012).

Chang, M.-K. & Wu, J.-C. Tracking Control of a 2-DOF Arm Actuated by Pneumatic Muscle Actuators Using Adaptive Fuzzy Sliding Mode Control. *J. Syst. Des. Dyn.* **1,** 257–269 (2007).

Chang, M.-K. & Wu, J.-C. Tracking Control of a 2-DOF Arm Actuated by Pneumatic Muscle Actuators Using Adaptive Fuzzy Sliding Mode Control. *J. Syst. Des. Dyn.* **1,** 257–269 (2007).

Chao, Y.-C., Lai, W.-J., Chen, C.-Y., Meng, H.-F., Zan, H.-W. & Horng, S.-F. Low voltage active pressure sensor based on polymer space-charge-limited transistor. *Appl. Phys. Lett.* **95,** 253306 (2009).

Chen, Y.Y., J. Wang and Q.H. Wu, 2003. A software tool development for pneumatic actuator system simulation and design, Computers in industry, 51: 73-88.

Chitty, A., and T.H. Lambert, 1976. Modeling a loaded two-way pneumatic actuator, ASME, Journal of Measurement and Control, 9, 19-24.

Cho, D. and J.K. Hedrick, 1985. Pneumatic actuators for vehicle active suspension on applications, Journal of Dynamic Systems, Measurement, and Control, 107: 67-72.

Choi, R. *et al.* Soft Actuator for Robotic Applications Based on Dielectric Elastomer : Dynamic Analysis and Applications. in *Proc. 2002 IEEE lntemational Conf. Robot. 8 Autom.* (2002). at <http://ieeexplore.ieee.org/stamp/stamp.jsp?tp=&arnumber=1013722&userType=inst>

Choi, R., Ryew, M., Jung, M., Kim, M., Jeon, J. W. & Nam, J. D. Soft Actuator for Robotic Applications Based on Dielectric Elastomer : Dynamic Analysis and Applications. in *Proceedings of the 2002 IEEE lntemational Conference on Robotics 8 Automation* (2002). at <http://ieeexplore.ieee.org/stamp/stamp.jsp?tp=&arnumber=1013722&userType=inst>

Chou, C. & Hannaford, B. Measurement and modeling of McKibben pneumatic artificial muscles. *Robot. Autom. IEEE Trans.* **12,** 90–102 (1996).

Chou, C. & Hannaford, B. Measurement and modeling of McKibben pneumatic artificial muscles. *Robot. Autom. IEEE Trans.* **12,** 90–102 (1996).

Chou, C. P. & Hannaford, B. (1994, May, 8-13). Static and dynamic characteristics of McKibben pneumatic artificial muscles. IEEE Int. Conf. on Robotics and Automation, San Diego, CA

Chou, C. P. & Hannaford, B. (1996). Measurement and modeling of McKibben pneumatic artificial muscles. *IEEE Trans. on Robotics and Automation* 12(1):90-102.

Clements and Len., 1985. Electro-pneumatic positioners get electronics, Journal of control and Instrumentation, 17: 54-56.

Cocatre-Zilgien, J. H., Delcomyn, F. & Hart, J. M. Performance o f a Muscle-like “Leaky ” Pneumatic Actuator Powered by Modulated Air Pulses. *J. Robot. Syst.* **13,** 379–390 (1996).

Concu A. and C. Marcello 1993.Stroke volume response to progressive exercise in athletes engaged in different types of training. *Eur J Appl Physiol*. Vol. **66**, pp:11-17.

ContiTech AG (2011). ContiTech Luftfedersysteme. URL: http://213.164.133.30/lufecatalog/

Cowan, L.S. and A. Walker 2008. "Soft" Continuum Robots: the Interaction of Continuous and Discrete Elements, *Artificial Life,* Vol. **XI**, pp. 126, 133.

Craig, P. S. & Fisher, J. A. (1989). Grappling device. URL: http://www.freepatentsonline.com/4815782.html

Crisafulli A, R. Milia, S. Vitelli, M. Caddeo, F. Tocco, F. Melis and A. Concu 2009. Hemodynamic responses to metaboreflex activation: insights from spinal cord-injured humans, *Eur. J. Appl. Physiol.,* Vol. **106**, pp. 25-33.

Crisafulli, A., A.C. Scott, R. Wensel, C.H Davos, D.P. Francio, P. Pagliaro, A.J.S. Coats, A. Concu and M.F. Piepoli. 2003. Muscle Metaboreflex-induced Increases in Stroke Volume *Med Sci Sport Exe*. ,Vol. **35**, pp. 221-228.

D. De Rossi, E.P. Scilingo, Skin-like sensor arrays, in *Encyclopedia of Sensors*, vol. X, ed. by C.A. Grimes, E.C. Dickey, M.V. Pishko (American Scientific Publishers, Valencia, 2006), pp. 1–22

D. Um, B. Stankovic, K. Giles, T. Hammond, V.L. Lumelsky, A modularized sensitive skin for motion planning in uncertain environments, in *IEEE International Conference on Robotics and Automation*, Leuven, Belgium (1998), pp. 7–112

D.J. Beebe, A.S. Hsieh, D.D. Denton, R.G. Radwin, A silicon force sensor for robotics and medicine. Sens. Actuators A, Phys. **50**, 55–65 (1995)

D.S.Tawil,D.Rye,M.Velonaki,ImprovedimagereconstructionforanEIT-basedsensitive skin with multiple internal electrodes. IEEE Trans. Robot. **27**(3), 425–435 (2011)

Daerden, F. & Lefeber, D. (2000). Pneumatic artificial muscles: actuators for robotics and automation, European journal of Mechanical and Environmental Engineering 47: 10–21.

Daerden, F., Lefeber, D., Verrelst, B. & Van Ham, R. (2001, July 8-12). Plated pneumatic artificial muscles: actuators for automation and robotics. *IEEE - ASME Int. Conf. On Advanced Intelligent Mechatronics,* Como, Italy.

Dahiya, R. S. & Valle, M. *Robotic Tactile Sensing*. (Springer Netherlands, 2013). doi:10.1007/978-94-007-0579-1

Damme, M. Van, Daerden, F. & Lefeber, D. A Pneumatic Manipulator used in Direct Contact with an Operator. in *Proceedings of the 2005 IEEE International Conference on Robotics and Automation* 4505–4510 (2005).

Damme, M. Van, Vanderborght, B., Ham, R. Van, Matthys, A., Cherelle, P. & Lefeber, D. The Role of Compliance in Robot Safety. *Context*

Davis, G. M., Servedio, G. J., Glaser, R. M., Gupta, S. C. & Suryaprasad, A. G. (1990). Cardiovascular responses to arm cranking and FNS-induced leg exercise in paraplegics. *J. Appl Physiol* 69: 671-677.

De Callafon, R. & Denny, M. Ask The Experts: Desperately Seeking Sensor. *IEEE Control Systems Magazine* 16–17;73 (2011).

De Greef, A., Lambert, P. & Delchambre, A. (2009). Towards flexible medical instruments: review of flexible fluidic actuators. *Precision Eng*. (33):311-321.

de Lavaud, D. S. (1929). Vorrichtung zur Erzeugung eines Über- oder Unterdruckes in Gasen oder Flüssigkeiten.

De Volder, M. & Reynaerts, D. Pneumatic and hydraulic microactuators: a review. *J. Micromechanics Microengineering* **20,** 043001 (2010).

Dela, F., Mohr, T., Jensen, C. M. R., Haahr, H. L., Secher, N. H., Biering-Sørensen, F. & Kjær, M. (2003). *Cardiovascular control during exercise. Insights from spinal cord-injured humans. Circulation* 107:2127-2133.

DeLepeleire, G. A. (1974). Bag diaphragms and bag diaphragm operated air dampers. URL: http://www.freepatentsonline.com/3804364.html

Ding, X. & Selig, J. M. (2003). Dynamic modeling of a compliant arm with 6-dimensional tip forces using screw theory. *Robotica* 21:193-197.

Djordje, D. and N. Novak, 2008. Simulation, animation and program suppot for a high performance pneumatic force actuator system, Mathematical and Computer Modelling.

Dohta, S., Ban, Y. & Matsushita, H. (2000, August 13-17). Application of a flexible strain sensor to a pneumatic rubber hand. *Proc. of the Sixth Triennal International Symposium on Fluid Control, Measurement and Visualization,* Sherbrooke (Qc), Canada.

E. Torres-Jara, I. Vasilescu, R. Coral, A soft touch: compliant tactile sensors for sensitive manipulation. Technical report, CSAIL, Massachusetts Institute of Technology (2006)

E. Torres-Jara, Sensitive manipulation. Ph.D. thesis, Massachusetts Institute of Technology (2007). http://hdl.handle.net/1721.1/36371

E.Cheung, V.L.Lumelsky, A sensitive skin system for motion control of robot arm manipu- lators. Robot. Auton. Syst. **10**, 9–32 (1992)

E.Cheung, V.L.Lumelsky, Proximity sensing in robot manipulation motion planning:system and implementation issues. IEEE Trans. Robot. Autom. **5**(6), 740–751 (1989)

E.M.Reimer,L.Danisch, Pressure sensor based on illumination of a deformable integrating cavity. U.S. Patent 5,917,180 (1999)

E.P.Scilingo, N.Sgambelluri, D.DeRossi, A.Bicchi, Haptic displays based on magnetorheological fluids: design, realization and psychophysical validation, in *The 11th Symposium on Haptic Interfaces for Virtual Environment and Teleoperator Systems (HAPTICS'03)* (2003), p. 10

Edmod, R. and H. Yildirim, 2001. A. high performance pneumatic force actuator system, ASME, Journal of Dynamic Systems, Measurement and Control, 122(3): 416-425.

Eric, J.B., Z. Jianlong and G. Michael, 2002. Sliding mode approach to PWM-controlled pneumatic systems, Proceedings of the American Control Conference, Anchorage, 2362-.

Ewing (1973). Flexible actuator. URL: http://www.freepatentsonline.com/3713685.html

Fernando Vidal-Verdú, Maria Jose Barquero, Julián Castellanos-Ramos, Rafael Navas-González, Jose Antonio Sánchez, J. S. and A. G. A Large Area Tactile Sensor Patch Based on Commercial Force Sensors. *Sensors (Basel).* **11,** 5489–5507 (2011).

Ferraresi, C., Franco, W. & Manuello, A. (1999, May, 26-28,). Straight fibers pneumatic muscle: an actuator with high traction force. *Sixth Scandinavian Int. Conf. on Fluid Power,* Tampere.

Ferraresi, C., Manuello Bertetto, A. & Mazza, L. (1997, May 28-30). Design and Realisation of a Flexible Pneumatic Actuator for Robotics. *5th Scandinavian Int. Conf. on Fluid Power, SICFP '97,* Linkoping, Sweden, 29-43.

Ferre, M., Galiana, I. & Aracil, R. Design of a lightweight, cost effective thimble-like sensor for haptic applications based on contact force sensors. *Sensors (Basel).* **11,** 11495–509 (2011).

Ferris, D. P., Gordon, K. E., Sawicki, G. S. & Peethambaran, A. An improved powered ankle-foot orthosis using proportional myoelectric control. *Gait Posture* **23,** 425–8 (2006).

Ferris, Daniel P. ; Czerniecki, Joseph M.; Hannaford, B. An Ankle-Foot Orthosis Powered by Artificial Pneumatic Muscles. *J Appl Biomech.* **21,** 189–197 (2006).

Festo AG & Co KG (1999). Betätigungseinrichtung.

Festo AG & Co. KG (2009). Fluidic Muscle DMSP/MAS.

French, L.G. and C.S. Cox, 1988. The robust control of a modern electropneumatic actuator, IFAC, Automatic Control In Space.

Freschi, C., Vecchi, F., Micera, S., Sabatini, A. M., Dario, P. & Sacchetti, R. Force Control during Grasp using FES Techniques : Preliminary Results. in *5th Annual Conference of the International Functional Electrical Stimulation Society* 6–9 (2000).

FSR Sensors, Interlink Electronics Inc.(2008). Available at: http://www.interlinkelectronics.com

Fu, S. H. & Cheng, C. in *Manufacturing the Future, Concepts - Technologies - Visions* (ed. Kordic, V.; Lazinica, A. & Merdan, M.) 857–902 (Kordic, V.; Lazinica, A. & Merdan, M., 2006). at <http://www.intechopen.com/search?q=Manufacturing+the+Future>

Fuchs, G. (1994). Faltenbalg.

Fueller, M. *Trunk Manipulator Final Report*. *Systems Technology* 1–14 (2010).

G.L. Kenaley, M.R. Cutkosky, Electrorheological fluid-based robotic fingers with tactile sensing, in *IEEE International Conference on Robotics and Automation*, USA, vol. 1 (1989), pp. 132–136

G.M. Krishna, K. Rajanna, Tactile sensor based on piezoelectric resonance. IEEE Sens. J. **4**(5), 691–697 (2004)

Gaiser, I., Wiegand, R., Ivlev, O., Andres, A., Breitwieser, H., Schulz, S. & Bretthauer, G. in *Smart Actuation and Sensing Systems – Recent Advances and Future Challenges* (ed. Berselli, Giovanni Vertechy, Rocco Vassura, G.) 567–604 (InTechOpen.com, 2012). at <http://www.intechopen.com/books/smart-actuation-and-sensing-systems-recent-advances-and-future-challenges/compliant-robotics-and-automation-with-flexible-fluidic-actuators-and-inflatable-structures>

Gary, M.B. and N. Shu, 2007. Experimental comparison of position tracking control algorithms for pneumatic cylinder actuators, IEEE/ASME Transactions on Mechatronics, 12(5): 557-561.

Gervaso, F., Capelli, C., Petrini, L., Lattanzio, S., Di Virgilio, L. & Migliavacca, F. On the effects of different strategies in modelling balloon-expandable stenting by means of finite element method. *J. Biomech.* **41,** 1206–1212 (2008).

Gordon, K. E. & Ferris, D. P. Learning to walk with a robotic ankle exoskeleton. *J. Biomech.* **40,** 2636–44 (2007).

Gorissen, B., M. De Volder, A. De Greef and D. Reynaerts 2011. Theoretical and experimental analysis of pneumatic balloon microactuators. *Sens. Actuators A* Vol. **168**, pp.58-65.

Granosik, G. & Borenstein, J. Minimizing air consumption of pneumatic actuators in mobile robots. *IEEE Int. Conf. Robot. Autom. 2004. Proceedings. ICRA '04. 2004* 3634–3639 Vol.4 (2004). doi:10.1109/ROBOT.2004.1308820

Granosik, G. in *Bioinspiration and Robotics: Walking and Climbing Robots* (ed. Habib, M. K.) (I-Tech, 2007).

Grating, P. F. B., Zhang, Y., Feng, D., Liu, Z., Guo, Z., Dong, X., Chiang, K. S. & Chu, B. C. B. High-Sensitivity Pressure Sensor Using a Shielded. *Technology* **13,** 618–619 (2001).

H. Alirezaei, A. Nagakubo, Y. Kuniyoshi, A highly stretchable tactile distribution sensor for smooth surfaced humanoids, in *7th IEEE-RAS International Conference on Humanoid Robots*, Pittsburgh, USA (2007)

H. Shinoda, K. Matsumoto, S. Ando, Tactile sensing based on acoustic resonance tensorcell, in *Proceedings of TRANSDUCERS 1997, International Conference Solid-State Sensors and Actuators* (1997), pp. 129–132

H. Takao, K. Sawada, M. Ishida, Monolithic silicon smart tactile image sensor with integrated strain sensor array on pneumatically swollen single-diaphragm structure. IEEE Trans. Electron Devices **53**(5), 1250–1259 (2006)

H. Yussof, J. Takata, M. Ohka, Measurement principles of optical three-axis tactile sensor and its application to robotic fingers system, in *Sensors: Focus on Tactile, Force and Stress Sensors*, ed. by J.G. Rocha, S. Lanceros-Mendez (I-Tech Publishers, Vienna, 2008), pp. 123– 142

H. Zhang, E. So, Hybrid resistive tactile sensing. IEEE Trans. Syst. Man Cybern., Part B, Cybern. **32**(1), 57–65 (2002)

H.-K. Lee, S.-I. Change, E. Yoon, A flexible polymer tactile sensor: fabrication and mod- ular expandability for large area deployment. J. Microelectromech. Syst. **15**(6), 1681–1686 (2006)

H.Liu, P.Meusel, G.Hirzinger, A tactile sensing system for the DLR three-finger robot hand, in International *Symposium on Measurement and Control in Robotics* (1995), pp. 91–96

H.R. Nicholls, M.H. Lee, A survey of robot tactile sensing technology. Int. J. Robot. Res. **8**(3), 3–30 (1989)

Ham, B. Y. R. V. A. N., Sugar, T. G., Vanderborght, B., Hollander, K. W. & Lefeber, D. Compliant Actuators Designs Review of Actuators with Passive Adjustable Compliance/Controllable Stiffness for Robotic Applications. *IEEE Robotics & Automation Magazine* 81–94 (2009). doi:10.1109/MRA.2009.933629

Ham, R. Van, Daerden, F., Verrelst, B., Lefeber, D. & Vandenhoudt, J. Control of Pneumatic Artificial Muscles with Enhanced Speed Up Circuitry . in *Proceedings of the 5th International conference on Climbing and Walking Robots and the Support Technologies for Mobile Machine* (2002). at <http://mech.vub.ac.be/multibody/publications.htm>

Han K.L., S.C. Gi and H.C. Gi, 2002. A study on tracking position control of pneumatic actuators, Mechatronics, 12: 813-831.

Hannaford, B. Static and dynamic characteristics of McKibben pneumatic artificial muscles. *Proc. 1994 IEEE Int. Conf. Robot. Autom.* 281–286 (1994). doi:10.1109/ROBOT.1994.350977

Hannan, M. W. & Walzer, I. D. (2001). Analysis and experiments with an Elephant's Trunk Tobot. *The Int. J. of the Robotics society of Japan,* 15(8):847-858.

Hannan, M. W. and I. D. Walker 2003. Kinematics and the implementation of an elephant's trunk manipulator and other continuum style robots, *Journal of Robotic Systems*, Vol. **20**, No. 2, pp. 45-63

Hills, N.H., Pflug, J.J., Jeyasingh, K., Boardman. L. & Calnan. J.S. (1972). Prevention of deep vein thrombosis by intermittent pneumatic compression of calf. *Br Med J.* 1:131-135.

Hirai, S., Cusin, P., Tanigawa, H., Masui, T., Konishi, S. & Kawamura, S. (2000). Qualitative Syn-thesis of Deformable Cylindrical Actuators through Constraint Topology. *Proc. of the 2000 IEEE/RSJ int. Conf. on Int. Robots and Systems,* Kagawa, Japan.

Hollinger, A. & Wanderley, M. M. Evaluation of Commercial Force-Sensing Resistors. 1–4 (2006).

Holzapfel, G. a. & Gasser, T. C. Finite element modeling of balloon angioplasty by considering overstretch of remnant non-diseased tissues in lesions Finite element modeling of balloon angioplasty by considering overstretch of remnant non-diseased tissues in lesions. *Comput. Mech.* (2006).

Hopman, M. T. E. (1994). Circulatory responses during arm exercise in individuals with parap-legia. *Int J Sports Med*, 15:126-131.

Ilievski, F., Mazzeo, A. D., Shepherd, R. F., Chen, X. & Whitesides, G. M. (2011). Soft robotics for chemists, Angewandte Chemie International Edition 50(8): 1890–1895. URL: http://dx.doi.org/10.1002/anie.201006464

Ingold, J.B. and J.K. Tice, 1988. Development of an electro-pneumatic system for prestarified charge emission control, (PSC), Proceedings of Energy Source Technology Conference and Exhibition, USA.

Ivlev, O. (2009). Soft fluidic actuators of rotary type for safe physical human-machine interaction, Rehabilitation Robotics, 2009. ICORR 2009. IEEE International Conference on, pp. 1 –5.

J. Dargahi, M. Parameswaran, S. Payandeh, A micromachined piezoelectric tactile sensor for an endoscopic grasper—theory, fabrication and experiments. J. Microelectromech. Syst. **9**(3), 329–335 (2000)

J. Dargahi, S. Najarian, Advances in tactile sensors design/manufacturing and its impact on robotics applications—a review. Ind. Robot **32**, 268–281 (2005)

J.-S. Heo, J.-H. Chung, J.-J. Lee, Tactile sensor arrays using fiber Bragg grating sensors. Sens. Actuators A, Phys. **126**, 312–327 (2006)

J.-S. Heo, J.-Y. Kim, J.-J. Lee, Tactile sensors using the distributed optical fiber sensors, in *Proceedings of the 3rd International Conference on Sensing Technology* (2008), pp. 486–490

J.D. Carlson, S.P. Koester, Magnetically-controllable active haptic interface system and apparatus. U.S. Patent 6,283,859 B1

J.Winger,K.-M.Lee,Experimentalinvestigationofatactilesensorbasedonbendinglosses in fiber optics, in *Proceedings of the IEEE International Conference on Robotics and Automation*, Raleigh, North Carolina, USA (1988), pp. 754–759

Jacobs, P. L., Mahoney, E. T., Robbins, A. & Nash, M. (2002). Hypokinetic circulation in persons with paraplegia. *Med Sci Sports Exerc.* 34:1401-1407.

Jeong, O. C. & Konishi, S. (2006). All PDMS pneumatic microfinger with bidirectional motion and its application. *J. Microelectromech. Syst*. 15(4):896-903.

Jeyasingh, K., Boardman, L. & Calnan, J. S. Prevention of Deep Vein Thrombosis by Intermittent Pneumatic Compression of Calf. *Br. Med. J.* 131–135 (1972).

Jihong, W., K. Ulle and K. Jia, 2007. Tracking control of nonlinear pneumatic actuator systems using static state feedback linearization of the input-output map,

Proceedings Estonian Academic Science of Physics and Mathematics, 56: 47-66.

Jihong,, W., P. Junsheng and M. Philip, 1999. Accurate position control of servo pneumatic actuator systems: an application to food packaging, Control Engineering Practice, 7: 699-706.

Joachim, S. and E. Duygun, 2003. Dynamic pneumatic actuator model for a model-based torque controller, Proceedings IEEE International Symposium on Computational Intelligence in Robotics and Automation, Kobe, Japan, 342-347.

Johnston, L. B. (1965). Fluid actuated displacement and positioning system. URL: http://www.freepatentsonline.com/3202061.html

Junbo, S. and I. Yoshihisa, 1997. Robust tracking controller design for pneumatic servo system, International Journal of Engineering Science, 35(10/11): 905-920.

K. Hosoda, Y. Tada, M. Asada, Anthropomorphic robotic soft fingertip with randomly distributed receptors. Robot. Auton. Syst. **54**, 104–109 (2006)

K. Nakamura, H. Shinoda, A tactile sensor instantaneously evaluating friction coefficients, in Proceedings *of TRANSDUCERS 1997, International Conference Solid-State Sensors and Actuators* (1997), pp. 1430–1433

K. Weiss, H. Worn, Tactile sensor system for an anthropomorphic robotic hand, in *IEEE International* Conference *on Manipulation and Grasping*, Genoa, Italy (2004)

Kalamdani, A., Messom, C. & Siegel, M. Tactile Sensing by the Sole of the Foot Part II : Calibration and Real-time Processing. in *3rd International Conference on Autonomous Robots and Agents 2006* 1–6 (2006).

Kanellos, G. T., Papaioannou, G., Tsiokos, D., Mitrogiannis, C., Nianios, G. & Pleros, N. Two dimensional polymer-embedded quasi-distributed FBG pressure sensor for biomedical applications. *Opt. Express* **18,** 179–86 (2010).

Kang, B., Kothera, C. S., Woods, B. K. S. & Wereley, N. M. Dynamic Modeling of Mckibben Pneumatic Artificial Muscles for Antagonistic Actuation. in *IEEE International Conference on Robotics and Automation* 182–187 (2009). at <http://ieeexplore.ieee.org/xpls/abs_all.jsp?arnumber=5152280>

Karim, K., B. Pascal and A.D. Louis, 2008. Force control loop affected by bounded uncertainties and unbounded inputs for pneumatic actuator systems, ASME, Journal of Dynamic Systems, Measurement, and Control, 130: 1-9.

Khayati, K., Bigras, P., Dessaint, L. & Member, S. A Multistage Position / Force Control for Constrained Robotic Systems With Friction : Joint-Space Decomposition , Linearization , and Multiobjective Observer / Controller Synthesis Using LMI Formalism. **53,** 1698–1712 (2006).

Kinnunen, J. & Rahikka, V. *Ceilbot in home environment*. *Wire* at <http://autsys.tkk.fi/en/attach/Ceilbot/Hometeam_report-fix.pdf>

Konishi, S., Kawai, F. & Cusin, P. (2001). Thin flexible end-effector using pneumatic balloon ac-tuator. *Sens. Actuators A* 89:28-35.

Kotovsky, J., Tooker, A. & Horsley, D. Thin Silicon MEMS Contact-Stress Sensor. in *Hilton Head Solid-State Sensors, Actuators, and Microsystems Workshop 2010* (2010).

Kroll, A. & Schulte, H. Benchmark problems for nonlinear system identification and control using Soft Computing methods: Need and overview. *Appl. Soft Comput.* **25,** 496–513 (2014).

Kumar, V., Rahman, T. & Krovi, V. Assistive Devices For People With Motor Disabilities. *Mech. Eng.* (1997). at <http://www.wtec.org/robotics/us_workshop/June22/Wiley.pdf>

Kwak, B. M. & Lee, C. W. (2009). Contact Analysis by Shape Optimization (CASO), *Mechanics Based Design of Structures and Machines: An International Journal.* 37(2):113-142.

L.D.Harmon, Automated tactile sensing.Int.J.Robot.Res.**1**(2),3–31(1982)

Lachmann, E. A., Rook, J. L., Tunkel, R. & Nagler, W. Complications associated with intermittent pneumatic compression devices. in *the American Congress of Rehabilitation Medicine, and the American Academy of Physical Medicine and Rehabilitation* **93,** 1556–7 (1992).

Lachmann, E.A., Rook J.L., Tunkel, R. & Nagler, W. (1992). Complications associated with intermittent pneumatic compression. *Arch Phys Med Rehabil*. 73:482-5.

Larsson, Ove (Gothenburg, S. (1988). Flexible actuator. URL: http://www.freepatentsonline.com/4777868.html

Leitman, M. J. & Villaggio, P. (2006). The Dynamics of a Membrane Shock-Absorber , *Mechanics Based Design of Structures and Machines: An International Journal*. 34(3):277-292.

Lewis, D. J. (1974). Fiber reinforced inflatable restraining band for vehicles. URL: http://www.freepatentsonline.com/3830519.html

Lichtwark, G. a & Wilson, a M. Is Achilles tendon compliance optimised for maximum muscle efficiency during locomotion? *J. Biomech.* **40,** 1768–75 (2007).

Lightwave, J. re grating pressure sensor with enhanced sensitivity using a glass-bubble housing. *Electron. Lett.* **32,** 128–129 (1996).

Lilly, J. H. Adaptive tracking for pneumatic muscle actuators in bicep and tricep configurations. *IEEE Trans. Neural Syst. Rehabil. Eng.* **11,** 333–9 (2003).

L. Ljung, *System Identification Toolbox User's Guide*, 2003 The MathWorks, Inc.

Ljung, L. Some classical and some new ideas for identification of linear systems. *J. Control. Autom. Electr. Syst.* **24,** 3–10 (2013).

Lu, Y.-W., Kim, C. J. (2009). Microhand for biological applications, *Appl. Phys. Lett.,* 89:164101-164103.

M. Ohka, H. Kobayashi, J. Takata, Y. Mitsuya, Sensing precision of an optical three-axis tactile sensor for a robotic finger, in *15th International Symposium on Robot and Human Interactive Communication "RO-MAN"* (2006), pp. 214–219

M. Shimojo, A. Namiki, M. Ishikawa, R. Makino, K. Mabuchi, A tactile sensor sheet using pressure conductive rubber with electrical-wires stitched method. IEEE Sens. J. **4**(5), 589– 596 (2004)

M.A. Diftler, R. Platt Jr., C.J. Culbert, R.O. Ambrose, W.J. Bluethmann, Evolution of the NASA/DARPA robonaut control system, in *IEEE International Conference on Robotics and Automation* (2003), pp. 2543–2548

M.E.H.Eltaib, J.R.Hewit, Tactile sensing technology for minimal access surgery—a review. Mechatronics **13**, 1163–1177 (2003)

M.H.Lee,H.R.Nicholls, Tactile sensing for mechatronics—a state of the art survey. Mechatronics **9**, 1–31 (1999)

M.Maggiali, G.Cannata, P.Maiolino, G.Metta, M.Randazzao, G.Sandini, Embedded tactile sensor modules, in *11th Mechatronics Forum Biennial International Conference*, Limerick, Ireland (2008)

M.R.Cutkosky, R.D.Howe ,W.Provancher, Force and tactile sensors, in *Springer Handbook of Robotics*, ed. by B. Siciliano, O. Khatib (Springer, Berlin, 2008), pp. 455–476

M.R.Wolffenbuttel, P.P.L.Regtien, Polysilicon bridges for the realization of tactile sensors. Sens. Actuators A, Phys. **A2**(1–3), 257–264 (1991)

Macia, N. Thaler, G. J., Modeling and Control of Dunamic Systems, Cengage Learning, 2005

Manuello Berretto A. and M. Ruggiu 2001. In-pipe inch-worm pneumatic flexible robot, *2001 IEEE-ASME International Conference on Advanced Intelligent Mechatronics Proceedings*, 6-12 July Como, Italy, pp. 1226-1231.

Manuello Bertetto A., S. Meili, A. Concu and A. Crisafulli 2011. Flexible Pneumatic Actuation For Blood Pressure Recovery, *Proc. Of Musme 2011, The International Symposium On Multibody Systems And Mechatronics*, Valencia, Spain, 25-28 October, pp. 359- 370.

Manuello Bertetto A., S. Meili, A. Concu and A. Crisafulli 2012. An inflatable pneumatic device for blood pressure recovery, accepted for publication on *Mechanics based design of structures and machines* (DOI 10.1080/15397734.2012.687312)

Manuello Bertetto, A. & Ruggiu, M. (2002, November, 12-15). Pole Climbing Pneumatic Robot. *Proc. of the Fifth JFPS International Symposium on Fluid Power,* Nara, Japan.

Manuello Bertetto, A. & Ruggiu, M. (2004). Characterization and modeling of air muscles, *Me-chanics Research Communications* 31:185-194.

Manuello Bertetto, A., M. Ruggiu 2004. A Novel Fluidic Bellows Manipulator. *Journal of Robotics and Mechatronics*, Vol.**16**, No.6, pp. 604-612

Manunza, I., Sulis, a. & Bonfiglio, a. Pressure sensing by flexible, organic, field effect transistors. *Appl. Phys. Lett.* **89,** 143502 (2006).

Marette, R. T. (1961). Actuator. URL: http://www.freepatentsonline.com/2991763.html

Margineanu, D., Perju, D. , Lovasz, E. -C., Vacarescu, V. & Ciupe, (2008).. Consideration about one type of adaptive intelligent brace. *Buletin of the of the Transilvania University of Brasov*, (15):213-218.

Marumo, R. & Tokhi, M. O. Intelligent modeling and control of a pneumatic motor. in *Electrical and Computer Engineering, 2004. Canadian Conference on (Volume:2)* 1163 – 1166 (IEEE Comput. Soc. Press, 2004). doi:10.1109/CCECE.2004.1345327

Midorikawa, Y. & Nakamura, T. Variable Rheological Joints Using an Artificial Muscle Soft Actuator and Magneto-Rheological Fluids Brake. in *Intelligent Robotics and Applications: Second International Conference, ICIRA 2009* (ed. Xie, D. M.) 504–514 (Springer, 2009).

Monroe, JohnW. (Warren,M. (1994). Jointed assembly actuated by fluid pressure. URL: http://www.freepatentsonline.com/5351602.html

Morin, A. H. (1953). Elastic diaphragm. URL: http://www.freepatentsonline.com/2642091.html

Negishi, Koichi (Kodaira, J. (1991). Double-acting flexible wall actuator. URL: http://www.freepatentsonline.com/5067390.html (93)

Noritsugu, T., Kubota, M. & Yoshimatsu, S. (2000). Development of pneumatic rotary soft actua-tor. *Transactions of the Japan Society of Mechanical Engineers, Series C* 66:2280-2285.

O'Brien, D. J. & Lane, D. M. (2001, May, 21-26). 3D force control system design for a hydraulic parallel bellows continuum actuator. *Proc. of the 2001 IEEE International conference on Robotics & Automation,* Seoul, Korea.

Otto, J. K., Brown, T. D. & Callaghan, J. J. Static and Dynamic Response of a Multiplexed-array Piezoresistive Contact Sensor. *Exp. Mech.* **39,** 317–323

P. Dario, D. de Rossi, Tactile sensors and gripping challenge. IEEE Spectr. **22**(8), 46–52 (1985)

P. Dario, G. Buttazzo, An anthropomorphic robot finger for investigating artificial tactile perception. Int. J. Robot. Res. **6**(3), 25–48 (1987)

P. Puangmali, K. Althoefer, L.D. Seneviratne, D. Murphy, P. Dasgupta, State-of-the-art in force and tactile sensing for minimally invasive surgery. IEEE Sens. J. **8**, 371–381 (2008)

P. Svyatoslav, Touch screen control and calibration—four-wire, resistive. Application Note AN2173, Cypress Microsystems (2004)

P.A. Schmidt, E. Mael, R.P. Wurtz, A sensor for dynamic tactile information with applications in human–robot interaction & object exploration. Robot. Auton. Syst. **54**, 1005–1014 (2006)

Pack, R. T., Christopher, J. L. Jr. & Kawamura, K. (1997, April, 20-25). A rubbertuator-based structure-climbing inspection robot. *IEEE Int. Conf. on Robotics and Automation,* Albuquerque, New Mexico

Palmer, M. C., Rourke, T. D. O., Olson, Nathaniel A., Abdoun, T., Ha, D. & Rourke, M. J. O. Tactile Pressure Sensors for Soil-Structure Interaction Assessment. *J. Geotech. GEOENVIRONMENTAL Eng.* 1638–1646 (2009).

Parry, D. & Brown, R. (1959). The hydraulic mechanism of the spider leg. *J. Exp. Biol.,* (36):423-433.v

Paugh, B. & Sterry, K. Getting a (Gentle) Grip. *MachineDesign.com* (2007). at <http://machinedesign.com/archive/getting-gentle-grip>

Paugh, B. & Sterry, K. Getting a (Gentle) Grip. *MachineDesign.com* (2007). at <http://machinedesign.com/archive/getting-gentle-grip>

Paynter, H.M. (1974). Tension actuated pressurized gas driven rotary motors. URL: http://www.freepatentsonline.com/3854383.html

Paynter, Henry M. (35 Scotland Rd., R. M. . (1988a). High pressure fluid-driven tension actuators and method for constructing them. URL: http://www.freepatentsonline.com/4751869.html

Paynter, Henry M. (35 Scotland Rd., R. M. . (1988b). Hyperboloid of revolution fluid-driven tension actuators and method of making. URL: http://www.freepatentsonline.com/4721030.html

Pelrine, R. E., Kornbluh, R. D. & Joseph, J. P. Electrostriction of polymer dielectrics with compliant electrodes as a means of actuation. **64,** 77–85 (1998).

Pelrine, R., Kornbluh, R., Pei, Q., Stanford, S., Oh, S., Eckerle, J., Full, R., Rosenthal, M., *et al.* Dielectric Elastomer Artificial Muscle Actuators : Toward Biomimetic Motion. *Struct. Mater.* **4695,** 126–137 (2002).

Peratech Ltd., UK Patent PCT/GB98/00206 (WO 98/33193) Available at: http://www. peratech.co.uk

Pitetti, K. H., P. J. Barrett, K.D. Campbell and D.E. Malzahn 1994. The effect of lower body positive pressure on the exercise capacity of individuals with spinal cord injury. *Med Sci Sports Exerc,* Vol. **26**, pp. 463-468.

Pressure sensitive ink (2008). Available at:http://www.tekscan.com/

Prior, S.,Warner, P., White, A., Parsons, J. & Gill, R. (1993). Actuators for rehabilitation robots, Mechatronics 3(3): 285 – 294. Special Issue Robot Actuators. URL: http://www.sciencedirect.com/science/article/B6V43-47YVPRC-3/2/0a2fb2c92d4ec09d 6493c32cdf2ed09e

Qinghua, Y., Guanjun, B., Libin, Z. & Jian, R. Analysis and simulation of dynamic characteristics of flexible pneumatic actuator FPA. *2006 IEEE Int. Conf. Mechatronics Autom. ICMA 2006* **2006,** 1817–1821 (2006).

R.C.Luo,F.Wang,Y.Liu,Animagingtactilesensorwithmagnetorestrictivetransduction, in *Robot Sensors*, vol. 2, ed. by A. Pugh (Springer, Berlin 1985), pp. 113–122

R.D. Howe, Tactile sensing and control of robotics manipulation. Adv. Robot. **8**, 245–261 (1994)

R.D.Howe, M.R.Cutkosky, Dynamic tactile sensing: perception of fine surface features with stress rate sensing. IEEE Trans. Robot. Autom. **9**, 140–151 (1993)

R.M.Voyles, G.Fedder, P.K.Khosla, Design of a modular tactile sensor and actuator based on an electrorheological gel, in *IEEE International Conference on Robotics and Automation*, USA, vol. 1 (1996), pp. 13–17

R.S. Dahiya, G. Metta, G. Cannata, M. Valle, Guest editorial special issue on robotic sense of touch. IEEE Trans. Robot. **27**, 385–388 (2011)

R.S. Dahiya, G. Metta, M. Valle, G. Sandini, Tactile sensing—from humans to humanoids. IEEE Trans. Robot. **26**, 1–20 (2010)

R.S. Dahiya, M. Valle, G. Metta, L. Lorenzelli, POSFET based tactile sensor arrays,in *IEEE ICECS'07: The 14th International Conference on Electronics, Circuits and Systems*, Marrakech, Morocco (2007), pp. 1075–1078

R.S. Dahiya, M. Valle, L. Lorenzelli, Spice model of lossy piezoelectric polymers. IEEE Trans. Ultrason. Ferroelectr. Freq. Control **56**(2), 387–396 (2009)

Raparelli, T., Durante, F. & Beomonte Zobel, P. (1999). *Numerical modelling and experimental validation of a pneumatic muscle actuator.* Fourth JHPS, Int. Symp on Fluid PowerTokyo _99, Tokio

Repperger, D.W. ;Phillips, C.A. ; Krier, M. Controller design involving gain scheduling for a large scale pneumatic muscle actuator. in *Control Applications, 1999. Proceedings of the 1999 IEEE International Conference on* 285–290 (1999).

Reynolds, D. B., Repperger, D. W., Phillips, C. a. & Bandry, G. Modeling the Dynamic Characteristics of Pneumatic Muscle. *Ann. Biomed. Eng.* **31,** 310–317 (2003)

Richer, E. & Hurmuzlu, Y. A High Performance Pneumatic Force Actuator System Part 1 - Nonlinear Mathematical Model ∗. *ASME J. Dyn. Syst. Meas. Control* **122,** 416–425 (2001).

RITA MARIA CÂNDIDO, B. M. Development of a Control Architecture for a Musculoskeletal Model of the Human Ankle Joint Using Multibody Dynamics and Hill-Type Muscle Actuators R ITA M ARIA C ÂNDIDO B OAVIDA M ALCATA Dissertação para obtenção do Grau de Mestre em E NGENHARIA B IOMÉDIC. *Control* (Universidade de Lisboa, 2009). at <https://dspace.ist.utl.pt/bitstream/2295/578436/1/Tese_versao_55752.pdf>

Robinson, G. & Davies, J. B. C. Continuum robots - a state of the art. *Proc. 1999 IEEE Int. Conf. Robot. Autom. (Cat. No.99CH36288C)* **4,** 2849–2854 (1999).

Robinson, G. & Davies, J. B. C. Continuum robots - a state of the art. *Proc. 1999 IEEE Int. Conf. Robot. Autom. (Cat. No.99CH36288C)* **4,** 2849–2854 (1999).

Roboskin Project(2010).Available at: http://www.roboskin.eu/

RoboTouch(2007).Availableat:http://www.pressureprofile.com

Rodrigo, S. E., Ambrósio, J. A. C., Tavares da Silva, M. P. & Penisi, O. H. (2008): Analysis of Human Gait Based on Multibody Formulations and Optimization Tools , *Mechanics Based Design of Structures and Machines: An International Journal*, 36(4):446-477.

Rogers, C., Tseng, D. Y., Squire, J. C. & Edelman, E. R. Design as Contributors to Vascular Injury. *October* 378–383 (1999). doi:10.1161/01.RES.84.4.378

S. Ando, H. Shinoda, A. Yonenaga, J. Terao, Ultrasonic six-axis deformation sensing. IEEE Trans. Ultrason. Ferroelectr. Freq. Control **48**(4), 1031–1045 (2001)

S. Ando, H. Shinoda, Ultrasonic emission tactile sensing. IEEE Control Syst. Mag. **15**(1), 61–69 (1995)

S. Omata, Y. Murayama, C.E. Constantinou, Real time robotic tactile sensor system for the development of the physical properties of biomaterials. Sens. Actuators A, Phys. **112**(2–3), 278–285 (2004)

S.C. Jacobsen, I.D. McCammon, K.B. Biggers, R.P. Phillips, Design of tactile sensing sys- tems for dextrous manipulators. IEEE Control Syst. Mag. **8**, 3–13 (1988)

Saldien, J., Goris, K., Vanderborght, B., Verrelst, B., Ham, R. Van & Lefeber, D. ANTY : The development of an intelligent huggable robot for hospitalized children. in *9th International Conference on Climbing and Walking Robots and the Support Technologies for Mobile Machines, Proceedings}* 123–128 (2006). at <http://hdl.handle.net/1854/LU-3093456>

Schulte Jr, H. F. (1961). The characteristics of the McKibben artificial muscle. *Application of external power in prosthetics and orthotics.* Nat. Acad. Sci. Nat. Res. Council, Washington DC.

Schultz, S., Pylatiuk, C. & Bretthauer, G. (2001, May 21-26). A new ultra light anthropomorphic hand. *Proc. of the 2001 IEEE Int. Conf. on Robotics & Automation*, Seoul, Korea.

Schulz, S. (2004b). Vorrichtung mit fluidischem schwenkantrieb.

Schwörer, M., Kohl, M. & Menz, W. (1998). Fluidic microjoints based on spider legs, *Proc. Actuator 98*:103-106.

Sfakiotakis, M., Lane, D. M. & Davies, B. C. (2001, May 21-26). An experimental undulating-fin device using the parallel bellows actuators. *Proc. of the 2001 IEEE International conference on Robotics & Automation*, Seoul, Korea.

Shaw, A. J., Davis, B. a, Collins, M. J. & Carney, L. G. A technique to measure eyelid pressure using piezoresistive sensors. *IEEE Trans. Biomed. Eng.* **56,** 2512–7 (2009).

Shin, D., Khatib, O.& Cutkosky,M. (2009). Design methodologies of a hybrid actuation approach for a human-friendly robot, Robotics and Automation, 2009. ICRA '09. IEEE International Conference on, pp. 4369 –4374.

Sigmon, J.W. (1976). Rotary motion valve and actuator. URL: http://www.freepatentsonline.com/3977648.html

Slatkin, A. B. & Burdick, J. (1995, August 05-09). Development of a robotic endoscope. *Proceedings of the International Conference on Intelligent Robots and Systems*, Pittsburgh, Pennsylvania, USA.

Slatkin, a. B., Burdick, J. & Grundfest, W. The development of a robotic endoscope. *Proc. 1995 IEEE/RSJ Int. Conf. Intell. Robot. Syst. Hum. Robot Interact. Coop. Robot.* **2,** 162–171 (1995).

Someya, T., Sekitani, T., Iba, S., Kato, Y., Kawaguchi, H. & Sakurai, T. A large-area, flexible pressure sensor matrix with organic field-effect transistors for artificial skin applications. *Proc. Natl. Acad. Sci. U. S. A.* **101,** 9966–70 (2004).

Staines, A. J. (1962). Sheet lifting device. URL: http://www.freepatentsonline.com/3039767.html

Stiehl, W. D., Lieberman, J., Breazeal, C., Basel, L., Lalla, L. & Wolf, M. Design of a therapeutic robotic companion for relational, affective touch. *Rom. 2005. IEEE Int. Work. Robot Hum. Interact. Commun. 2005.* 408–415 (2005). doi:10.1109/ROMAN.2005.1513813

Suzumori, K. (1992). Gripping actuator with independently flexible cylinders. URL: http://www.freepatentsonline.com/5156081.html

Suzumori, K. (1995). Actuator with flexible cylinders. URL: http://www.freepatentsonline.com/5385080.html

Suzumori, K. (1996). Elastic materials producing compliant robots, Robotics and Autonomous Systems 18: 135–140(6).

Suzumori, K., Endo, S., Kanda, T., Kato, N. & Suzuki, H. (2007). A bending pneumatic rubber actuator realizing soft-bodied manta swimming robot, IEEE International Conference on Robotics and Automation, Roma, Italy, pp. 4975 – 4980.

Suzumori, K., Iikura, S. & Tanaka, H. (1992). Applying a flexible microactuator to robotic mechanisms, Control Systems Magazine, IEEE 12(1): 21 –27.

T. Mukai, M. Onishi, T. Odashima, S. Hirano, Z. Luo, Development of the tactile sensor system of a human-interactive robot "RI-MAN". IEEE Trans. Robot. **24**(2), 505–512 (2008)

T. Someya, T. Sekitani, S. Iba, Y. Kato, H. Kawaguchi, T. Sakurai, A large-area, flexible pressure sensor matrix with organic field-effect transistors for artificial skin applications. Proc. Natl. Acad. Sci. USA **101**(27), 9966–9970 (2004)

T.J.Nelson, R.B. VanDover, S.Jin,S.Hackwood,G.Beni, Shear-sensitive magnetoresistive robotic tactile sensor. IEEE Trans. Magn. **Mag-22**(5), 394–396 (1986)

Takagi, Takeo (Yokohama, J.& Sakaguchi, Yuji (Kawasaki, J. (1986). Pneumatic actuator for manipulator. URL: http://www.freepatentsonline.com/4615260.html

Tanaka, D., Maeda, H. & Nakamura, T. Joint Stiffness and Position Control of an Artificial Muscle Manipulator Considering Instantaneous Load. in *Ind. Electron. 2009. IECON '09. 35th Annu. Conf. IEEE* 2259–2264 (2009). at <http://ieeexplore.ieee.org/stamp/stamp.jsp?tp=&arnumber=5415203>

Taro Nakamura, Yuichiro Midorikawa, H. T. Position and Vibration Control of Variable Rheological Joints Using Artificial Muscles and Magneto-Rheological Brake. *Int. J. Humanoid Robot.* **8,** 205–222 (2011).

Taro Nakamura, Yuichiro Midorikawa, H. T. Position and Vibration Control of Variable Rheological Joints Using Artificial Muscles and Magneto-Rheological Brake. *Int. J. Humanoid Robot.* **8,** 205–222 (2011).

Tillett, N., Vaughan, N. & Bowyer, A. (1994). An improved flexible pneumatic joint for horticultural robots, Mechatronics 4(7): 653 – 671. URL: http://www.sciencedirect.com/science/article/B6V43-480TWR6-T/2/59208c93bf4b07b44 17f3c73d0a3efd1

TL, C. The prevention of deep vein thrombosis, with particular reference to mechanical methods of prevention. *Surgery* **2,** 228–35 (1977).

Todorov, E., Hu, C., Simpkins, A., Movellan, J. & Science, C. Identification and control of a pneumatic robot. in *Proceedings of the 2010 3rd IEEE RAS & EMBS International Conference on Biomedical Robotics and Biomechatronics* (2010). at <http://ieeexplore.ieee.org/xpls/abs_all.jsp?arnumber=5627779&tag=1>

Tomori, H. & Nakamura, T. Theoretical Comparison of McKibben-Type Artificial Muscle and Novel Straight-Fiber-Type Artificial Muscle. *Technology* **5,** 4–5 (2011).

Tri Vo Minh, Tegoeh Tjahjowidodo, Herman Ramon, H. V. B. Non-local Memory Hysteresis in A Pneumatic Artificial Muscle (PAM). in *17th Mediterranean Conference on Control & Automation* 640–645 (2009).

Trivedi, D., Lotfi, A. & Rahn, C. D. Geometrically exact dynamic models for soft robotic manipulators. *2007 IEEE/RSJ Int. Conf. Intell. Robot. Syst.* 1497–1502 (2007). doi:10.1109/IROS.2007.4399446

V.Maheshwari, R.Saraf, Tactile devices to sense touch on a par with a human finger. Angew. Chem., Int. Ed. Engl. **47**, 7808–7826 (2008)

V.Maheshwari, R.Saraf,High-resolution thin-film device to sense texture by touch. Science **312**, 1501–1504 (2006)

Van Damme, M. *et al.* Proxy-based Sliding Mode Control of a Planar Pneumatic Manipulator. *Int. J. Rob. Res.* **28,** 266–284 (2009).

Van Damme, M., Vanderborght, B., Verrelst, B., Van Ham, R., Daerden, F. & Lefeber, D. Proxy-based Sliding Mode Control of a Planar Pneumatic Manipulator. *Int. J. Rob. Res.* **28,** 266–284 (2009).

Van Varseveld, R. B. & Bone, G. M. Accurate position control of a pneumatic actuator using on/off solenoid valves. *IEEE/ASME Trans. Mechatronics* **2,** 195–204 (1997).

Vanderborght, B., Ham, R. Van, Van, M., Saldien, J. & Lefeber, D. Using Compliant Actuators in the Mechanical Design of Robots developed at the VUB Overview • Classical approach : the stiffer the better Good for tracking precision • New generation : introducing compliance – Active compliance (using software). *Program* 1–20 (2010).

Vanderborght, B., Ham, R. Van, Van, M., Saldien, J. & Lefeber, D. Using Compliant Actuators in the Mechanical Design of Robots developed at the VUB Overview • Classical approach : the stiffer the better Good for tracking precision • New generation : introducing compliance – Active compliance (using software). *Program* 1–20 (2010).

Vecchi, F., Freschi, C., Micera, S., Sabatini, A. M., Dario, P. & Sacchetti, R. Experimental Evaluation of Two Commercial Force Sensors for Applications in Biomechanics and Motor Control. in *5th Annual Conference of the International Functional Electrical Stimulation Society* 4–7 (2000).

Verdejo, H. E., Castro, P. F., Concepción, R., Ferrada, M. a, Alfaro, M. a, Alcaíno, M. E., Deck, C. C. & Bourge, R. C. Comparison of a radiofrequency-based wireless

pressure sensor to swan-ganz catheter and echocardiography for ambulatory assessment of pulmonary artery pressure in heart failure. *J. Am. Coll. Cardiol.* **50,** 2375–82 (2007).

Vidal-Verdu, Fernando Estı´balitz, Ochoteco Castellanos-Ramos, Juliàn Navas-Gonzàlez, Rafael Macicior, Haritz Sikora, T. Tactile sensors based on conductive polymers. *Microsyst Technol* 765–776 (2010). doi:10.1007/s00542-009-0958-3

Vimieiro,Claysson Bruno Santos; do Nascimento,Breno Gontijo; Nagem, Danilo Alves Pinto; de Oliveira Costa, Charles; Amaral, Giovanna Mendes; Pinotti, M. DEVELOPMENT OF A HIP ORTHOSIS USING PNEUMATIC ARTIFICIAL MUSCLES TO CONTROL THE JOINT ROTATION. Proc. COBEM 2005 i, 2–7 (2005).

W.C.Nowlin, Experimental results on Bayesian algorithms for interpreting compliant tactile sensing data, in *IEEE International Conference on Robotics and Automation*, Sacramento, California, USA (1991)

W.D.Hillis, Active touch sensing.Int.J.Robot.Res.**1**(2),33–44(1982)

Wang, J., Pu, J. & Moore, P. A practical control strategy for servo-pneumatic actuator systems. *Control Eng. Pract.* **7,** 1483–1488 (1999).

Wilkening, A., Baiden, D. & Ivlev, O. Assistive control of motion therapy devices based on pneumatic soft-actuators with rotary elastic chambers. *IEEE Int. Conf. Rehabil. Robot.* **2011,** 5975361 (2011).

Wissler, M. & Mazza, E. Modeling and simulation of dielectric elastomer actuators. *Smart Mater. Struct.* **14,** 1396–1402 (2005).

Xiang, F. Block-Oriented Nonlinear Control of Pneumatic Actuator Systems. (inflatable actuators dynamics, 2001).

Xin-tao, M. A. O., Qing-jun, Y., Jin-jun, W. U. & Gang, B. A. O. Control strategy for pneumatic rotary position servo systems based on feed forward compensation pole-placement self-tuning method. *J. Cent. South Univ. Technol* 608–613 (2009). doi:10.1007/s11771

Y. Ohmura, Y. Kuniyoshi, A. Nagakubo, Conformable and scalable tactile sensor skin for curved surfaces, in *IEEE International Conference on Robotics and Automation*, Orlando, Florida, USA (2006)

Y.Kato,T.Mukai,T.Hayakawa,T.Shibata,Tactilesensorwithoutwireandsensingelement in the tactile region based on EIT method, in *IEEE Sensors Conference* (2007), pp. 792–795

Y.Liu, R.I.Davidson, P.M.Taylor, J.D.Ngu, J.M.C.Zarraga, Single cell magnetorheological fluid based tactile displays. Displays **26**, 29–35 (2005)

Yan, T. H., Chen, X. D., Dou, W. F. & Lin, R. M. Feedback Control of Disk Vibration and Flutter by Distributed Self-Sensing Piezoceramic Actuators. Mech. Based Des. Struct. Mach. 283–305 (2008). at <http://www.tandfonline.com/doi/pdf/10.1080/15397730802400433>

Yoshikama, T. & Hosoda, K. (1996). Modeling of flexible manipulators using virtual rigid links and passive joints. *International Journal of Robotics Research* 15:290-299.

Zentner, L. & Böhm, V. (2007). Nachgiebige monolithische fluidisch angetriebene aktuatoren mit neuartigem verformungsverhalten, Technische Mechanik 27(1): 18–27.

Zentner, L., Böhm, V. & Minchenya, V. (2009). On the new reversal effect in monolithic compliant bending mechanisms with fluid driven actuators, Mechanism and Machine Theory 44(5): 1009 – 1018.

Zentner, L., Petkun, S. & Blickhan, R. (2000). From the spider leg to a hydraulic device, *Technische Mechanik* (20):21-29.

Zhang, Z. & Philen, M. Pressurized artificial muscles. *J. Intell. Mater. Syst. Struct.* **23,** 255–268 (2011).

Zhao, M., Zheng, W., Fan, C. & Pan, E. Nonlinear elastic mechanics of the ball-loaded blister test. *Int. J. Eng. Sci.* **49,** 839–855 (2011).

Zhu, X., Tao, G., Yao, B. & Cao, J. Adaptive robust posture control of a parallel manipulator driven by pneumatic muscles. *Automatica* **44,** 2248–2257 (2008).